The Dissertation Committee for Ye Shi Certifies that this is the approved version of the following dissertation:

Rational Design of 3D Nanostructured Conductive Polymer Gels for Electrochemical Energy Storage and Responsive Electronic Devices

Committee:

Guihua Yu, Supervisor

Christopher J. Ellison

Nanshu Lu

Wei Li

Rational Design of 3D Nanostructured Conductive Polymer Gels for Electrochemical Energy Storage and Responsive Electronic Devices

by

Ye Shi, B.E.; M.E.

Dissertation

Presented to the Faculty of the Graduate School of

The University of Texas at Austin

in Partial Fulfillment

of the Requirements

for the Degree of

Doctor of Philosophy

The University of Texas at Austin

May 2017

Dedication

To my parents and my wife for their endless love and support.

Acknowledgements

I would like to express my special appreciation and thanks to my supervisor Prof. Guihua Yu for his continuous support of my PhD study and research. His guidance helped me throughout my research and allowed me to grow as a research scientist. I would also like to express my gratitude to my committee members, Prof. Nanshu Lu, Prof. Christopher J. Ellison, and Prof. Wei Li for serving as my committee members and for their brilliant comments and suggestions on my thesis.

My sincere thanks go to my colleagues in Yu Lab, who are just like family to me. My work would not be half of what it is without their great support of my research and living life.

I want to express special thanks to Prof. Christopher J. Ellison (UT Austin), Prof. Xiaopeng Li (Texas State University), Prof. Esther S. Takeuchi (Stony Brook University), Prof. Amy C. Marschilok (Stony Brook University), and Prof. Lijia Pan (Nanjing University) for collaborating with me on different projects. I also want to appreciate Dr. Heonjoo Ha, Dr. Jun Zhang, and Dr. Ming Wang for sharing with me their insightful thoughts and rich experience in scientific research.

Finally, I would like to acknowledge the financial support from National Science Foundation, 3M Company, and Department of Energy.

Rational Design of 3D Nanostructured Conductive Polymer Gels for Electrochemical Energy Storage and Responsive Electronic Devices

Ye Shi, PhD

The University of Texas at Austin, 2017

Supervisor: Guihua Yu

This work presents the rational design and synthesis of conductive polymer gels (CPGs) using doping molecules as crosslinkers. Molecules with multiple functional groups are used to crosslink the conductive polymer chains, leading to CPGs with 3D networked structures. These dopant molecules crosslinked CPGs exhibit both high electrical and ionic conductivities since they construct heavily doped and interconnected polymer network for electron transport and hierarchically porous structure for ion diffusion. The chemical and physical properties of dopant molecules crosslinked CPGs can be facilely tuned by controlling the dopants and synthetic conditions.

With improved electrochemical properties, CPGs have been applied as an electrode material in supercapacitors and as a binder material in lithium ion batteries. CPGs establish a continuous network to promote the transport of electrons, provide short ion diffusion path and large surface area for redox reactions, and construct a porous architecture with intrinsic elasticity to accommodate the volume change, thus showing high capacitance and rate capability as supercapacitor electrode materials. High elasticity derived by the structure of CPGs further enables highly flexible supercapacitor. CPGs were also adopted as bifunctional binder materials for lithium ion battery electrodes, acting as both polymeric binder and a conductive additive. The gel framework based

electrode exhibits greatly improved rate and cyclic performance owing to improved electronic and ionic transport. In addition, both inorganic and organic components are uniformly distributed within the electrode due to the polymer coating. The robust framework further provides mechanical strength to support active electrode materials and improves the long-term electrochemical stability.

Combined with other functional gels, CPGs have been also adopted for smart electrochemical devices. Based on CPGs and a thermoresponsive electrolyte system, electrochemical energy storage devices with thermal self-protection behavior are developed. The smart electrolyte system is achieved by employing a commercially available thermoplastic elastomer, Pluronic, which shows a fast sol-gel transition process upon heating. The gelation of Pluronic solution based electrolytes significantly inhibits the migration of ions, leading to a nearly 100% decrease in specific capacitance. The responsive behavior is highly reversible and tunable. Various electrode materials and conductive ions are compatible with this system.

Finally, multifunctional hybrid gel materials based on CPGs are developed by introducing a second responsive polymeric network, forming an interpenetrating double network structure. A highly thermoresponsive and conductive hybrid gel is synthesized by in situ polymerization of CPGs within PNIPAM matrix and a room-temperature self-healing hybrid gel is prepared by introducing a supramolecular gel into PPy gel framework.

Table of Contents

List of Tables

List of Figures

Chapter 1 Introduction*

1.1 NANOSTRUCTURED CONDUCTIVE POLYMERS: SYNTHESIS AND PROPERTIES

Conductive polymers are a class of functional polymers that have a delocalized π-system backbone along the polymeric chains. They have received great research interests from both academia and industry since the discovery of conductive polyacetylene in the 1970s because conductive polymers offer tunable electrical and optical properties similar to those of metals and inorganic semiconductors while maintaining advantageous features associated with conventional polymers, such as ease of synthesis and flexibility in processing.[1-3] A variety of conductive polymers with different molecular structures have been developed, showing quite different chemical/physical properties (Figure 1a). Typical conductive polymers include polyacetylene (PA), polyaniline (PANI), polypyrrole (PPy), polythiophene (PTh), poly(phenylenevinylene) (PPV), polyfuran (PF), etc. These conjugated polymeric chains can be synthesized by various methods such as chemical polymerization, electrochemical polymerization, photochemical polymerization and so on.[4] However, the polymerizations of conductive polymers with different methods usually share similar processes with an electrochemical process of oxidation, a chemical process of coupling and eliminating protons.[4] A widely accepted mechanism of conductive polymer polymerization is shown in Figure 1b.[5] Firstly, the oxidation of one monomer generates a radical cation which couples with another radical cation and forms a dimer after the loss of two protons. The dimer could be further oxidized and coupled with radical cations to form oligomers. This propagation continues via the same sequence of oxidation, coupling, deprotonation until the polymer is finally obtained.

---

* Y. Shi, L. Peng, Y. Ding, Y. Zhao and G. Yu, Nanostructured Conductive Polymers for Advanced Energy Storage, *Chem. Soc. Rev.*, 2015, 44, 6684.
Y. S. participated in the preparation of manuscript.

The conductive property of conductive polymers is not only determined by their molecular structures and orders of molecular packing but also associated with doping molecules and level of doping.[4, 6-9] Doping is a reversible process which brings the backbone of conductive polymer positive (p-doping) or negative charge carriers (n-doping) (Figure 1c).[10] And counter ions with opposite charges would be entrapped or released from the polymer matrix to maintain the charge neutrality of the polymer. Polymer doping leads to the formation of conjugational defects such as solitons, polarons or bipolarons in conductive polymer chains, thus significantly enhancing the conductivity of conductive polymers. The conductivity of neutral conductive polymers is rather low, which is usually in the range of 10^{-10} to 10^{-5} S cm^{-1}, but they could be tuned in a wide range up to 10^{4} S cm^{-1} by doping. This unique feature endows conductive polymers with the ability to act as insulators, semiconductors or conductors.

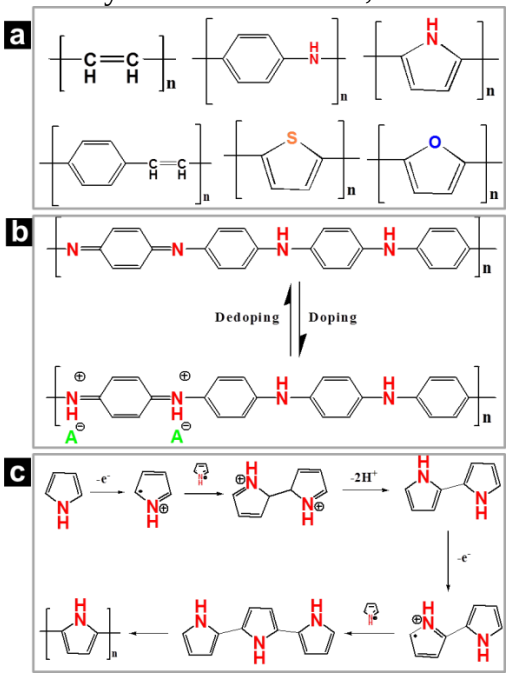

Figure 1.1 (a) The chemical structures of typical conductive polymers; (b) The mechanism of doping/dedoping process of PPy; (c) Schematic illustration of the mechanism of polymerization of conductive polymers.

The chemical/physical properties of conductive polymers can be further tuned by controlling their micro- or nano-structures. With rapid advancement in nanoscale science and technology, nanostructured conductive polymers have been intensively researched due to the unusual physical/chemical properties associated with confined dimensions of nano-scale structures.[11-14] Compared with their bulk form, nanostructured conductive polymers exhibit several advantageous features including:[15] (1) enhanced electrical conductivity; (2) large surface area of the interfaces between the electronic transporting phase and the ionic transporting phase, or between biological and synthetic materials; (3) shortened pathway for charge/mass transport; (4) improved mechanic properties; (5) mixed conductive mechanism which lowers the interfacial impedance between electrode and electrolyte, thus both electronic and ionic conductivity are enhanced. Various nanostructured conductive polymers have been developed including 1D, 2D, 3D nanostructures and nanostructured composites.

1.1.1 Conductive polymers with 1D nanostructures

1D nanostructured conductive polymers including nanowires, nanorods, nanofibers, nanobelts, and nanotubes show enhanced electrical conductivity, high charge-carrier mobility, good mechanical properties, and unique electrochemical activity due to improved alignment of polymeric chains, thus becoming one important family of conductive polymer nanostructures. The controlled synthetic strategies for 1D nanostructured conductive polymers could be classified into two main categories: template-based methods and template-free methods.[16]

Template-based methods are powerful tools for the controllable synthesis of 1D nanostructures of conductive polymers and two kinds of templates including hard templates and soft templates have been used (Figure 2a). Commonly used hard templates

include porous membrane materials such as anodic aluminum oxide (AAO), block copolymers, porous silicate, and mesoporous zeolites and pre-existing nanostructured materials such as inorganic nanowires and nanofibers.[17, 18] The pores of the porous membrane or the surface of inorganic 1D nanostructures can be loaded with the monomer solution of conductive polymer followed by in-situ chemical or electrochemical polymerization of the monomer, forming 1D nanostructured conductive polymers. It is possible to tune the dimension, aspect ratio and orientation of 1D polymer structures either by adjusting experimental parameters or by the template. Soft templates can be also used for 1D conductive polymer nanostructures. The soft templates are usually made from mesophase structures of self-assembled amphiphilic molecules through hydrophilic-hydrophobic interactions, hydrogen bonds, and van der Waals forces, etc. Surfactant micelles, liquid crystals, copolymers etc. are commonly used soft templates. By tuning the chemical properties and chain length of the surfactants, as well as the concentrations of both polymer monomers and surfactants, the morphology of resulted 1D nanostructured conductive polymers can be controlled. For examples, nanowire- or nanoribbon-like of PPy, PANI have been synthesized with cationic surfactants of cetyltrimethylammonium bromide (CTAB) and anionic surfactants of sodium dodecyl sulfate (SDS),[19] while hollow 1D nanostructure of PPy has been achieved with sodium bis(2-ethylhexyl) sulfosuccinate (AOT) as surfactants due to the reverse micro-emulsion polymerization.[20]

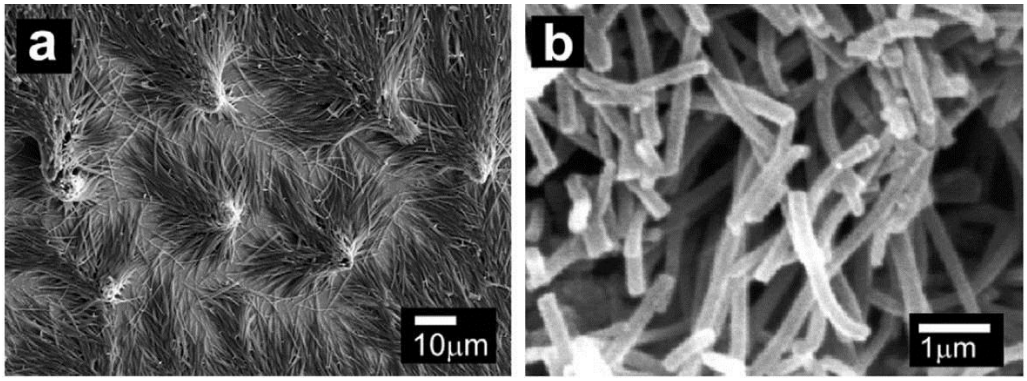

Figure 1.2 SEM images of 1D conductive polymer nanostructures synthesized with (a) template-based method and (b) self-assembly method.

The template-based methods show not only advantages of universality and controllable dimensions but also poor scalability and harsh post treatment. Large-scale fabrication of polymer nanostructures using template-based methods is limited by the size and amount of the template and the post treatment for template removal may destroy or harm the formed nanostructures and increase the processing cost.

Template-free methods including self-assembly or electrospinning have been developed to overcome the drawbacks of template-based methods (Figure 2b).[5] The self-assembly method is induced by non-covalent forces between polymer chains such as π-π stacking, dipole-dipole, hydrophobic, van der Waals forces, hydrogen bonding, electrostatic and ion-dipole interactions. For example, β-naphthalene sulfuric acid (β-NSA) can introduce these interactions into conductive polymer chains and help them self-assemble to 1D nanostructures. PANI, PPy, PEDOT nanowires and nanotubes have been successfully obtained by this dopant-enabled self-assembly method. It is facile to control the size and structure by adjusting the kinds of dopants, molar ratios of monomers to dopant, as well as reaction temperature and time. Interfacial polymerization is another self-assembly method in which nanofibers or nanotubes of conductive polymers are self-

assembled on the interfaces of aqueous/organic solvents. People also use electrospinning to synthesize 1D polymer nanostructures. In a typical synthesis, a high electrical field is applied between a polymer fluid and a conductive collector to form a liquid line. The nanofibers are produced as the solvent is evaporated. PANI, PPy, PPV and P3HT nanofibers have been successfully prepared via this method.[5]

1.1.2 Conductive polymers with 2D nanostructures

2D nanostructured films of conductive polymers show unique features of controllable thickness, modifiable porosity and surface morphology, and processability over a large range of areas.[21] There are two types of nanostructured films of conductive polymers: non-porous films and nano-porous films, which are usually synthesized on pre-treated substrates or well-defined surfaces.

Non-porous nanofilms can be prepared by synthetic strategies including electrochemical polymerization, spin coating, and layer-by-layer (LBL) techniques. Electrochemical polymerization has been used to deposit a ultra-thin film of conductive polymer on the substrate and modify the film by introducing other molecules or particles which can act as functional components such as conductive additives, reaction sites, catalysts and surface modifiers, resulting in multi-functional and high-performance devices. For example, an ultrathin (~55 nm) PPy film modified by glucose oxidase (GOD) has been fabricated by employing a simple electrochemical polymerization process in an electrolyte-free monomer solution with a low current density and long period.[22] Spin coating is also able to prepare non-porous films of soluble conductive polymers. For example, ultra-thin Poly(3,4-ethylenedioxythiophene)-Polystyrene sulfonate (PEDOT-PSS) films on different substrates have been obtained through this method with controllable thickness by varying the speed of spin coating or the solution

concentration.[23] LBL technique is another technique for non-porous film fabrication.[21] A layer-by-layer manner is used to deposit conductive polymers with other polymers like polystyrene sulfuric acid (PSSA), as well as with some inorganic materials such as graphene and carbon nanotubes. The conductive polymer can act as weak polyelectrolyte with surface charge and is processed by the LBL technique, and the film thickness is controlled by the number of individual layers.

Conductive polymers networks formed by the interconnection of nanoscale domains or nanopores of conductive polymers on a substrate or surface are called nanoporous films. These films show advantages including large surface area, fast diffusion of molecules and strong interaction between molecules and exposed areas. Hard-template, soft-template method and template-free electrosynthesis have been developed to fabricate the nano-porous films of conductive polymers. Colloidal particles are one of the commonly used hard-templates. For examples, a porous film of 3-methylthiophene (MTH) and thiophene-3-acetic acid (TAA) is electrochemical copolymerized onto ITO-coated glass with different sizes of polystyrene (PS) particles on the surface to act as templates.[24] Aniline monomers are electrochemical polymerization within the interstitial voids in assemblies of polystyrene nanospheres pre-coated with multilayers polyelectrolyte, forming 2D PANI films with honeycomb structures (Figure 3a).[25] Soft template method is also useful for the synthesis of nanoporous conductive polymer films. For example, PEDOT and PPy can grow along the nanostructures of rod-like PSA with during electrochemical polymerization, resulting in the formation of conductive polymer nanofiber networks on the electrodes.[26] Nanoporous films of conductive polymers on electrode surface can be synthesized by template-free electrosynthesis. The fabrication of a superhydrophilic PPy nanofiber porous film has been achieved by using a template-free electrochemical approach in which phosphate

buffer solution (PBS) is applied (Figure 3b).[27] Another template-free synthesis is the interfacial electropolymerization technique which successfully prepares PPy nanoporous films by using ionic liquid as the electrolyte.[28]

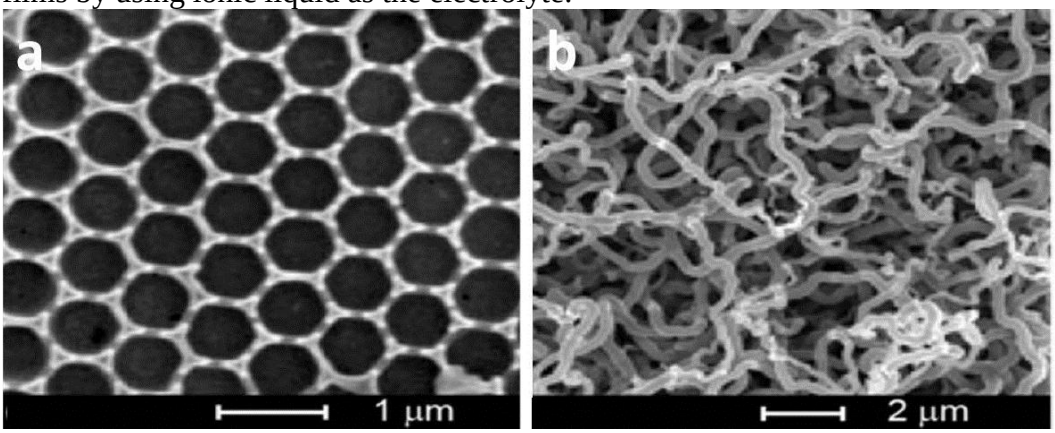

Figure 1.3 (a) PPy network prepared by the template-free approach. (b) PPy network prepared by the template-free approach.

1.1.3 Nanostructured composites based on conductive polymers

Nanostructured composites based on conductive polymers are attractive because they combine the intrinsic properties of each component and may produce synergistic effect.[29] Synthetic routes such as physical mixing, electrochemical synthesis, epitaxial growth and in-situ polymerization etc., have been used to incorporate one or more foreign components into conductive polymers and thus tune the electrochemical activity, mechanical strength, conductivity, and stability etc. of nanostructured composites.

Hybrid materials based on carbon nanomaterials and conductive polymers are one of the most important composite materials. In such nanostructured composites, conductive polymers often act as an active redox-reactive component due to their high electrochemical activity while carbon nanomaterials play the role as a framework which promotes charge transport and reinforces the composite. Carbon nanotube (CNT), graphene, activated carbon, and other nanostructured carbon materials are commonly

used materials for composites with promising electrochemical, optical and mechanical properties. For example, composite nanofibers consisting of integrated PANI nanofiber shells and single-walled carbon nanotube (SWCNT) core nanostructures with average diameters of 20-50 nm have been explored as high-performance chemosensors (Figure 4a).[30] Another composite combining reduced graphene oxide (RGO) and PANI through in-situ polymerization in the RGO suspensions has been prepared for high-performance supercapacitor electrodes.[31]

Transition metal oxides is another candidate for composite synthesis owing to their advantageous features including high energy storage capacity, rich redox activity, long cycle life and good mechanical stability. Conductive polymer/MnO_2 nanocomposites have been synthesized by simply soaking the polymer nanowire arrays in $KMnO_4$ solution through a redox exchange reaction between $KMnO_4$ and the functional groups of selected polymers (Figure 4b).[32] As another example, Co_3O_4/PANI core/shell nanowire arrays were also synthesized for Li-ion battery anode application.[33]

In addition to binary hybrids, ternary hybrid structures have also been explored. Common ternary composites with nanostructures usually consist of carbon-based nanomaterials, transition metal oxides, and conductive polymers and combine the advantages from all components. For instance, a ternary hybrid material of MnO_2/CNT/PEDOT-PSS has been proposed, in which CNTs provide large surface for the deposition of hierarchical porous MnO_2 nanospheres and improve the electrical conductivity as well as the mechanical stability of the composite; PEDOT-PSS acts as an effective dispersant for MnO_2/CNTs structures and a binder material that helps adhesive and connect MnO_2/CNTs particles in the film; and MnO_2 nanospheres provide improved specific capacitances (Figure 4c).[34]

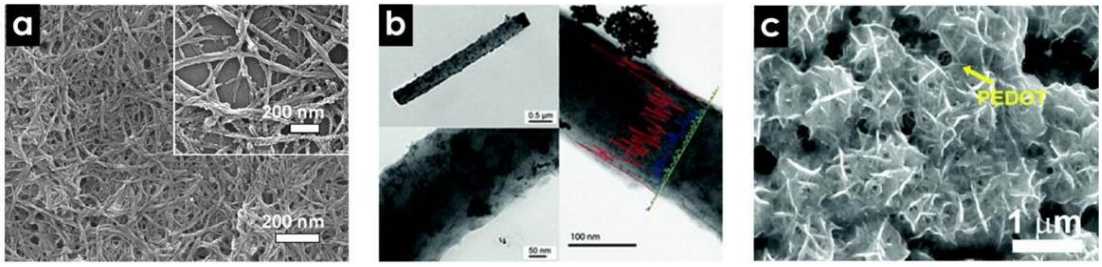

Figure 1.4 (a) SEM image of SWCNT/polyaniline composite nanofibers. (b) TEM images of MnO_2–PPy nanowires. (c) SEM image of the graphene/MnO_2 /PEDOT: PSS ternary electrode.

1.2 NANOSTRUCTURED CONDUCTIVE POLYMERS: APPLICATIONS IN ENERGY STORAGE DEVICES

1.2.1 Nanostructured conductive polymers for electrochemical capacitors

Electrochemical capacitors are expected to be one of the most promising future power sources owing to their high power densities. Distinct from conventional electrostatic capacitors which store charges in an electric field imposed across a thin layer of dielectric material, electrochemical capacitors store charges at the electrochemical interfaces between the high surface area, porous electrode material, and the electrolyte. The larger specific surface area and shorter distance between the electrode and electrolyte ions can significantly increase the effective capacitances of electrochemical capacitors with several orders of magnitude. In general, a high-performance electrochemical capacitor electrode requires the simultaneous minimization of the four primary resistances present during charging and discharging: (1) ion transport in the electrolyte, (2) ion transport in the electrode, (3) electrochemical reactions in the electrode and (4) electron conduction in the electrode and current collector (Figure 5).[35]

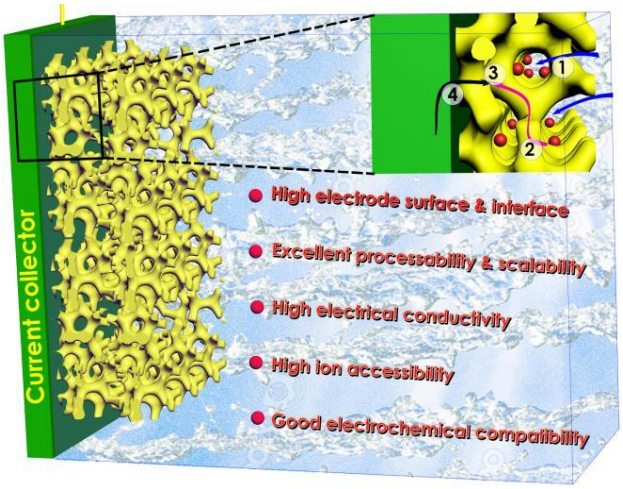

Figure 1.5 Schematic of a high-performance EC electrode with the following desired characteristics: large electrode surface & interface, high electrical conductivity, high ion accessibility, good electrochemical compatibility, and excellent processability and scalability.

Conductive polymers are a class of pseudocapacitive materials which utilize fast and reversible electron exchange reactions at or near the electrode surface to store energy.[36] Conductive polymers show the following advantages: high electrical conductivity, large ion-accessible surface and interface area, high ionic transport, and good processability and scalability.[9, 37] However, conductive polymers such as PANI and PPy usually suffer from poor cycling stability maybe due to the unstable chemical structures and the low charge transfer of the conductive polymers, as well as the volume change caused by swelling and shrinking of the polymer structures during charging and discharging processes.[38] Also, penetration of electrolyte ions is blocked in bulk films of conductive polymers, hindering the high performance. To solve these problems, various nanostructures have been designed to fulfill the high capacitance of conductive polymers.

Conductive polymer nanowire arrays are used as electrodes to improve the electrochemical performance. The vertical nanowire array electrodes exhibit several advantages for energy storage devices compared with disordered nanowire networks.

Firstly, all nanowires contribute to the storage capacity since they are all electrically connected to the conductive substrate. Secondly, 1D electronic pathways promote efficient charge transport and reduced ions-transport length. Lastly, volume change can be accommodated by the interspace between oriented nanowires without the initiation of fracture in bulk or micron-sized materials. Conductive PANI nanowire arrays are grown vertically on graphene oxide (GO) sheets by Wei et al.[39] The PANI nanowire/GO composite showed a synergistic effect when used as supercapacitor electrode, yielding high specific capacitance of 555 F g^{-1} at a discharge current density of 0.2 A g^{-1} and excellent capacitance retention of 92% after 2000 consecutive cycles. Their results indicated that optimizing the structures at the nanoscale is an effective way to improve practical capacitance and stability of conductive polymer based electrodes.

Nanostructured composite materials are another important material platform for fabricating high-performance electrochemical capacitors. Hybrid materials based on conductive polymers and various inorganic components such as carbon-based nanomaterials, transition metal oxides with controlled nanostructures have been widely studied to take advantage of the unique synergic properties inherited from individual components. In these nanostructured composites, conductive polymers provide improved electrode conductivity and interfaces between the electrodes and the electrolytes while the inorganic components can act as conductive pathways, mechanical reinforcement framework and/or redox-reaction materials.

Carbon nanomaterials transport charge carriers and relief the strains during electrochemical processes, thus improving the stability of pure conductive polymer based electrodes. For example, paper-like composite films of chemically converted graphene (CCG) and PANI-NFs (G-PNF) are fabricated by Shi et al.[40] and applied for supercapacitors. The G-PNF film is self-standing, highly flexible, and highly conductive

to eliminate the need of conducting additive. Compared to carbon–conductive polymer composites, hybrids of conductive polymers and pseudocapacitive transition metal oxides like RuO_2, NiO, and MnO_2 would have higher electrochemical activities due to their high energy density and large pseudocapacitance from metal oxides.[41] Transition metal oxides are considered to be one of the most attractive material platforms for electrochemical capacitors owing to their rich redox activity and high energy density. They also show poor conductivity (usually around 10^{-5}~10^{-8} S cm^{-1}). Conductive polymers have been proved to solve these critical problems. MnO_2/PEDOT coaxial nanowires are synthesized by Lee et al.[42] by co-electrodeposition with tunability in terms of the dimensions, shell thickness, and nanowire length. The coaxial nanowires exhibited a high specific capacitance, good capacitance retention, and excellent rate capability. In another example, Liu et al.[43] reported a 3D CoO-based nanowire electrode with PPy as a nanosized thin layer which is firmly attached to the nanowires in the form of nanoparticles to enhance the conductivity of the 3D electrode. The electrode shows very high capacitance and good rate capability. The binary electrodes maintain a good electrochemical reversibility with 99.86% Coulombic efficiency even after 2000 cycles, and the asymmetric supercapacitors deliver a high energy density of 43.5 Wh kg^{-1} at a power density of 87.5 W kg^{-1}.

Besides binary composites, ternary hybrid materials based on conductive polymers and inorganic materials have been also developed to improve their electrochemical properties. Liu et al.[34] developed a ternary MnO_2/CNT/conductive polymer composite for high-performance electrochemical supercapacitor electrodes. The ternary MnO_2/CNT/conductive polymer composite exhibits not only the high specific capacitance and stable capacitance at high current density but also showed great potential for the use in power applications. Such electrode design provides the possibility to solve

the potential problems such as the dense morphology and the intrinsically poor electrical conductivity of transition metal oxides.

1.2.2 Nanostructured conductive polymers as active electrodes and functional materials for lithium ion batteries

Lithium ion batteries are extensively investigated as a new generation of energy storage devices due to their high theoretical capacity, relatively light weight, enhanced safety, and low toxicity. Pure conductive polymers have been explored as electrode materials since the 1980s in which[44] they can serve as both anodic and cathodic materials while they are commonly used as a cathode in lithium ion battery. Although conductive polymers show several advantages such as good processability, low cost, convenient molecular modification, and light weight when applied as electrodes, their application is inhibited by poor stability during cycling and low conductivity at reduced state.

The adoption of nanostructured conductive polymers can partially overcome this problem, owing to their high surface and fast diffusion kinetics for Li ions. PANI nanotubes doped with $HClO_4$ are synthesized by Chen et al.[45] and utilized as positive electrode materials in lithium ion battery, showing better performance than the commercial PANI powders. The Li/PANI battery achieved a high practical discharge capacity of 75.7 mAh g^{-1} but the capacity and power density is still relatively low and the stability of organic materials remains a serious problem.[46] Redox-active components are added into a polymeric matrix or linked to polymer chains to act as a counterion dopant and function as redox-active sites, thus enhancing capacity density. Goodenough et al.[47] covalently anchored ferrocene groups to the PPy backbone, thus increasing the specific capacity and rate capability, as well as lowering the overpotential at high discharge rates. Conductive polymers are combined carbon materials such as graphene and carbon nanotubes to form nanostructured composites, in which carbon nanomaterials can

improve the electrical conductivity as well as the mechanical properties of the conductive polymer matrix. Hammond et al.[48] prepared electrodes consisting of PANI nanofibers and multiwall carbon nanotubes, resulting in the electrodes with a high specific capacity of 147 mAh g^{-1} and excellent charge/discharge stability over 10,000 cycles.

The conductive polymers are more commonly used as modification material to enhance the performance of other cathodes and anodes battery materials. For example, Co_3O_4/PANI core/shell nanowire arrays were synthesized to overcome the poor rate capabilities of Co_3O_4 anodes due to its low intrinsic electronic conductivity. The composite anode exhibited superior Li-ion storage capability compared to the bare Co_3O_4 nanowires arrays.[33] Olivine $LiFePO_4$ is combined with the conducting polymer PEDOT. Polymerization propagation requires the reinsertion of lithium into the partially delithiated lithium iron phosphate, as well as the transport of Li ions and electrons through the deposited polymer coating. In turn, these are also the functional characteristics of an effective conducting coating for $LiFePO_4$. As such, the $LiFePO_4$/PEDOT composites exhibited greatly improved rate capability (125 mAh g^{-1} at 10 C) and power density.[49]

Recently, conductive polymers are developed as binder system for lithium-ion battery electrodes, which holds the active material together in the electrodes of a Li-ion battery (Figure 6). They show various advantageous features: a continuous electrically conductive framework, binding with the hosted active materials, and porous space for volume change upon repeated Li^+ insertion/de-insertion. Nanostructured conductive polymers can work well in materials with large volume change such as alloying-type electrodes (silicon, germanium, etc) and avoid aggregation during volume expansion, owing to their distinctive characteristics: (1) good electronic conductivity inherited from the conductive polymer framework, (2) good mechanical adhesion and ductility with

tolerance of large volume change, and (3) good electrolyte uptake to warrant high ionic conductivity.[50]

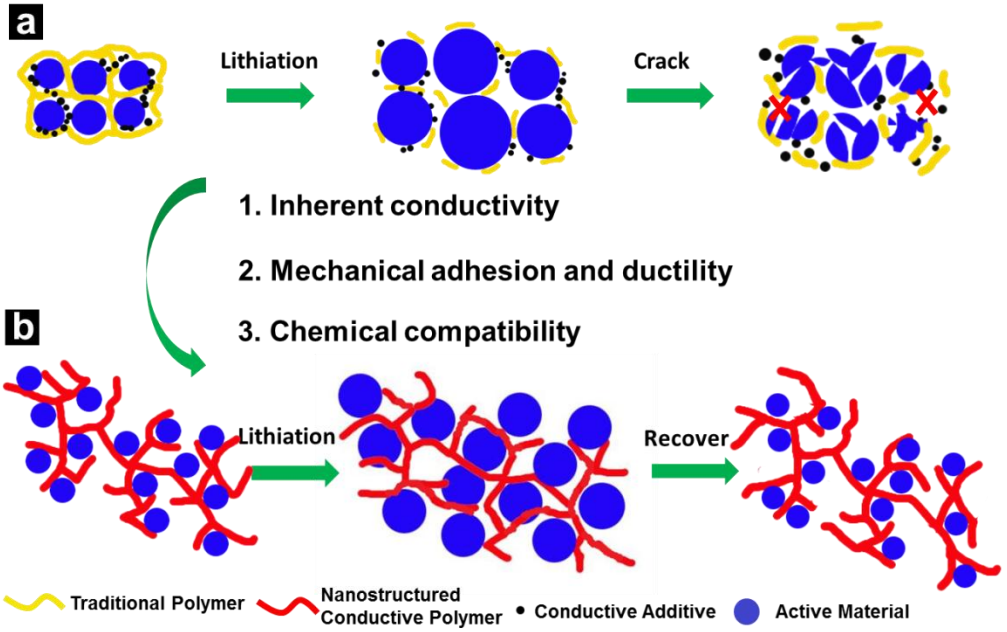

Figure 1.6 (a) Traditional approach using conductive additive and polymer as a mechanical binder may result in broken electric contacts. (b) Conductive polymers can play multi-functions, as a conductor and binder, thus keeping both electrical and mechanical integrity of the electrode during cycling

Liu et al.[51] developed a promising conductive polymer which can be cathodically doped under reducing environments for silicon anodes. They tailored the lowest unoccupied molecular orbital (LUMO) electronic states and the mechanical binding force of polymer binder to achieve both high conductivity for electron conduction and mechanical integrity, resulting in high specific capacity and stable cycling performance. The polymer binder can be further modified with other functional groups. Fluorenone (F) was incorporated to tailor the electronic structure of the polymer and methyl benzoate ester (M) groups were used to improve the chain flexibility of the polymer and the

mechanical binding force between the active materials and the polymer binder. In addition, triethyleneoxide monomethylether (E) side chains were introduced to enhance its electrolyte uptake capability. Besides the molecular tailoring of conductive polymers, the micro/nano-structure design is another efficient way to enhance their performance when acting as electrode binders. PPy nanotubes are used as a conductive matrix to support sulfur cathode in lithium-sulfur batteries. The PPy-S composites exhibited nearly a constant capacity of ~650 mAh g^{-1} after 80 cycles. The enhanced performance could be mainly attributed to the improved conductivity of PPy nanotubes based composites, favorable distribution of the nanosized sulfur in the PPy matrix and excellent retention of the polysulfides within the electrode.

1.3 CONDUCTIVE POLYMER GELS (CPGS): NANOSTRUCTURED CONDUCTIVE POLYMER WITH 3D NETWORK STRUCTURE

Gels are defined as cross-linked network systems that exhibit properties ranging from soft and weak to hard and tough. Conventional gels, especially hydrogels, are synthesized by crosslinking homopolymer or copolymer chains through physical interactions or chemical bonds.[52] Physical gels are networks formed through non-covalent interactions including hydrophobic interactions, charge interactions and hydrogen bonds, which usually lead to junction zones in which separated polymer chains interact over a certain length but not in a point-to-point manner. Chemical gels are crosslinked with covalent bonds, which typically exhibit enhanced mechanical stability because covalent interactions are much stronger. Chemical crosslinking methods include radical polymerization, the chemical reaction of complementary groups, high-energy irradiation and the use of other functional crosslinking agents.

Gels, especially hydrogels, have been widely studied and applied in bio-related fields, such as tissue engineering, controlled drug delivery, the development of medical

and biological sensors, and diagnostic imaging,[53] owing to their advantageous features from chemical and physical structures.[54] Gel networks have a high affinity for solvents but are prevented from dissolving because of their crosslinked nature. Solvents can penetrate between the chains, and the mechanical properties of gels can be modulated over a wide range. Biologically active entities such as enzymes and cells can be incorporated into gel networks and well dispersed by means of physical or chemical entrapment to produce hybrid materials owing to large surface area and biocompatibility of hydrogel. In addition, it is possible to precisely control the molecular architecture and morphology of gels. Finally, gel networks can be made to interact with their environments in an intelligent manner via molecular tailoring. Various responsive gels have been synthesized that are capable of sensing and responding to external stimuli, such as pH, light, mechanical stress, and temperature.

These appealing features of gel materials as demonstrated in bio-applications are also desirable in energy applications. Gel materials offer many advantages: 1. The 3D network of a gel can promote the transport of electrons along the backbone while facilitating the diffusion of ions through hierarchical pores, which is appealing in energy devices. 2. The network structure can avoid the stacking of materials by mitigating the effects of strong interactions such as π-π interactions and can accommodate the volume changes. 3. Energy conversion and storage involve physical interactions and/or chemical reactions at surfaces and interfaces; therefore, the surface area and surface chemistry of a material play very important roles in these processes.[55] Gel materials with enhanced surface areas can provide large numbers of active sites for reactions, and their surfaces can be chemically modified. 4. Hybrid materials also play important roles in high-performance energy devices. Gel materials offer an excellent platform to support other active materials and its porous structure permits the introduction of a second network,

thus enabling the development of various hybrid materials. The hydrophilic nature of hydrogels also makes them compatible with bio-environments. 5. Gel materials exhibit beneficial mechanical properties, including tunable strength and high flexibility, which enable the development of flexible and stretchable devices. 6. Finally, the chemical, mechanical, and electrochemical properties of gels are tunable by adopting different functional crosslinkers and applying chemical modifications, thereby further extending their applications and improving their performance.

With structural features derived from gel materials and electrical properties of conductive polymers, conductive polymer gels (CPGs) with three-dimensional (3D) hierarchical structures are emerging as a promising class of polymeric materials for energy applications because they could provide an electrically conductive yet monolithic framework to promote transport of electrons, offer micro- and meso-scale pores within the polymeric matrix to facilitate the diffusion of ions and molecules, as well as extending effective interface between molecular chains and electrolyte for redox reactions.[56-58] The porous structure of CPGs can also help accommodate the strain caused by volume change during electrochemical reaction and offer the possibility to fabricate light-weight and flexible devices.

Several synthetic strategies for CPGs have been developed including polymerization of monomers in existing non-conductive hydrogel matrix, copolymerization of conductive polymer with non-conductive polymers, or crosslinking conductive polymers by multivalent metal ions (Fe^{3+} or Mg^{2+}).[59] In a typical synthesis using commonly used hydrogel template (Figure 7), a hydrogel is firstly prepared and de-swollen, and then re-swollen in the solution of conductive polymer monomers which is in-situ polymerized either by electrochemical polymerization or by exposure to chemical oxidants. However, this route usually results in the low surface area of the conductive

hydrogel. A micro or nanostructured template is introduced to increase the surface area but leads to poor scalability. Another method to fabricate CPGs is the copolymerization of conductive polymer monomers with other hydrogel monomers. Non-conductive polymers can act as a component of main chains of the copolymer or the crosslinking part to crosslink conductive counterparts. In this route, non-conductive hydrogel and conductive polymer precursors are placed together and polymerized either simultaneously or in a two-step process by chemical oxidation or electrochemical polymerization. PPy-pHEMA hybrid hydrogel is synthesized with this method and tuned by further adding other acrylate, methacrylate and acrylamide monomers.[60] These traditional methods result in composite gels of both conductive and nonconductive polymers in which the electrical properties are deteriorated. Moreover, excessive metal ions adopted in the polymerization may reduce the compatibility of hydrogels with other molecules. The conventionally synthesized CPGs can hardly be micropatterned which is important for fabricating large-scale arrays of electronic devices.

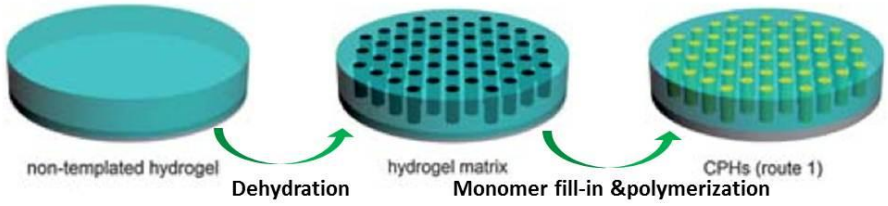

Figure 1.7 Schematic illustration of a template-guide method for the synthesis of conductive polymer gels.

1.4 RESEARCH MOTIVATIONS

Various nanostructured conductive polymers have been successfully synthesized and they have been applied for a wide range of applications. As a special class of nanostructured conductive polymers, CPGs with 3D network structure show advantageous features such as high conductivity, a porous structure for ion transport, and

large surface. However, the conventional method for synthesis of CPGs with templates usually results in limited conductivity. New methods need to be developed for the facile synthesis of CPGs with decent electrical properties. The synthetic strategies should also be tunable to further improve physical/chemical properties of CPGs.

With improved properties, CPGs need to be extended to wider applications. By proper modification and device design, CPGs could play an increasingly important role in the applications of energy storage devices such as supercapacitors and lithium ion batteries.

With hierarchically porous structure and high surface area, CPGs can act as the matrix for the introduction of second gel network, thus enabling the development of hybrid gel systems with interpenetrated network structure. Hybrid gel systems could bring additional new features, such as stimuli-responsive property, self-healing property, and enhanced biocompatibility, thus opening the door to new functional energy devices such as self-healing and/or responsive energy devices. Thus it is worthy to study the synthesis and applications of hybrid gel materials based on CPGs.

1.5 REFERENCES

1. A. G. Macdiarmid, J. C. Chiang, A. F. Richter and A. J. Epstein, *Synthetic Metals*, 1987, **18**, 285-290.
2. R. Gangopadhyay and A. De, *Chemistry of Materials*, 2000, **12**, 608-622.
3. G. Wegner, *Angewandte Chemie International Edition in English*, 1981, **20**, 361-381.
4. S. Sadki, P. Schottland, N. Brodie and G. Sabouraud, *Chemical Society Reviews*, 2000, **29**, 283-293.
5. Z. Yin and Q. Zheng, *Advanced Energy Materials*, 2012, **2**, 179-218.
6. G. Giri, E. Verploegen, S. C. B. Mannsfeld, S. Atahan-Evrenk, D. H. Kim, S. Y. Lee, H. A. Becerril, A. Aspuru-Guzik, M. F. Toney and Z. Bao, *Nature*, 2011, **480**, 504-508.
7. A. J. Heeger, *Angewandte Chemie International Edition*, 2001, **40**, 2591-2611.

8. K. Lee, S. Cho, S. Heum Park, A. J. Heeger, C.-W. Lee and S.-H. Lee, *Nature*, 2006, **441**, 65-68.

9. D. Li, J. Huang and R. B. Kaner, *Accounts of Chemical Research*, 2009, **42**, 135-145.

10. C. Li, H. Bai and G. Shi, *Chemical Society Reviews*, 2009, **38**, 2397-2409.

11. Y. Shi, L. Peng, Y. Ding, Y. Zhao and G. Yu, *Chemical Society Reviews*, 2015, **44**, 6684-6696.

12. R. K. Joshi and J. J. Schneider, *Chemical Society Reviews*, 2012, **41**, 5285-5312.

13. H. D. Tran, K. Shin, W. G. Hong, J. M. D'Arcy, R. W. Kojima, B. H. Weiller and R. B. Kaner, *Macromolecular Rapid Communications*, 2007, **28**, 2289-2293.

14. L. Qu, G. Shi, F. e. Chen and J. Zhang, *Macromolecules*, 2003, **36**, 1063-1067.

15. L. Pan, H. Qiu, C. Dou, Y. Li, L. Pu, J. Xu and Y. Shi, *International Journal of Molecular Sciences*, 2010, **11**, 2636.

16. Y.-Z. Long, M.-M. Li, C. Gu, M. Wan, J.-L. Duvail, Z. Liu and Z. Fan, *Progress in Polymer Science*, 2011, **36**, 1415-1442.

17. L. J. Pan, L. Pu, Y. Shi, S. Y. Song, Z. Xu, R. Zhang and Y. D. Zheng, *Advanced Materials*, 2007, **19**, 461-464.

18. X. Zhang and S. K. Manohar, *Journal of the American Chemical Society*, 2004, **126**, 12714-12715.

19. X. Zhang, J. Zhang, Z. Liu and C. Robinson, *Chemical Communications*, 2004, 1852-1853.

20. J. Jang and H. Yoon, *Chemical Communications*, 2003, 720-721.

21. L. Xia, Z. Wei and M. Wan, *Journal of Colloid and Interface Science*, 2010, **341**, 1-11.

22. S. J. Killoran and R. D. O'Neill, *Electrochimica Acta*, 2008, **53**, 7303-7312.

23. D. Xie, Y. Jiang, W. Pan, D. Li, Z. Wu and Y. Li, *Sensors and Actuators B: Chemical*, 2002, **81**, 158-164.

24. C. Liu, H. Ohta, T. Kuwahara and M. Shimomura, *European Polymer Journal*, 2008, **44**, 1114-1122.

25. S. Han, A. L. Briseno, X. Shi, D. A. Mah and F. Zhou, *The Journal of Physical Chemistry B*, 2002, **106**, 6465-6472.

26. G. Lu, C. Li and G. Shi, *Polymer*, 2006, **47**, 1778-1784.

27. J. Zang, C. M. Li, S.-J. Bao, X. Cui, Q. Bao and C. Q. Sun, *Macromolecules*, 2008, **41**, 7053-7057.

28. J. M. Pringle, M. Forsyth, G. G. Wallace and D. R. MacFarlane, *Macromolecules*, 2006, **39**, 7193-7195.

29. X. Lu, W. Zhang, C. Wang, T.-C. Wen and Y. Wei, *Progress in Polymer Science*, 2011, **36**, 671-712.

30. Y. Liao, C. Zhang, Y. Zhang, V. Strong, J. Tang, X.-G. Li, K. Kalantar-zadeh, E. M. V. Hoek, K. L. Wang and R. B. Kaner, *Nano Letters*, 2011, **11**, 954-959.

31. J. Zhang, J. Jiang, H. Li and X. S. Zhao, *Energy & Environmental Science*, 2011, **4**, 4009-4015.

32. Z. Gui, J. Duay, J. Hu and S. B. Lee, *Physical Chemistry Chemical Physics*, 2014, **16**, 12332-12340.

33. X. Xia, D. Chao, X. Qi, Q. Xiong, Y. Zhang, J. Tu, H. Zhang and H. J. Fan, *Nano Letters*, 2013.

34. Y. Hou, Y. Cheng, T. Hobson and J. Liu, *Nano Letters*, 2010, **10**, 2727-2733.

35. H. Zhang, X. Yu and P. V. Braun, *Nat Nano*, 2011, **6**, 277-281.

36. G. Yu, X. Xie, L. Pan, Z. Bao and Y. Cui, *Nano Energy*, 2013, **2**, 213-234.

37. J. Huang and R. B. Kaner, *Journal of the American Chemical Society*, 2003, **126**, 851-855.

38. D. P. Dubal, S. H. Lee, J. G. Kim, W. B. Kim and C. D. Lokhande, *Journal of Materials Chemistry*, 2012, **22**, 3044-3052.

39. J. Xu, K. Wang, S.-Z. Zu, B.-H. Han and Z. Wei, *ACS Nano*, 2010, **4**, 5019-5026.

40. Q. Wu, Y. Xu, Z. Yao, A. Liu and G. Shi, *ACS Nano*, 2010, **4**, 1963-1970.

41. G. Wang, L. Zhang and J. Zhang, *Chemical Society Reviews*, 2012, **41**, 797-828.

42. R. Liu and S. B. Lee, *Journal of the American Chemical Society*, 2008, **130**, 2942-2943.

43. C. Zhou, Y. Zhang, Y. Li and J. Liu, *Nano Letters*, 2013, **13**, 2078-2085.

44. P. Novák, K. Müller, K. S. V. Santhanam and O. Haas, *Chemical Reviews*, 1997, **97**, 207-282.

45. F. Cheng, W. Tang, C. Li, J. Chen, H. Liu, P. Shen and S. Dou, *Chemistry – A European Journal*, 2006, **12**, 3082-3088.

46. M. Zhou, J. Qian, X. Ai and H. Yang, *Advanced Materials*, 2011, **23**, 4913-4917.

47. K. S. Park, S. B. Schougaard and J. B. Goodenough, *Advanced Materials*, 2007, **19**, 848-851.

48. M. N. Hyder, R. Kavian, Z. Sultana, K. Saetia, P.-Y. Chen, S. W. Lee, Y. Shao-Horn and P. T. Hammond, *Chemistry of Materials*, 2014, **26**, 5310-5318.

49. D. Lepage, C. Michot, G. Liang, M. Gauthier and S. B. Schougaard, *Angewandte Chemie International Edition*, 2011, **50**, 6884-6887.

50. M. Wu, X. Xiao, N. Vukmirovic, S. Xun, P. K. Das, X. Song, P. Olalde-Velasco, D. Wang, A. Z. Weber, L.-W. Wang, V. S. Battaglia, W. Yang and G. Liu, *Journal of the American Chemical Society*, 2013, **135**, 12048-12056.

51. G. Liu, S. Xun, N. Vukmirovic, X. Song, P. Olalde-Velasco, H. Zheng, V. S. Battaglia, L. Wang and W. Yang, *Advanced Materials*, 2011, **23**, 4679-4683.

52. K. Deligkaris, T. S. Tadele, W. Olthuis and A. van den Berg, *Sensors and Actuators B: Chemical*, 2010, **147**, 765-774.

53. R. Chakrabarty, P. S. Mukherjee and P. J. Stang, *Chemical Reviews*, 2011, **111**, 6810-6918.

54. N. A. Peppas, J. Z. Hilt, A. Khademhosseini and R. Langer, *Advanced Materials*, 2006, **18**, 1345-1360.

55. Q. Zhang, E. Uchaker, S. L. Candelaria and G. Cao, *Chemical Society Reviews*, 2013, **42**, 3127-3171.

56. L. Pan, G. Yu, D. Zhai, H. R. Lee, W. Zhao, N. Liu, H. Wang, B. C.-K. Tee, Y. Shi, Y. Cui and Z. Bao, *Proceedings of the National Academy of Sciences*, 2012, **109**, 9287-9292.

57. C. R. Martin, *Accounts of Chemical Research*, 1995, **28**, 61-68.

58. L. Li, Y. Shi, L. Pan, Y. Shi and G. Yu, *Journal of Materials Chemistry B*, 2015, **3**, 2920-2930.

59. Y. Zhao, B. Liu, L. Pan and G. Yu, *Energy & Environmental Science*, 2013.

60. S. Brahim, D. Narinesingh and A. Guiseppi-Elie, *Biomacromolecules*, 2003, **4**, 497-503.

Chapter 2 Controlled synthesis of conductive polymer gels using dopants as crosslinking molecules*

2.1 INTRODUCTION

Due to their unusual physical/chemical properties associated with confined dimensions, nanostructured materials become critically important in a wide range of applications from renewable energy, electronics, to medical and life science,.[1-3] It is promising to address critical challenges in fields of energy and electronic technologies by these materials, owing to their advantageous features, such as high electrode/electrolyte contact area, shortened pathways for charge/mass transport, and better accommodation of the strain within electrodes. Gels with highly crosslinked networks stand out from various nanostructured materials because of their 3D structures at both microscale and nanometer levels. Gels exhibit mechanical properties ranging from soft and weak to hard and tough, owing to their unique composition with a large quantity of liquid dispersed within a solid.[4] The crosslinking structure and swelling nature endow gels a highly porous microstructure, high surface area, good compatibility with bio- or other hydrophilic molecules, and tunable mechanical property, thus making them an ideal material for diverse applications in energy, electronics, and medical/life science.[5, 6]

As a special class of conductive polymer materials, conducting polymer gels synergize the advantages of hydrogels and organic conductors.[7] CPGs with 3D network structures provide an electrically conductive yet mechanically robust framework: charge transportation is promoted by the continuous conductive backbones, the diffusion of ions

* Y. Shi, L. Pan, B. Liu, Y. Wang, Y. Cui, Z. Bao, G. Yu, Nanostructured conductive polypyrrole hydrogels as high-performance, flexible supercapacitor electrodes, *J. Mater. Chem. A*, 2014, 2, 6086.
Y. Wang, Y. Shi, L. Pan, Y. Ding, Y. Zhao, Y. Li, Y. Shi and G. Yu, Dopant-Enabled Supramolecular Approach for Controlled Synthesis of Nanostructured Conductive Polymer Hydrogels, *Nano Lett.*, 2015, 15, 7736.
Y. S. carried out the experimental work and participated in the preparation of manuscript.

and molecules is facilitated by the porous structure, and effective interface between molecular chains and solution phase is increased by the swelling nature. Compared with their bulk form, CPGs also exhibit other unique properties such as improved mechanical properties due to effective accommodation of the strain, light weight and good processability.[8, 9] As a result, CPGs have been explored for various applications such as energy conversion and storage, sensors, actuators, medical and bio-devices, and superhydrophobic coatings.

Recently, a novel method for the synthesis of CPGs has been developed in which dopants are adopted as crosslinking molecules.[5] Other than conventional methods which usually use a non-conductive template for CPG synthesis, the dopant molecules crosslinked CPGs show advantages such as facile synthesis, high conductivity, and low cost. The chemical and physical properties of dopant molecules crosslinked CPGs can be facilely tuned by changing the dopants during polymerization. In addition, the structure and properties of CPGs can further be tuned by controlling the synthetic conditions.

In this chapter, the controlled synthesis of CPGs using doping molecules as crosslinkers is discussed. PPy gel with an interconnected fiber structure is synthesized using CuTcPs as the crosslinker owing to the supramolecular aligning effect.[10] The crosslinked nanofibers structure greatly improves the electrical and electrochemical properties of resulting CPGs through nanoconfinement effect. In addition, the structure and properties of CPGs can further be tuned by controlling the synthetic conditions such as solvents, precursor ratio, temperature, etc. An interfacial synthesis is developed to generate an interconnected hollow-sphere microstructure of PPy gel.[11] By using different organic solvents and varying the ratio of polymer monomers to crosslinkers, the microstructures and resulted properties of PPy gels can be further adjusted.

2.2 GENERAL SYNTHESIS AND PROPERTIES OF DOPANTS CROSSLINKED CONDUCTIVE POLYMER GELS

Recently, a novel synthetic route for conductive polymer gels which exhibit facile processability, excellent electronic property, high electrochemical activity and high biocompatibility has been developed.[5, 12] Phytic acid is adopted as the gelator and dopant in the synthetic process and conductive gel networks could be directly formed (Figure 1). PANI gel is firstly synthesized via this method. In a typical synthesis, two precursor solutions containing monomers, dopant molecules, and oxidative initiator, respectively, are mixed together and the gelation is typically completed within several minutes. The gelation mechanism of the CPG could be explained by the ability of each phytic acid molecule to interact with more than one conductive polymer chain. The gelation can be induced in a wide range of molar ratios of monomer to phytic acid, and with diverse oxidative initiators such as APS and hydrogen peroxide.

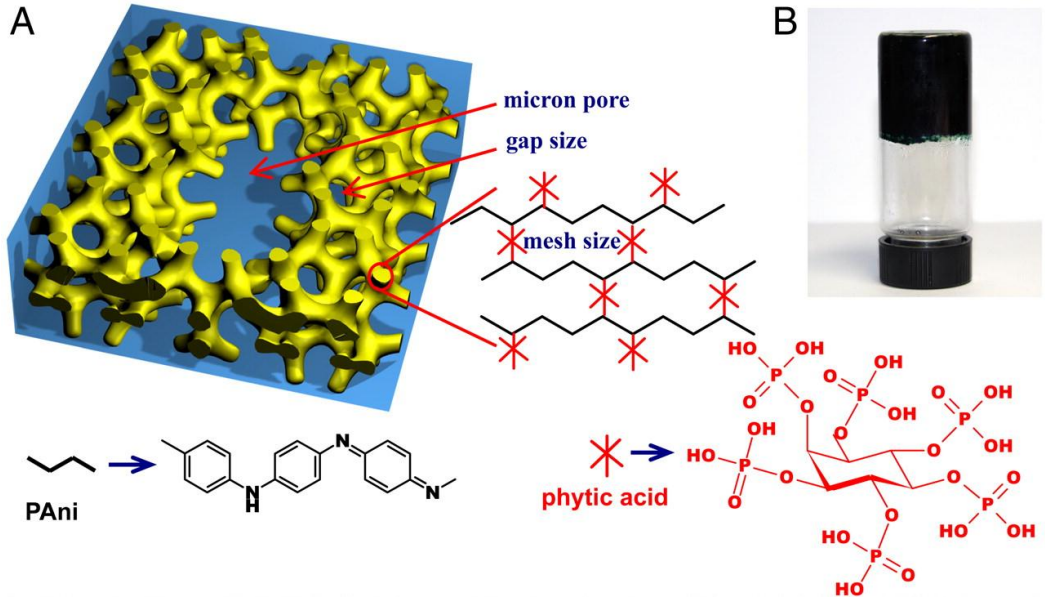

Figure 2.1 PANI gel with 3D nanostructure was synthesized by using phytic acid as the gelator and dopant.

The SEM and TEM images of as-synthesized PANI gel show that the dehydrated PANI gels are constructed with coral-like dendritic nanofibers with uniform diameters of 60–100 nm (Figure 2) while the fully swollen PANI gels are demonstrated to consist of nanofibers about 200–300 nm in diameter, showing their high level of hydration. In addition, the phytic acid renders CPGs improved hydrophilicity owing to an excess of phosphorous groups. The swelling nature and hydrophilic property of CPGs may provide additional interface areas between polymer chains and solution phase to support more active reaction sites and anchoring sites for active molecules or particles. The framework of the as-prepared CPG is free of insulating polymers, thus providing an ideal 3D interconnected path for electron transport. The obtained PANI hydrogel reaches a conductivity of 0.11 S cm^{-1} at room temperature, which is the highest reported value for conducting polymer hydrogels. A highly porous 3D nanostructure with two levels of pores (the first level is the pores between the branched nanofibers and the second level was the bigger micron size pores) can be achieved on a large-scale and with long-term stability in this synthesis. Such 3D porous structures offer large open channels on the microscale and mesoscale pores which facilitate the diffusion of ions and molecules and also provide large specific surface area. Moreover, the synthetic route needs no external ingredients such as surfactants or templates, thus greatly enhancing its processability and universality.

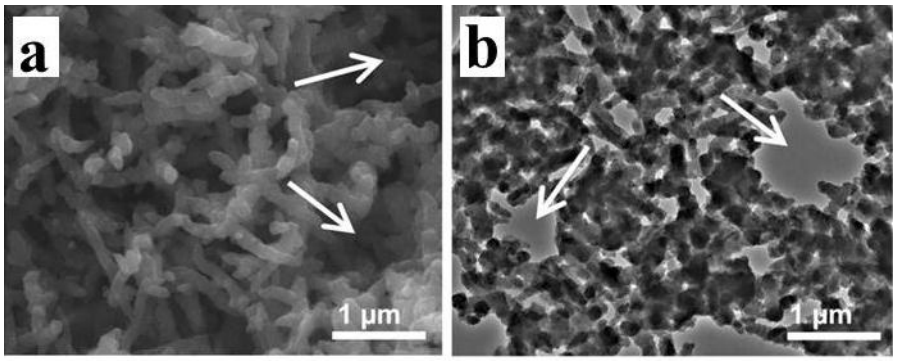

Figure 2.2 SEM (a) and TEM (b) image of PANI gel crosslinked by phytic acid.

In terms of processing properties, CPGs synthesized with novel method exhibit advantageous features when compared to conventional gel materials owing to the unique synthetic methods for CPGs in which two precursor solutions are used. Unlike conventional polymeric materials which usually possess high viscosity in solution or melting states, CPGs can be processed by scalable techniques such as ink-jet printing or spray coating because two precursor solutions could be separately deposited onto the substrate and gels will form in the area that both solutions overlapped, thus avoiding the block of inkjet nozzle by gelation and high viscosity of conventional gel materials. With the appealing processing properties, CPGs can be employed to fabricate desired micropatterns for large arrays of devices.

This dopant enabled crosslinking method provides great potential to be extended to other conductive polymers and to further modify the physical/chemical properties of resulted CPGs.

2.3 CONTROLLED SYNTHESIS OF CONDUCTIVE POLYMER GELS THROUGH DOPANT-ENABLED SUPRAMOLECULAR APPROACH

The PANI gel synthesized by using phytic acid as both crosslinker and dopant shows improved conductive property and processing ability. However, when phytic acid

is used to crosslink PPy chains, although PPy gel can be obtained, the conductivity still remains low. This result can be attributed to two aspects. Firstly, PANI intrinsically favors its growth into fiber-like structures[13] while PPy tends to grow into nanoparticles due to preferred formation of branched and cross-linked chains.[14] These branched chains lead to intermolecular electron transport, which harms the conductivity of conductive polymers. Secondly, phytic acid itself is an insulating molecule,[5] which decreases the conductivity of resulted conductive polymer gels. Thus new crosslinking molecules are needed to control the nanostructure of PPy gel and improve its conductivity. And applications involving the structure-related properties of nanostructured materials call for a scalable and effective method for morphologically tunable synthesis.

Functional nanomaterials via noncovalent interactions can be designed through supramolecular self-assembly.[15-17] A novel supramolecular strategy was presented in this chapter to prepare morphology-controlled nanostructured conductive gels (with PPy as a model material) using a dopant molecule of copper phthalocyanine-3,4′,4″,4‴-tetrasulfonic acid tetrasodium salt (CuPcTs), which is a disc-shaped liquid crystal. The CuPcTs acts as both the dopant and crosslinker, enabling the supramolecular self-assembly of PPy into nanostructured gels through electrostatic interaction and hydrogen bonding between the tetra-functional CuPcTs and PPy chain, as well as, a self-sorting mechanism caused by the planar structure of CuPcTs molecules. As a result, the PPy chains are aligned to form 1D nanostructures, as shown in Figure 3. This approach can in situ generate hierarchically interconnected nanofiber monolithic, which is distinct from other syntheses of conducting polymer nanofibers.

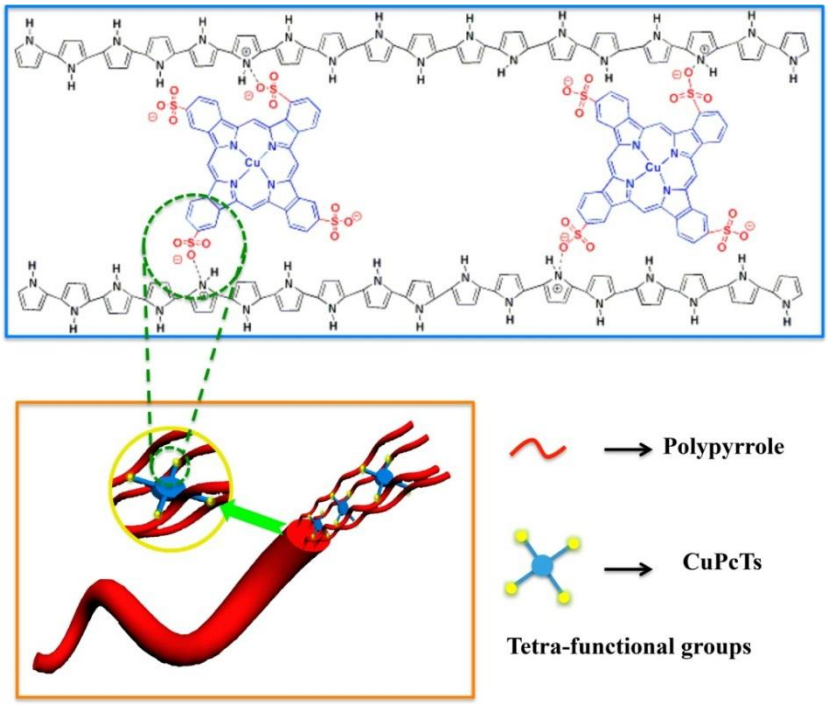

Figure 2.3 Illustration depicting controlled synthesis of the CuPcTs doped PPy hydrogel. The CuPcTs act as both the cross-linker and protonic dopant for the PPy hydrogel and align the PPy chains into ordered nanostructure through a steric effect. Note that the special disc-shaped structure and the tetra-sulfonic acid functional groups enabled the CuPcTs for a supramolecular self-sorting mechanism that align the PPy chains to form 1D nanostructured PPy.

In a typical synthesis, two precursor solutions were prepared and mixed: a pyrrole solution in isopropanol, and an aqueous solution of an oxidative initiator and CuPcTs. As the reaction progressed, the color of the solution changed from blue (the color of the CuPcTs) to black (the color of PPy) within a few seconds. The mixed solution gelated to form a hydrogel and lost its fluidic properties in approximately 2 min. The PPy gel was then rinsed with deionized (DI) water to remove residual ions and oligomers.

SEM was used to observe the morphology of the PPy gels. They possess interconnected nanofibers with a diameter of ~60 nm rather than agglomerated bundles (Figure 4a). Compared to agglomerated nanoparticles, this structure with interconnected nanofibers offers a greater effective surface area and porosity and may facilitate the transport of electrons and ions. In contrast, the control sample synthesized without CuPcTs consisted of only granular particles (Figure 4f). The role of CuPcTs in supramolecular assembly of PPy nanofibers is firstly demonstrated by the control experiment in which the concentration of CuPcTs is tuned. When CuPcTs concentration decreases, the diameter of the PPy nanofibers increases to approximately 400−500 nm and some granular particles appeared on the nanofiber surface with 0.45 mM of the CuPcTs solution. This reveals that the counterion of CuPcTs strongly affects on the supramolecular self-assembly and morphologic tuning of PPy (the concentration of CuPcTs in the PPy gels was proportional to the concentration of the CuPcTs in the precursor solution). The rigid disc-shape and the sulfonic acid functional groups of the CuPcTs align the PPy chains to form 1D nanostructure through supramolecular self-sorting. Moreover, the formation of side chains and cross-linked structures between the PPy main chains in pristine PPy hinders the 1D growth of PPy, leading to a granular morphology.[18] Notably, the relatively large size of the disc-shaped CuPcTs may sterically hinder the formation of these cross-linked structures and enhance the 1D growth of PPy.

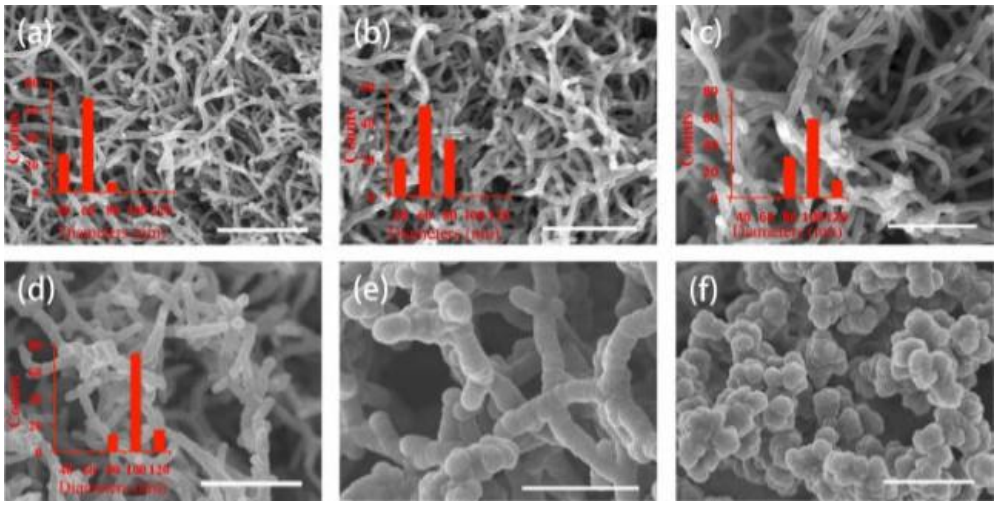

Figure 2.4 SEM images of nanostructured PPy hydrogels with various morphologies prepared by chemical oxidative polymerization with different concentrations of CuPcTs dopant: (a) 0.015 M CuPcTs; the CuPcTs concentration in (b − f) is 1/2, 1/4, 1/8, 1/16, and none that of sample (a), respectively. Scale bar: 1 μ m.

To further confirm the role of the CuPcTs molecule on the supramolecular self-assembly of the PPy gels, we used indigo carmine and indigo carmine dehydrate which have molecular structures similar to a half and a quarter of CuPcTs molecule, respectively as the control dopants (Figure 5). As shown in Figure 4, different dopants lead to morphology change from 1D nanofibers, to a nanoparticle necklace (quasi-1D), to granular particles. The disc-shaped CuPcTs enables the PPy gel with a smooth nanofiber morphology while the binary-functional sulfonic acid group of indigo carmine results in the PPy gel consisted of agglomerated bundles of nanofibers with particles present on the surface of the nanofibers. This indicates that the binary-functional sulfonic acid group shows a less effective steric effect on the alignment of PPy chains to form 1D nanostructure. The isatin-5-sulfonic acid sodium salt leads to a granular nanostructure of PPy with a morphology similar to that of the PPy synthesized without dopants. This

implies that the single sulfonic acid group molecule is not effective enough to enable supramolecular self-assembly.

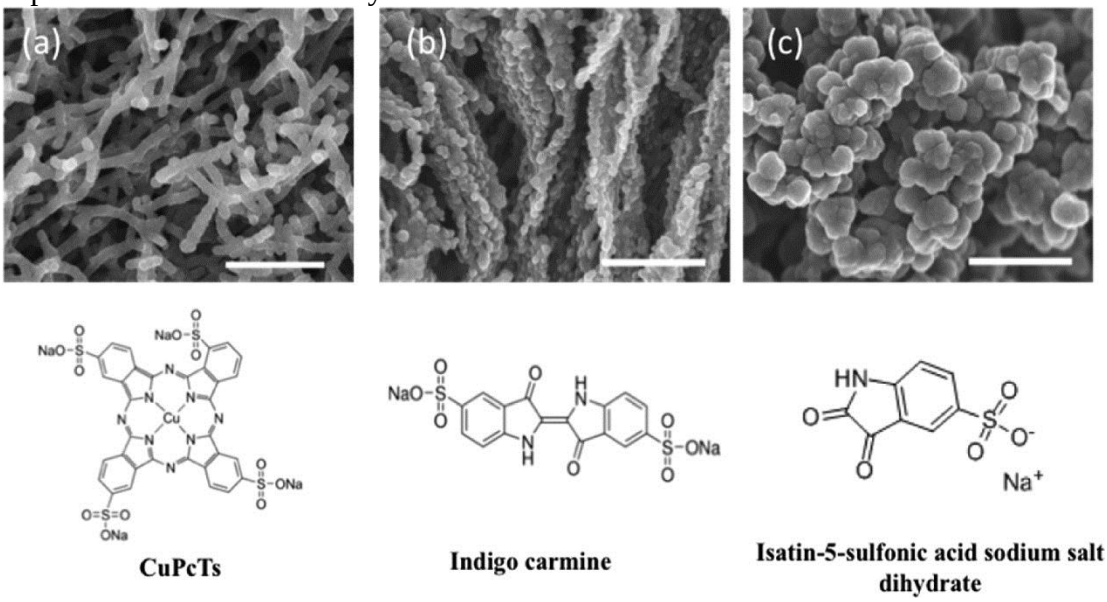

Figure 2.5 SEM images of different nanostructured PPy hydrogels with various dopants: (a) CuPcTs as a dopant, (b) indigo carmine as a dopant, and (c) isatin-5-sulfonic acid sodium salt dehydrate as a dopant. Scale bar: 1 μ m. The morphology of the as-synthesized PPy hydrogels changed from 1D nanofibers, a nanoparticle necklace (quasi-1D), to granular particles in the presence of different dopant molecules, corresponding to the change of steric effect from strong to weak between the dopants and PPy chains, respectively.

The chemical structure of resulted PPy gel was investigated by the Fourier transform infrared (FTIR) spectra, as shown in Figure 6a. The absorption peak at 1548 cm^{-1} and 1472 cm^{-1} can be assigned to the in-plane bending of C=N bonds and the stretching vibrations of C=C bonds, respectively.[19] The peak around 1340 cm^{-1} (D-band) is related to the ring stretching mode, while the 1592 cm^{-1} (G-band) is due to the C=C backbone stretching of PPy.[20] The peak at 1297 cm^{-1} was attributed to the C−C stretching and the characteristic peak at 1042 cm^{-1} is due to in-plane deformation of the C−H bond and N−H bond. The peak at 1174 and 903 cm^{-1} can be attributed to the stretching

vibrations of C−N^+ bonds and C=N^+−C bonds, respectively. The absorption of these two peaks of CuPcTs crosslinked PPy has a blue shift in contrast to that of the PPy without doping, indicating the doping states of PPy−CuPcTs.

The aggregation states of polymer chains in the pristine PPy and CuPcTs doped PPy were investigated by the X-ray diffraction (XRD) (Figure 6b). A characteristic broad peak of PPy centered at approximately 22.8 °, and the high angle asymmetric scattering peak of PPy−CuPcTs from 20 to 30° implies the orientation of polymer along the molecular chain direction.[21] This peak of PPy−CuPcTs could be deconvoluted to two separate peaks situated at ~22 ° and 27 °, corresponding to d-spacing of 0.404 and 0.330 nm which can be attributed to the π−π stacking between polypyrrole units and the interplanar distance of pyrrole−counterions, respectively.[22] The CuPcTs reorganized in the PPy matrix which can be demonstrated by the disappearance of the peak at 10.7 °. Moreover, a peak at ~0.8° shows up for PPy−CuPcTs only, indicating the long-range ordering structure of PPy−CuPcTs.

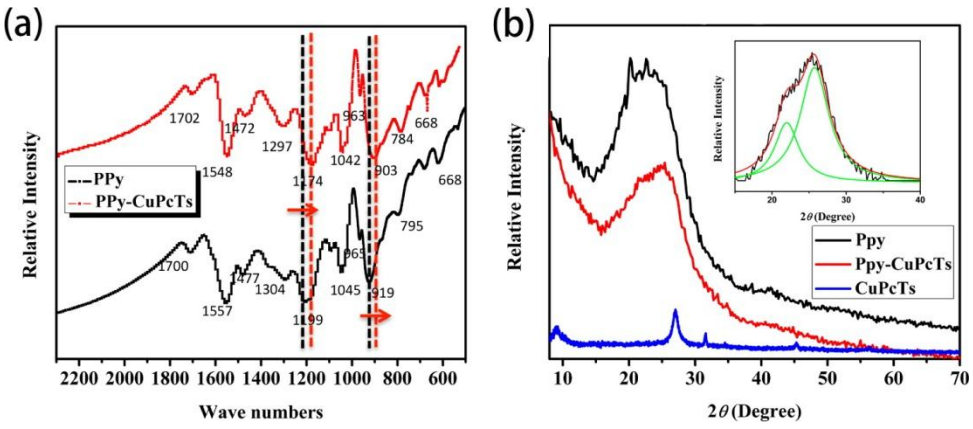

Figure 2.6 (a) FTIR spectra of CuPcTs-doped PPy nanofiber sample (PP −CuPcTs) and granular PPy sample (PPy). (b) XRD of CuPcTs-doped PPy nanofiber sample (PPy−CuPcTs), granular PPy (PPy) sample, and CuPcTs-only sample (inset, deconvoluted XRD of PPy−CuPcTs sample).

The supramolecular self-assembled PPy gel shows much improved electrical conductivity owing to the improved ordering of polymer chains. The conductivities of different samples measured by the four-probe method are summarized in Table 1. The conductivities of CuPcTs−PPy, indigo carmine−PPy, isatin-5-sulfonic acid sodium salt dehydrate−PPy, and pristine PPy were measured to be 7.8, 0.4, 0.06, and 0.07 S cm^{-1}, respectively. These samples were synthesized in solutions with similar pH values. The results confirmed that the CuPcTs dopant molecule favors for the enhancement of directional charge transport among conducting polymer chains.[23]

Samples	Conductivity (S cm^{-1})
CuPcTs−PPy	7.8
indigo carmine−PPy	0.4
isatin-5-sulfonic acid sodium salt dehydrate−PPy	0.06
pristine PPy	0.07

Table 2.1 Measured Conductivities of Different PPy Samples with Different Dopants

2.4 INTERFACIAL SYNTHESIS OF CONDUCTIVE POLYMER GELS WITH STRUCTURE-DERIVED ELASTICITY

CPGs provide intrinsic conducting frameworks that promote the transport of charges, ions, and molecules and the ideal interface between electronic-transporting and ionic-transporting phases, between biological and synthetic systems, as well as between soft and hard materials, thus becoming an ideal candidate for energy storage, molecular and bioelectronics and medical electrodes. However, traditional conductive polymers show poor elasticity due to their rigid backbones caused by the highly conjugated ring structure. CPGs with decent mechanical strength and flexibility are critically important

for development of flexible, lightweight and efficient energy storage and electronic devices.[24-26]

The mechanical properties of CPGs can be improved by controlling their microstructures. With spherical shell geometry, inherently stiff and brittle CPGs can exhibit effective elastic modulus that is capable of withstanding large effective strains and stresses.[27] To realize the spherical shell geometry, a synthetic approach called 'interfacial synthesis' is developed for the synthesis of CPGs (Figure 7a),[28] in which two precursor solutions which are aqueous solution of oxidative reagent and organic solution containing a mixture of the conductive polymer monomer, organic solvent, and phytic acid are prepared and mixed together. The monomers would polymerize at the interface, resulting in hollow sphere microstructures, which are further interconnected by the crosslinker.

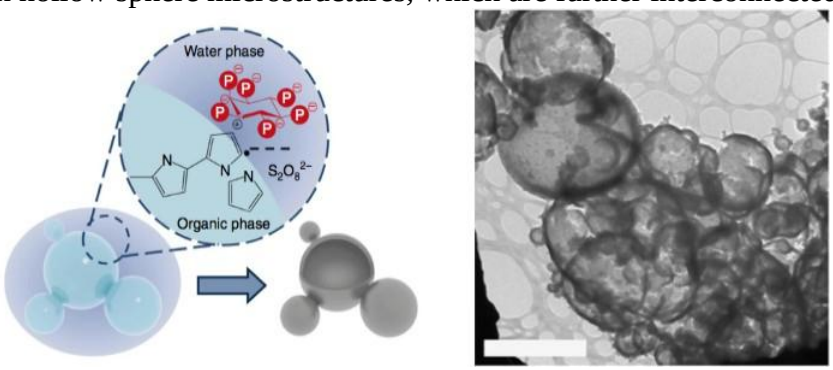

Figure 2.7 Illustration of interfacial synthesis and the microstructure of resulted PPy gel.

The PPy gel was successfully synthesized by this liquid phase interfacial reaction, exhibiting hollow sphere structure. In a typical synthesis, solution A was prepared by dissolving 1.2 mmol of ammonium persulfate in 0.5 mL deionized (DI) water. Solution B was prepared by mixing 0.084 mL pyrrole into 0.5 mL isopropanol alcohol (IPA), followed by the addition of 0.184 mL phytic acid. After gentle shaking, solution B will become an ivory-white mixture. The solutions were rapidly cooled to roughly 0 ℃ using

dry ice to slow down the rate of reaction. Right after mixing A and B solutions, the gelation occurs within seconds, and black PPy gel can be obtained.

The FTIR spectra (Figure 8a) provide information on the chemical structure of the as-synthesized PPy gel. The absorption peak at 1552.4 cm^{-1} and the band at 1397.4 cm^{-1} can be assigned to the in-ring stretching of C=C bonds in the pyrrole rings and the vibrations of C–H bonds, respectively. The peaks at 1296.2 cm^{-1} and 1045.1 cm^{-1} could be attributed to the C-C stretching and the in-plane deformation of C-H bond and N-H bond, respectively. The formation of PPy could be confirmed by these characteristic absorption peaks.[29] SEM and TEM images (Figure 8b) show the microstructure of PPy gel. The 3D porous morphology of PPy gel with foam-like microstructure constructed by interconnected hollow spheres with diameters in the range of 500 nm to 3 μm can be observed in SEM images. The shell thickness of PPy hollow spheres is of 50~100 nm, as revealed in TEM image (Figure 8c). The structure of interconnected hollow spheres is caused by the crosslinking effects from phytic acid and bi-phase synthesis. The large open channels between the branches and nanoscale porosities formed within hierarchical structure facilitate the transport of electrons and ions. More importantly, the hollow sphere structure endows PPy gel excellent elasticity and mechanical strength as shown in the inset photo in Figure 8a, making it being able to withstand 100 g weight. The formation of spherical shell geometry with a structural hierarchy could overcome the inherent brittleness of PPy caused by its rigid polymer backbone since the PPy with hollow sphere structure can elastically deform and recover upon the application and release of external pressure, thus showing tunable effective elasticity.

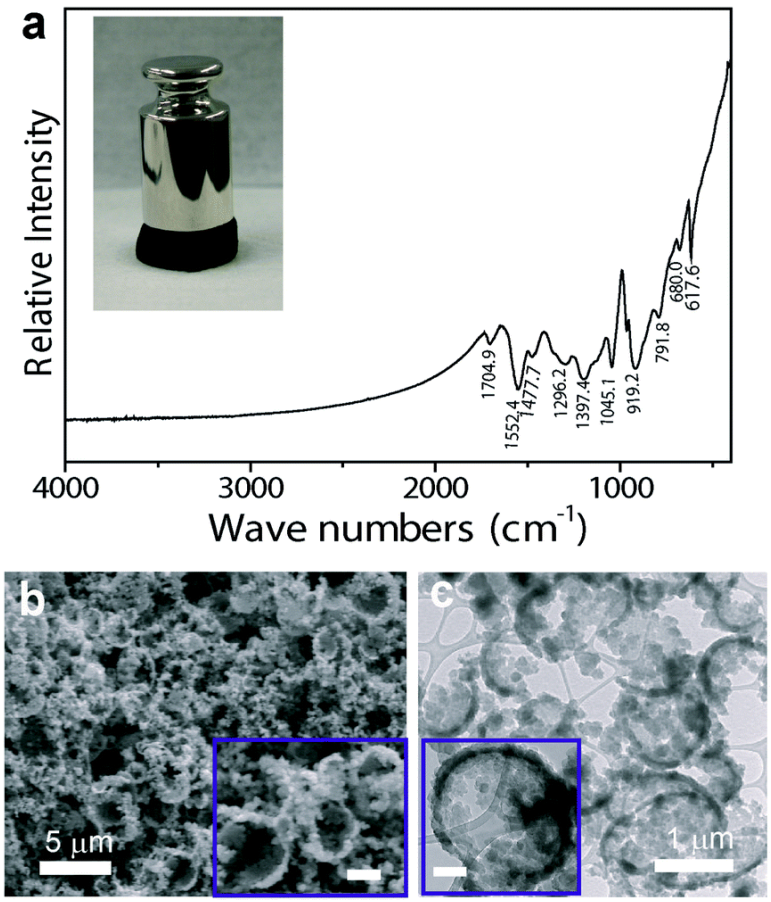

Figure 2.8 Interconnected hollow sphere conducting PPy hydrogel. (a) The FT-IR spectrum of the as-synthesized conductive polypyrrole (PPy) hydrogel with peaks labeled. Inset, a photograph showing a spongy PPy hydrogel sample placed under a balance weight of 100 g. (b) SEM image showing the microstructure of a piece of the dehydrated hydrogel. Inset scale bar: 1 μm. (c) TEM image showing the top view. Inset, TEM image of the dehydrated PPy hydrogel. Inset scale bar: 200 nm.

The size and size distribution of hollow spheres in the PPy gel can be further tuned by using different solvents. Figure 9 shows that using IPA as the organic solvent to prepare precursor solution B, the PPy gel possesses large size hollow sphere with diameter around 3600 nm. When butanol is used as the solvent, the size of the hollow spheres decreased significantly to around 1300 nm. This is due to miscibility between

water and organic solvents. Better miscibility leads to smaller liquid drops and thus enables the smaller size of PPy hollow spheres.

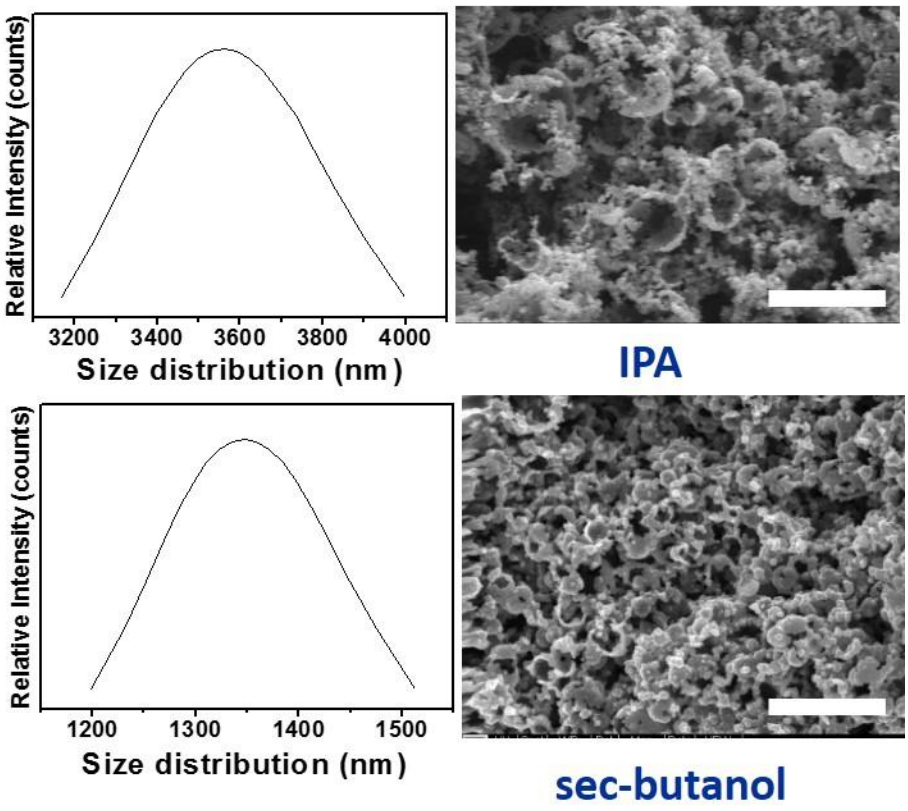

Figure 2.9 Size distribution of hollow spheres and their SEM images in PPy gels synthesized with different organic solvents. The scale bar is 1 μm.

2.5 CONCLUSIONS

In summary, 3D nanostructured CPGs have been successfully synthesized by using dopant molecules as crosslinkers. These dopants have several functional groups on each of the molecule, which can react with conductive polymeric chains, thus crosslinking them into a 3D network structure. This dopant enabled crosslinking method provides great tunability in terms of microstructures and resulted physical/chemical properties by tuning dopants and synthetic conditions during polymerization.

Supramolecular self-assembled PPy gels are synthesized using CuPcTs as a new type of crosslinker. CuPcTs favors 1D alignment of PPy chains, thus leading to PPy gels with interconnected nanofibers. Owing to the improved ordering of polymeric chains, the conductivity of PPy gels is significantly improved. An interfacial synthetic approach is also adopted to improve the mechanical properties of conductive polymer gels. This novel method leads to PPy gels with interconnected hollow sphere structure, which endows the gels structure derived elasticity.

2.6 REFERENCES

1. A. S. Arico, P. Bruce, B. Scrosati, J.-M. Tarascon and W. van Schalkwijk, *Nat Mater*, 2005, **4**, 366-377.
2. R. K. Joshi and J. J. Schneider, *Chemical Society Reviews*, 2012, **41**, 5285-5312.
3. D. R. Rolison, J. W. Long, J. C. Lytle, A. E. Fischer, C. P. Rhodes, T. M. McEvoy, M. E. Bourg and A. M. Lubers, *Chemical Society Reviews*, 2009, **38**, 226-252.
4. N. Sahiner, *Progress in Polymer Science*, 2013, **38**, 1329-1356.
5. L. Pan, G. Yu, D. Zhai, H. R. Lee, W. Zhao, N. Liu, H. Wang, B. C.-K. Tee, Y. Shi, Y. Cui and Z. Bao, *Proceedings of the National Academy of Sciences*, 2012, **109**, 9287-9292.
6. J. Janata and M. Josowicz, *Nat Mater*, 2003, **2**, 19-24.
7. Y. Zhao, B. Liu, L. Pan and G. Yu, *Energy & Environmental Science*, 2013.
8. L. Xia, Z. Wei and M. Wan, *Journal of Colloid and Interface Science*, 2010, **341**, 1-11.
9. H. D. Tran, D. Li and R. B. Kaner, *Advanced Materials*, 2009, **21**, 1487-1499.
10. Y. Wang, Y. Shi, L. Pan, Y. Ding, Y. Zhao, Y. Li, Y. Shi and G. Yu, *Nano Letters*, 2015.
11. Y. Shi, L. Pan, B. Liu, Y. Wang, Y. Cui, Z. Bao and G. Yu, *Journal of Materials Chemistry A*, 2014, **2**, 6086-6091.
12. Y. Shi and G. Yu, *Chemistry of Materials*, 2016, **28**, 2466-2477.
13. J. Huang and R. B. Kaner, *Angewandte Chemie International Edition*, 2004, **43**, 5817-5821.
14. W. Zhang, Z. Pan, F. K. Yang and B. Zhao, *Advanced Functional Materials*, 2015, **10**, 1588-1597.

15. T. Aida, E. W. Meijer and S. I. Stupp, *Science*, 2012, **335**, 813-817.

16. S. I. Stupp, V. LeBonheur, K. Walker, L. S. Li, K. E. Huggins, M. Keser and A. Amstutz, *Science*, 1997, **276**, 384-389.

17. S. I. Stupp and L. C. Palmer, *Chemistry of Materials*, 2014, **26**, 507-518.

18. H. D. Tran, Y. Wang, J. M. D'Arcy and R. B. Kaner, *ACS Nano*, 2008, **2**, 1841-1848.

19. R. Buitrago-Sierra, M. J. Garcia-Fernandez, M. M. Pastor-Blas and A. Sepulveda-Escribano, *Green Chemistry*, 2013, **15**, 1981-1990.

20. S. P. Lim, A. Pandikumar, Y. S. Lim, N. M. Huang and H. N. Lim, *Scientific Reports*, 2014, **4**, 5305.

21. J.-G. Wang, B. Wei and F. Kang, *RSC Advances*, 2014, **4**, 199-202.

22. M.-K. Song, Y.-T. Kim, B.-S. Kim, J. Kim, K. Char and H.-W. Rhee, *Synthetic Metals*, 2004, **141**, 315-319.

23. M. Massi, C. Albonetti, M. Facchini, M. Cavallini and F. Biscarini, *Advanced Materials*, 2006, **18**, 2739-2742.

24. V. L. Pushparaj, M. M. Shaijumon, A. Kumar, S. Murugesan, L. Ci, R. Vajtai, R. J. Linhardt, O. Nalamasu and P. M. Ajayan, *Proceedings of the National Academy of Sciences*, 2007, **104**, 13574-13577.

25. M. Armand and J. M. Tarascon, *Nature*, 2008, **451**, 652-657.

26. T. Janoschka, M. D. Hager and U. S. Schubert, *Advanced Materials*, 2012, **24**, 6397-6409.

27. L. Pan, A. Chortos, G. Yu, Y. Wang, S. Isaacson, R. Allen, Y. Shi, R. Dauskardt and Z. Bao, *Nat Commun*, 2014, **5**, 3002.

28. J. M. Pringle, O. Ngamna, C. Lynam, G. G. Wallace, M. Forsyth and D. R. MacFarlane, *Macromolecules*, 2007, **40**, 2702-2711.

29. S. Konwer and S. K. Dolui, *Materials Chemistry and Physics*, 2010, **124**, 738-743.

Chapter 3 Electrochemical properties of dopants crosslinked conductive polymer gels and their applications in electrochemical energy storage devices*

3.1 INTRODUCTION

Supercapacitors and lithium ion batteries are key members of electrochemical energy storage systems and have been widely used in applications such as consumer electronics, electrical vehicles, and large industrial scale power sources.[1, 2] Supercapacitors utilize the near surface charge storage, thus showing high power density and exceptional cyclic performance. Compared to supercapacitors, the lithium-ion batteries show limitations on charge/discharge rate and cycle life since their charge/discharge processes rely on motions of lithium ions between the negative and positive electrode, as well as the chemical reactions between lithium ions and cathode/anode materials.[3, 4] However, the lithium ion batteries possess high energy density, high efficiency, and portability. Owing to the chemical, structural and electrical features of CPGs, they have been successfully applied for high-performance supercapacitor and lithium ion battery devices, as capacitor electrode material and bi-functional binder, respectively.

Conductive polymers have been studied for supercapacitors as pseudocapacitive materials which take advantage of fast and reversible electron exchange reactions at or

* Y. Shi, L. Pan, B. Liu, Y. Wang, Y. Cui, Z. Bao, G. Yu, Nanostructured conductive polypyrrole hydrogels as high-performance, flexible supercapacitor electrodes, *J. Mater. Chem. A*, 2014, 2, 6086.
Y. Wang, Y. Shi, L. Pan, Y. Ding, Y. Zhao, Y. Li, Y. Shi and G. Yu, Dopant-Enabled Supramolecular Approach for Controlled Synthesis of Nanostructured Conductive Polymer Hydrogels, *Nano Lett.*, 2015, 15, 7736.
Y. Shi, J. Zhang, A. Bruck, Y. Zhang, J. Li, E. Stach, K. Takeuchi, A. Marschilok, E. Takeuchi, G. Yu, A Tunable 3D Nanostructured Conductive Gel Framework Electrode for High-Performance Lithium Ion Batteries, *Adv. Mater.*, 2017, DOI: 10.1002/adma.201603922.
Y. Shi, X. Zhou, J. Zhang, A. Bruck, A. Bond, A. Marschilok, K. Takeuchi, E. Takeuchi, G. Yu, Nanostructured Conductive Polymer Gels to Improve Electrochemical Performance of Cathode Materials in Li-Ion Batteries, *Nano Lett.*, 2017, 17, 1906.
Y. S. carried out the experimental work and participated in the preparation of manuscript.

near the electrode surface.[5, 6] Although they show high pseudocapacitance and mechanical flexibility, these conjugated polymers suffer from poor cycle life and fast decayed capacitance in high rate cycling process, possibly due to high volume change and the change of doping states during electrochemical reactions. As mentioned in Chapter 1, building up nanostructured conductive polymer has been demonstrated to be a promising strategy to solve these problems and greatly improve the performance of supercapacitors.[7] CPGs represent a special 3D nanostructure of conductive polymers. The 3D network establishes a continuous network to promote the transport of electrons, provides short ion diffusion path and large surface area for redox reactions, and constructs a porous architecture with intrinsic elasticity to accommodate the volume change and facilitate the diffusion of electrolyte ions. Thus CPGs can be adopted as high-performance supercapacitor electrode materials. An example of PANI gel has been tested to demonstrate the advantageous features of CPGs used as supercapacitor electrode materials.[7] However, the electrochemical properties of CPGs as supercapacitor electrode material can be further improved due to the limited conductivity of CPGs crosslinked by non-conductive dopant molecules. The mechanical properties of CPGs need also to be improved to enable the fabrication of novel devices such as flexible and stretchable supercapacitors.

Beyond the application in supercapacitors, CPGs are promising to act as a binder in the electrode owing to their 3D network structure and highly conductive nature. In an ideal electrode, every active particle should be wired to the current collector and to the solid or liquid electrolyte to reach the entire volume of the battery and maximize energy use.[8] However, in traditional binder system, the conductive phases consisting of polymer and conductive additives are randomly distributed and thus may lead to bottlenecks and poor contacts that impede effective access to parts of the battery.[9, 10] Different from the

traditional binder system, the CPGs are intrinsically conductive and their networks can serve as electrically conductive pathways to interconnect each active particles and current collector. In addition, the porous structure can facilitate the ion diffusion from the electrolyte to active particles.

In this chapter, we firstly discuss the strategies to improve the electrochemical properties of CPGs by using novel crosslinkers such as CuPcTs to enhance the electronic conductivity of the gel framework[11] and by using interfacial synthesis to develop CPGs with structure derived elasticity for flexible supercapacitor.[12] Then we discuss the application of CPGs as bifunctional binder material for lithium-ion battery electrodes, acting as both polymeric binder and conductive additive.[13] This gel framework based electrode exhibits greatly improved the rate and cyclic performance because the highly conductive and hierarchically porous network of the hybrid gel framework promotes both electronic and ionic transport. In addition, both inorganic and organic components are uniformly distributed within the electrode since the polymer coating prevents active particles from aggregation, enabling full access to each particle. The robust framework further provides mechanical strength to support active electrode materials and improves the long-term electrochemical stability.

3.2 CPGS WITH IMPROVED ELECTROCHEMICAL PROPERTIES FOR HIGH-PERFORMANCE SUPERCAPACITOR

3.2.1 Supramolecular self-assembled PPy gels with improved conductivity for high-performance supercapacitor

The 3D nanostructured conductive polymers have also emerged as a promising class of electrochemical capacitor electrodes. They offer an array of features such as intrinsic 3D conductive frameworks that promote the transport of charges, ions, and molecules. An example is the 3D nanostructured PANI hydrogel which shows great

potential for high-performance electrochemical capacitors.[7] The conductive nature of PANI brings the PANI hydrogel based electrode very low electrical resistance. The 3D continuous nanostructured framework also favors fast ion transport during charging/discharging. The PANI hydrogel materials (dry weight) yield a specific capacitance of ~480 F g^{-1} at a current density of 0.2 A g^{-1}. In addition, the PANI hydrogel based electrodes exhibit promising rate performance with only ~7% capacitance loss when the current density was increased by a factor of 10, indicating an exceptional rate capability for high power performance. This is in sharp contrast to previously reported PANI-based electrodes, in which a typical 25–40% capacitance loss was seen at high power. Moreover, PANI hydrogel-based electrodes also exhibited good cycling stability, which is another key requirement in the operation of supercapacitors. The 3D nanostructures provide structure derived elasticity and highly porous interconnected nanostructures that can accommodate the swelling and shrinking of the polymer network during intensive cycling processes.

The electrochemical properties of CPGs can be further improved. As discussed in Chapter 1, a high-performance electrochemical electrode requires the simultaneous minimization of the four primary resistances present during charging and discharging: (1) ion transport in the electrolyte, (2) ion transport in the electrode, (3) electrochemical reactions in the electrode and (4) electron conduction in the electrode and current collector. CPGs synthesized with non-conductive crosslinking molecules such as phytic acid shows limited electrical conductivity, thus impeding the electron transport through the conductive gel matrix and to the current collector. The conductivity of CPGs can be improved through utilizing novel crosslinking molecules which provide intrinsic conductive property and modify the microstructure of CPGs.

As discussed in Chapter 2, PPy gels with supramolecular self-assembled

nanofiber structure have been synthesized by using CuPcTs as crosslinker and dopants.[11] The conductivity of resulted PPy gels is significantly improved to 7.8 S cm^{-1}, while pristine PPy only shows conductivity of 0.07 S cm^{-1} and PANI gel synthesized with phytic acid shows conductivity of 0.11 S cm^{-1}. As a result, the electrochemical performance of PPy gels when applied for supercapacitor electrode is also greatly improved.

The electrochemical properties of PPy gels crosslinked by CuPcTs molecules are firstly investigated with electrochemical impedance spectroscopy (EIS). Figure 1a shows impedance curves measured in a 1 M H_2SO_4 electrolyte for electrodes based on CuPcTs-doped PPy gel and pristine PPy. The CuPcTs−PPy gel shows substantially smaller impedance than pristine PPy which is demonstrated by equivalent series resistance (ESR) extracted from high-frequency (100 kHz) data. This smaller impedance stems from PPy nanofibers owing to the alignment and orientation of PPy chains. An ideal capacitive behavior of the CuPcTs−PPy gel was indicated by the nearly vertical shape of the obtained curve at lower frequencies. Cyclic voltammetry (CV) tested in a conventional three-electrode system further confirmed the greatly enhanced electrochemical activity of CuPcTs−PPy, indicating a boosted redox peak of CuPcTs-PPy compared with pristine PPy shown in Figure 1b. Notably, the CuPcTs-PPy exhibits a higher conductivity, 1D morphology, and more porous structure than the pristine PPy, which favors the transfer of electrons and ions. In addition, the galvanostatic charge/discharge tests of the CuPcTs−PPy and pristine PPy electrodes were shown in Figure 1c. The specific capacitance of the CuPcTs-doped PPy was calculated to be as high as ~400 F g^{-1} at 0.2 A g^{-1}, whereas that of pristine PPy was only 232 F g^{-1} (Figure 1d). CuPcTs−PPy also shows better rate capability than pristine PPy.

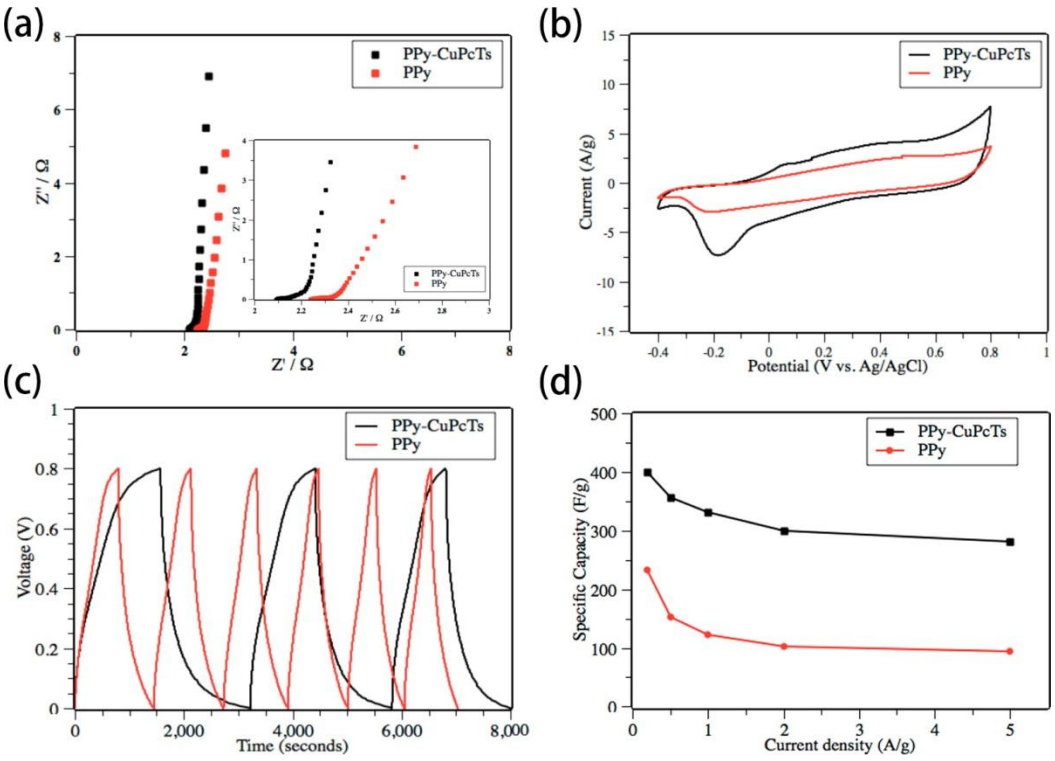

Figure 3.1 Electrochemical characteristics of different PPy samples showing greatly enhanced the electrochemical activity of CuPcTs-doped PPy compared with pristine PPy. (a) Electrochemical impedance plot (inset, zoom in of the plot), (b) cyclic voltammogram (scan rate: 10 mV/s), (c) charge/discharge curves (current density: 0.2 A/g), and (d) specific capacitance as a function of current density for CuPcTs−PPy and pristine PPy.

3.2.2 Interfacial synthesis enabled PPy gels with structure derived elasticity for flexible supercapacitor

Flexible and portable electronic devices such as wearable electronic devices, flexible displays, and bendable television screens have been attracting interests from both academia and industry in the past decades.[14] The rapid development of portable electronic equipment requires the development of flexible, lightweight and cost-effective power sources.[15-17] Flexible solid-state supercapacitors are promising candidates for portable energy storage devices because they can provide high power density, long cycle life and the potential to achieve relatively high energy density.[18-20]

CPGs have been successfully demonstrated to be a high-performance capacitive material with high rate capability and cyclic stability. However, their applications in flexible and portable energy storage devices are hindered by relatively poor mechanical properties. PANI hydrogels crosslinked by phytic acid with interconnected nanofibers show relatively poor mechanical strength while PPy gels are inherently rigid and fragile although they are mechanically strong. Limited by the mechanical properties of CPGs without synthetic modification, flexible supercapacitors based on CPGs are hard to be achieved.

As discussed in Chapter 2, PPy gels with a structure derived elasticity have been synthesized through an interfacial synthesis. These gels possess hollow sphere structure and show excellent elasticity and mechanical strength since the spherical shell geometry with a structural hierarchy could overcome the inherent brittleness of PPy by elastically deforming and recovering upon the application and release of external pressure. With improved mechanical properties, PPy gels can be used for the fabrication of highly flexible supercapacitor.

The electrochemical performance of PPy gels enabled by interfacial synthesis was firstly investigated as supercapacitor electrodes in a conventional three-electrode system. Figure 2a shows the EIS curves of PPy gels based electrodes with different PPy mass loadings measured in a 1 M H_2SO_4 electrolyte. A small charge transfer resistance can be verified according to the small semicircles in the high-frequency range and nearly ideal capacitive behavior is confirmed by approximately vertical EIS curve tails in the low-frequency range. Figure 2b shows the rate-dependent CV curves of the PPy gel based supercapacitor electrodes, showing good rate performance since the current densities increase along with increasing scan rates. Fig. 2c shows the discharge profiles of the PPy hydrogel electrode at current densities from 0.14 to 2.8 A g^{-1}. Specific capacitances as

high as 300–400 F g^{-1} were achieved at a low current density of ~0.2 A g^{-1} even at relatively high mass loadings, revealing excellent capacitive performance. Figure 2e shows corresponding data in the form of areal capacitance vs. current density. Figure 2f shows the excellent cycling stability of the PPy gel electrodes at a current density of 2.8 A g^{-1}. More than 93% capacitance retention was achieved for all three samples after 2000 cycles. The exceptional performance could be explained by the following reasons. Firstly, the polymer backbones of PPy CPG are intrinsically conductive, providing a 3D continuous pathway for electron transport. Secondly, the micro-/nano-porous structures of PPy gel electrode offered by ruptured PPy hollow spheres allow fast ionic migration between the aqueous electrolyte and the electrode and favor a rapid adsorption/desorption redox process. In addition, the PPy gel is hydrophilic which can ensure a thorough wetting of the electrode by the aqueous electrolyte. Moreover, the unique hydrogel viscosity ensures the good contact between the PPy gel and the carbon cloth. Finally, the rapidly charged/discharged redox-active sites incorporated into the polymer matrix can increase the overall capacitance of the supercapacitor at fast cycling rates.[21]

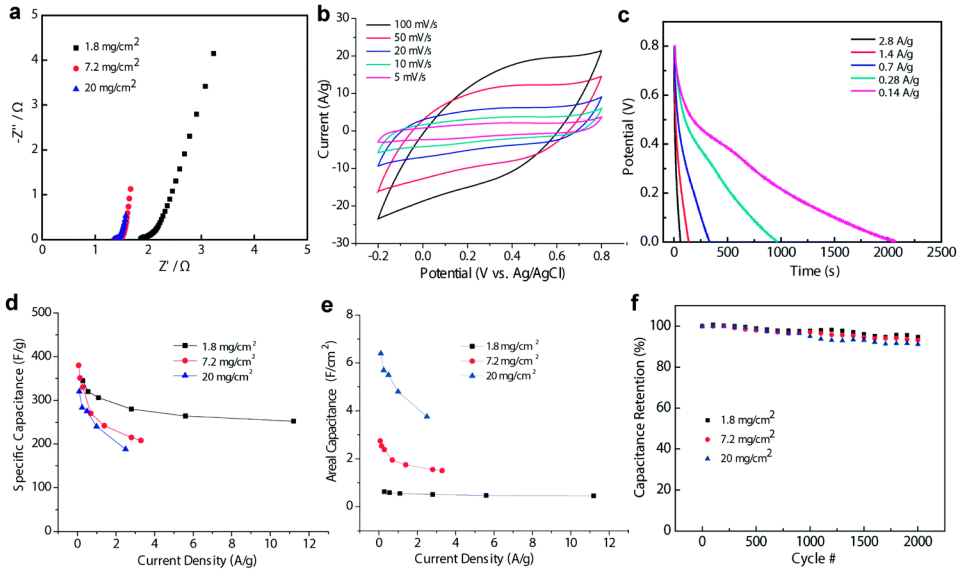

Figure 3.2 Electrochemical performance of the PPy hydrogel based electrodes. (a) EIS curves of PPy electrodes with active material loadings of 1.8, 7.2 and 20 mg cm^{-2}. (b) Cyclic voltammograms of the PPy electrode (7.2 mg cm^{-2}) at various scan rates of 5–100 mV s^{-1}. (c) Representative galvanostatic discharge curves of PPy electrodes at different current densities of 0.14–2.8 A g^{-1}. (d) Specific capacitance *versus* current density for PPy electrodes with different material loadings. (e) Corresponding areal capacitance *versus* current density with different active materials. (f) Cycling performance of PPy hydrogel based electrodes with various active material loadings at a current density of ~2.8 A g^{-1}.

The application of PPy gels with a structure derived elasticity in flexible supercapacitor was then demonstrated. The flexible device was assembled by sandwiching a PVA–H_2SO_4 gel-like electrolyte with two pieces of PPy gel electrodes, as illustrated in the inset of Figure 3a. The electrochemical properties of the flexible supercapacitor were examined with different tests. The EIS curve of the PPy gel based flexible supercapacitor in Figure 4a indicates good ionic conductivity of the PVA–H_2SO_4 electrolyte based supercapacitor and ideal capacitive properties of the all-solid-state supercapacitor.

The flexibility of PPy gel based supercapacitor was then demonstrated by testing its electrochemical performance under bending conditions (with radii of curvature of ∞ (flat), 8 mm, and 3 mm). CV data are shown in Figure 3b in which the encircled areas of CV curves remain almost the same (less than 3% decrease) as the curvature of the supercapacitor increases. Even at a highly bent status, the capacitance change is still negligible compared to that of a flat one. This can be attributed to the mechanical flexibility of the sponge-like PPy network. The porous space enclosed in the PPy network will largely accommodate the deformation of the PPy backbone during bending. The flexibility-related rate performance of PPy gel based solid-state supercapacitor was further evaluated by galvanostatic charge–discharge tests. Specific capacitance was calculated and plotted vs. current density in Figure 3c in which we can see that the specific capacitance retains ~81% and ~61% of the initial value when the current density is increased by ~10× and ~25×, respectively. In the cyclic test, the flexible solid-state supercapacitor retains ~90% of initial capacitance after 3000 charge–discharge electrochemical cycles (Figure 3d), indicating good electrochemical stability of the assembled supercapacitor device.

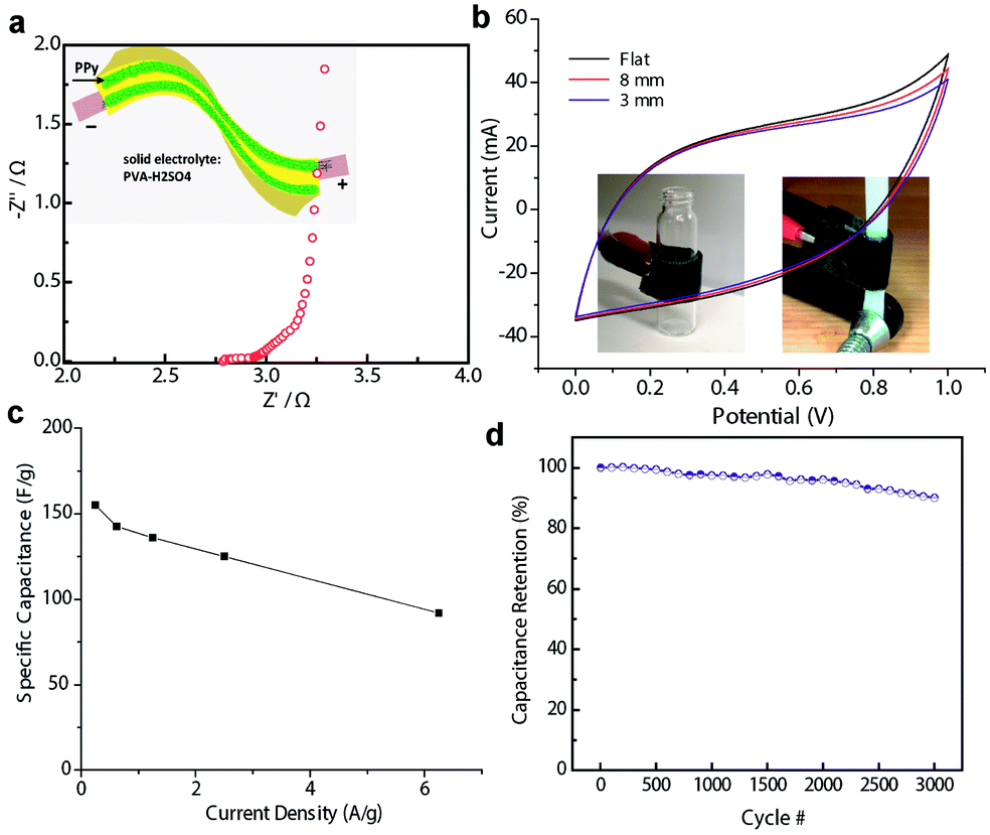

Figure 3.3 Electrochemical characteristics of flexible PPy hydrogel based supercapacitors. (a) EIS curve of a full cell based on symmetric electrodes. Inset: schematic of the makeup of the flexible supercapacitor. (b) CV curves of the fabricated supercapacitor under different bending conditions at a scan rate of 100 mV s^{-1}. (c) The specific capacitance of the full cell as a function of current densities. (d) Cycling performance over 3000 charge–discharge cycles under a bending curvature of 3 mm.

3.3 CONDUCTIVE POLYMER GELS AS BINDER MATERIALS FOR LITHIUM ION BATTERY ELECTRODES

Lithium ion batteries are dominating power sources in the market of consumer electronics for decades owing to their advantageous features such as high energy density, high efficiency, light weight and portability.[2, 4] Now the performance of lithium ion batteries in various aspects including energy density, rate capability, cyclic stability and safety need to be further improved to meet the growing demand for large-scale energy

storage such as power sources for electric vehicles and stationary energy storage.[3] However, in conventional battery electrodes, active particles are connected by the binder system which consists of conductive additives (usually carbon nanoparticles) and non-conductive polymer.[9, 22] In such system, the active materials and other additives are adhered together by polymer binders such as polyvinylidene fluoride (PVDF) to hold the mechanical integrity while conductivity is ensured by conductive additives. Electrons transport through chains of additive particles from the composite to the current collector while ions move through the liquid or solid electrolyte that fills the pores of the electrode. However, due to randomly distributed conductive phases within the active battery material, bottlenecks and poor contacts occur and impede effective access to parts of the battery.[8, 23]

In principle, the intrinsic energy capacity is determined by the charge transfer reactions which occur when a Li-ion encounters an electron at an active site within the electrode.[24] To maximize energy use, low-resistance and continuous pathways for both electrons and ions must be built within the electrode, reaching the entire volume of the battery. [8] However in conventional electrodes, carbon additives are randomly distributed and tend to aggregate during electrochemical reactions, leading to poor contacts of electronic connections.[9, 25] Although these negative effects can be avoided by increasing the amount of binder, the decreased porosity would impede ion conduction.[24, 26]

The distribution of both active particles and binder materials greatly affects the performance of battery electrodes.[16, 27, 28] In an ideal situation, the active particles should be uniformly distributed and thus every particle is electronically and ionically ‘wired’ to the current collector and electrolyte. However in conventional electrodes, due to lack of mechanical binding forces and good compatibility of inorganic particles with polymer binder, aggregation of both inorganic and organic components happens and hinders

electronic and ionic transport within the electrode.[8, 29, 30] If active particles possess the nano-level size or a large size distribution such as commercialized cathode materials, the problem will become even more serious since the small particles tend to be adsorbed on the surface of large particles, forming large size aggregates.[16, 31-33]

Different strategies have been proposed to improve the electron and ion transport within battery electrodes. For example, 3D network structured carbon materials which act as a conducting framework matrix and create porosity to facilitate the ion diffusion have been introduced to connect the active particles to the current collector. A cathode was prepared by Ruoff et al.[34] through loading lithium iron phosphate on highly conductive ultrathin graphite foam, which achieved a higher rate capability and specific capacity simultaneously, owing to the conductive and 3D graphitic structure of graphite foam. However, mass loading of active materials would be low with the employment of 3D carbon materials and can not avoid the aggregation of particles on the carbon framework surfaces. Conductive or conjugated polymers have been also adopted as a binder for battery electrode with potentially dual functionalities of adhesive and conductive nature.[35, 36] Liu et al.[9, 37] developed a promising conductive polymer binder with tailored electronic conductivity and mechanical binding force. Conjugated polymers could improve the dispersion of active particles within electrode due to the surface coating. Reichmanis et al.[38] wrapped P3HT polymer on the surface of nanomaterials and significantly enhanced material dispersity over the composite electrode. However, conductive polymers could cause low ionic transport property because the pores within the electrode are filled with soft polymers. Another recent example is the in-situ formed conductive coating for some special cathode materials, such as $Ag_2VP_2O_8$, which covers the surfaces of each particle.[39] Ideally, a binder system that can combine the advantageous features of 3D network structured materials and conductive polymers may

be a promising candidate for advanced battery electrodes.

Here a novel binder system based on 3D nanostructured CPG framework for high-capacity nanoparticles based LIB electrodes is presented (Figure 4). The highly conductive and continuous CPG framework provides a good electrical connection among the particles, as well as between particles and the current collector, thereby enabling outstanding rate capability. The hierarchical pores within electrode could maximize the interface between active material and electrolyte and facilitate the transport of ions. A polymeric ultrathin coating also forms due to the hydrophilic nature of hydrogel on the surface of active particles, preventing the aggregation of active particles. The conformal coating wired every active particle to the current collector and to the solid or liquid electrolyte. In addition, the mass ratio of active particles and gravimetric energy density of the battery is significantly enhanced since the gel framework serves dual functionalities in the binder system. At last, it is facile to tune the chemical structures and electrochemical properties of CPG framework via adopting different doping agents.

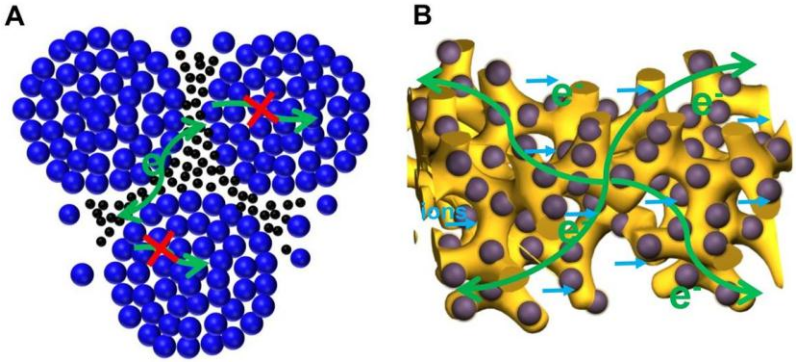

Figure 3.4 (A) In a traditional electrode system, bottlenecks and poor contacts may impede effective access to parts of the battery and aggregation of active particles occurs. (B) Conductive polymer gel framework constructs a 3D network for electron transport and a porous structure to facilitate the transport of ions in hybrid gel electrodes.

3.3.1 CPG/Fe_3O_4 nanoparticles hybrid gel electrode as high-performance lithium ion battery anode

The CPG-based binder system was firstly applied to Fe_3O_4 nanoparticles[40, 41] to build up hybrid gel electrode as an anode in lithium ion battery. The gel framework based electrode was synthesized by in-situ polymerization. Pyrrole monomers and the crosslinker were added into Fe_3O_4 NPs (~20 nm) dispersion by ultrasonication. Then two kinds of crosslinkers were adopted to crosslink conductive gel framework with modified properties, which are phytic acid (named as P-PPy/Fe_3O_4) and copper(II) phthalocyanine tetrasulfonate salts (CuPcTs) (named as C-PPy/Fe_3O_4). The multiple functional groups on crosslinker molecules could react with conductive polymer chains, thus crosslinking them into the 3D network, as well as doping polymer framework due to the protonated nature of crosslinker molecules. Ammonium persulfate (APS) solution is used to initiate polymerization and the gelation starts within half an hour, resulting in the hybrid gel in which Fe_3O_4 NPs were coated and connected by the conductive gel framework.

The SEM images in Figure 5 show the hierarchically porous structure of hybrid gels consisting of conductive polymer framework and connected active particles. It should be noted that the microstructure of C-PPy framework is a bit different from that of P-PPy, showing film- and fiber-like structure in the framework. This may result from that CuPcTs with planar structure can facilitate the supramolecular assembly of PPy chains, resulting in better aligned conductive polymer chains which may contribute to higher electronic conductivity.[42] Therefore different doping agents can be adopted to tune the microstructure of hybrid gel framework. In scanning transmission electron microscopy (STEM) images, it could be observed that the active particles were conformally coated by a polymer layer with thickness of 5-10 nm, which is further demonstrated in energy dispersive X-ray spectroscopy (EDX) mapping tests as shown in Figure 5E to 5G. The

results show that other than Fe element which can be only detected at locations of Fe_3O_4 particles, Cu element which is doping in the PPy gel can be found within the whole framework, covering entire Fe_3O_4 particles.

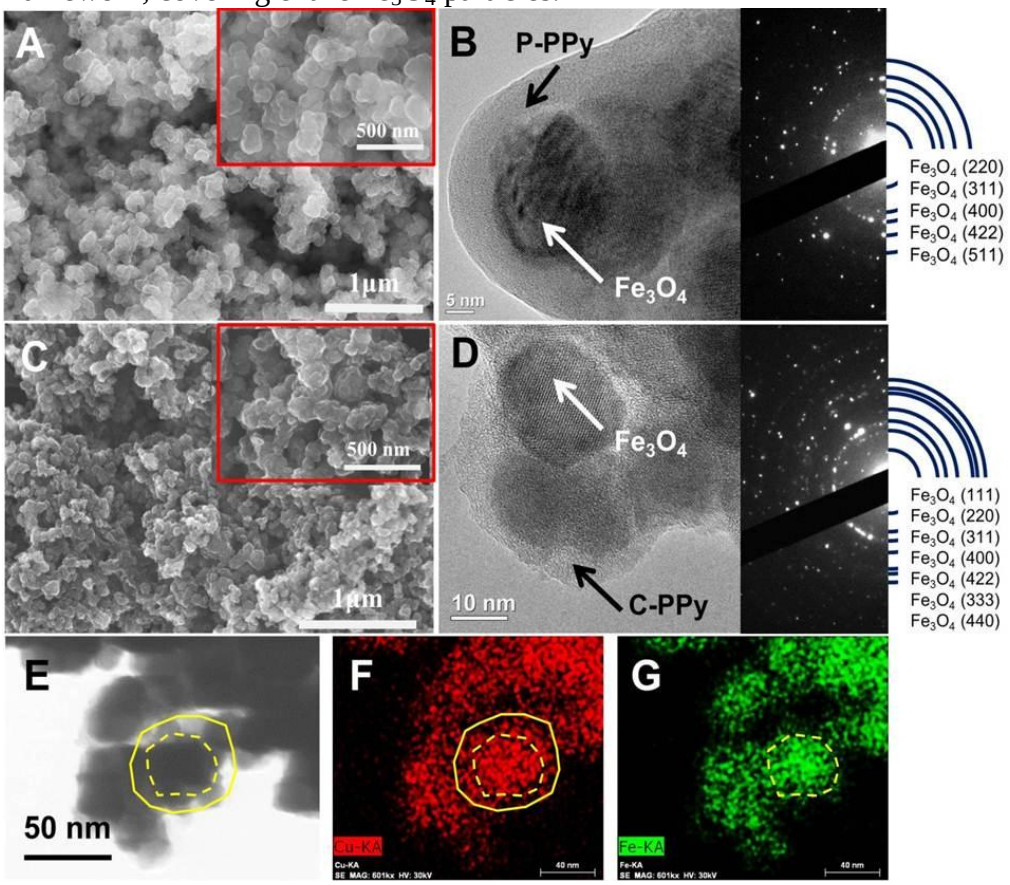

Figure 3.5 (A) and (B) SEM, TEM images and electron diffraction pattern of P-PPy/ Fe_3O_4 hybrid gel electrodes, (C) and (D) SEM, TEM images and electron diffraction pattern of C-PPy/ Fe_3O_4 hybrid gel electrodes, (E) STEM image of C-PPy/Fe_3O_4 hybrid gel, (F) and (G) EDX elemental mapping of C-PPy/ Fe_3O_4 hybrid gel.

EDX elemental mapping and Fourier transform infrared spectroscopy (FTIR) were used to investigate the chemical compositions of the PPy layer, especially the chemical states of N. Figure 6A and 6C show that N element can be detected from the whole area with hybrid gel, which demonstrates that PPy is coated on the active particles.

The FTIR spectra of P-PPy/Fe_3O_4 and C-PPy/Fe_3O_4 hybrid gels shown in Figure 6B and 6D, respectively, indicate the peak at 1045 cm^{-1} which can be attributed to the in-plane deformation of N-H bond. The FTIR spectra also demonstrate the existence of PPy in the gel framework.

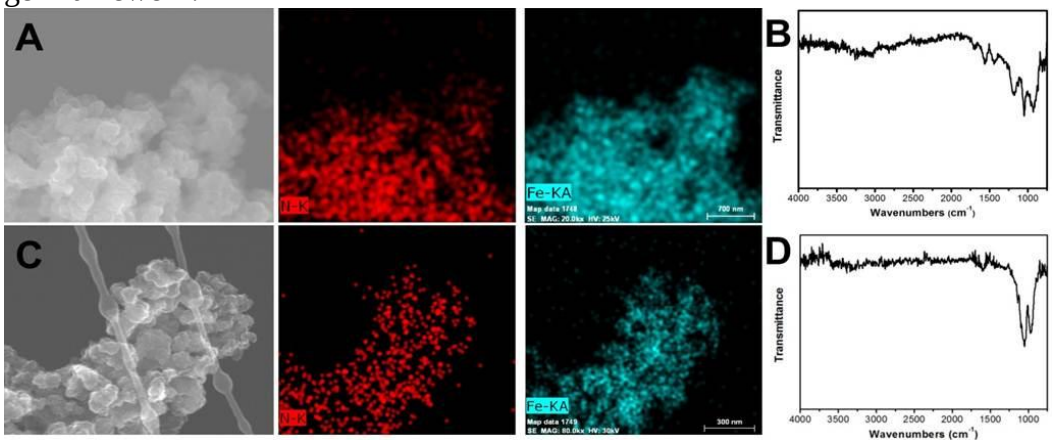

Figure 3.6 (A) and (B) EDX mapping and FTIR spectra of P-PPy/Fe_3O_4 hybrid gel. (C) and (D) EDX mapping and FTIR spectra of C-PPy/Fe_3O_4 hybrid gel.

The chemical and crystalline structure of hybrid gel was examined by X-ray diffraction (XRD). The XRD patterns of hybrid gel samples using different crosslinker molecules and corresponding PPy samples are shown in Figure 7. For both hybrid gel samples, sharp peaks which could be ascribed to the magnetite particles are observed at 30, 36, 43, 54, 57, and 63 degree, indicating that the crystal structure of active particles was well maintained after in-situ polymerization and no oxidization occurred.[43] The hybrid gels also show a broad peak between 20 and 30 degree which is similar to the one in pure PPy samples and could be ascribed to the amorphous PPy, confirming the existence of conductive polymer layer on the surface of Fe_3O_4 NPs.[44] Through thermogravimetric analysis (TGA) tests it is possible to evaluate the amount of each component in the hybrid gels. Hybrid gel samples were heated from 35 to 850 ℃ after drying in vacuum oven at 80 ℃ overnight to remove excess water. Figure 8 shows the

weight loss curves of both samples. The weight percentages of Fe_3O_4 NPs in P-PPy/ Fe_3O_4 and P-PPy/ Fe_3O_4 are calculated to be ~84% and ~83%, respectively. The second plateau in the TGA curve of P-PPy/ Fe_3O_4 could be ascribed to the decomposition of CuPcTs.[44] Note that in order to obtain best electrochemical performance, the weight ratio of Fe_3O_4 NPs in the hybrid gel electrode was optimized. Hybrid gels with ~80%, ~85%, and ~90% of Fe_3O_4 NPs were prepared and charge/discharge tests showed that only the sample with ~85% of Fe_3O_4 NPs exhibited stable capacity. The reason is that large size of polymer domains in the ~80% sample and serious aggregation of Fe_3O_4 NPs in the ~90% sample limit the electrodes' rate performance and harm cycling stability. The weight ratio of active materials in the CPG-based electrode is significantly higher compared with conventional PVDF-based or water-soluble binder systems, where a considerable amount of conductive additives are needed either in the composites or in the electrodes.[45, 46]

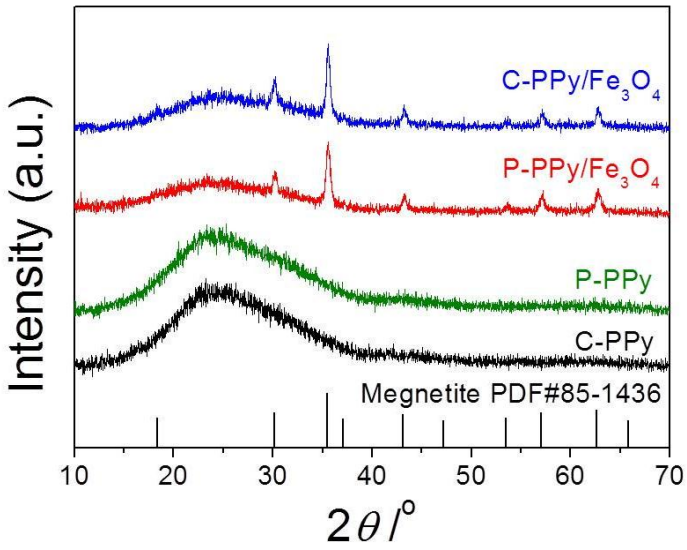

Figure 3.7 XRD patterns of phytic acid and CuPcTs doped PPy hydrogel and hybrid gels with Fe_3O_4.

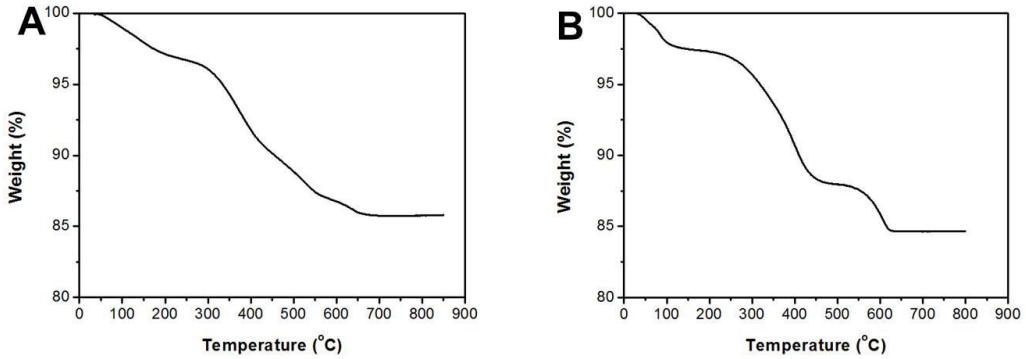

Figure 3.8 Typical TGA curves of (A) P-PPy/Fe_3O_4 and (B) C-PPy/Fe_3O_4 hybrid gel.

TEM microtome imaging of the bulk electrode was used to examine the dispersion of Fe_3O_4 NPs in the gel framework. A control electrode was prepared using a traditional binder system containing Fe_3O_4 NPs, acetylene black, and PVDF with a weight ratio of 75: 15: 10 and compared to hybrid gel electrode. Figure 9 shows that aggregations of Fe_3O_4 NPs and domains of pure polymer form in the control sample. The hybrid gel frameworks suppress the aggregation of active particles although it contains a higher weight ratio of Fe_3O_4 NPs. Uniformly distributed particles are connected with each other through polymer coating and gel network as shown in Figure 9D and 9G. C-PPy/Fe_3O_4 (Figure 9G) shows more homogeneous dispersion of both NPs and organic components since some domains containing pure polymer can be found in P-PPy/Fe_3O_4 hybrid electrode (Figure 9D). The TEM images demonstrated that conductive gel framework can prevent the aggregation of active particles and ensure both electrical and ionic connections between each active particle, between active particles and electrolyte, as well as between active particles and the current collector.

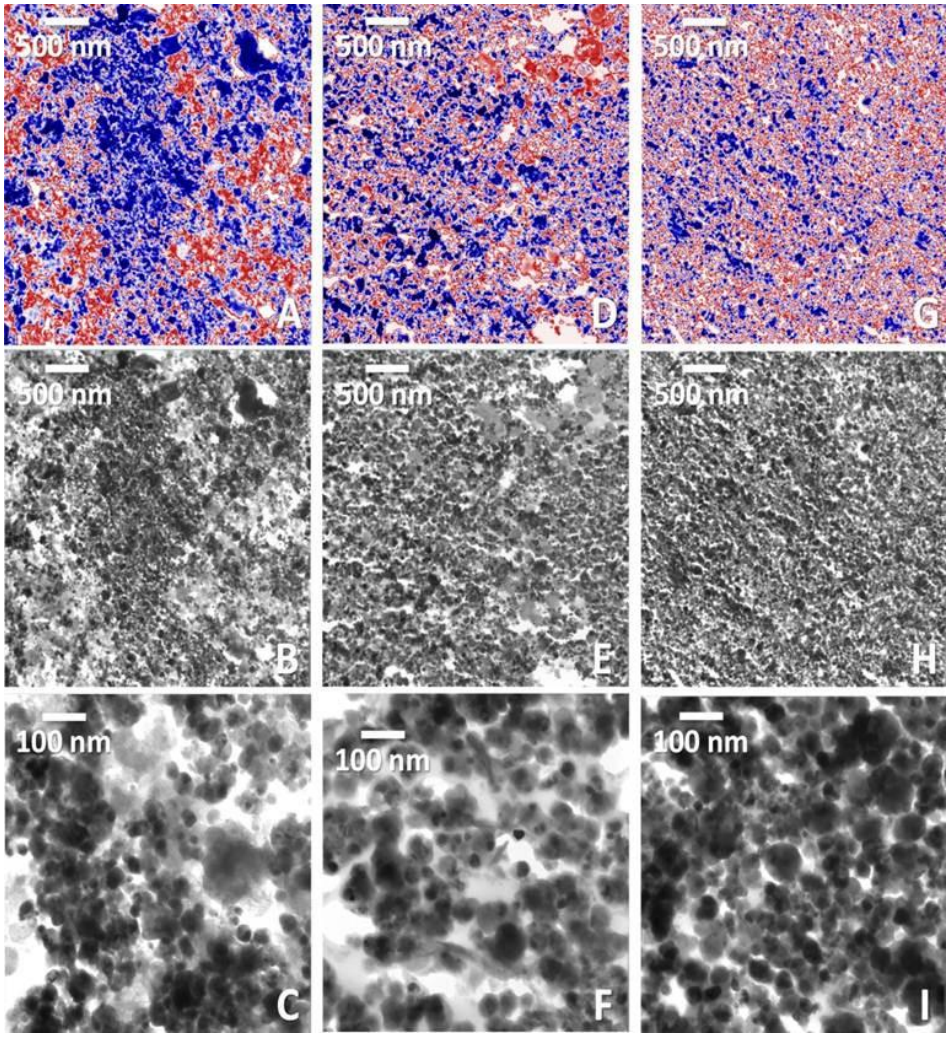

Figure 3.9 TEM microtome images of the (A) color enhanced, (B), (C) control sample. TEM microtome images of the (D) color enhanced, (E), (F) P-PPy/Fe_3O_4 hybrid gel. TEM microtome images of the (G) color enhanced, (H), (I) C-PPy/Fe_3O_4 hybrid gel. In the color enhanced images blue represents the Fe_3O_4 nanoparticles and red is organics (PVDF/carbon/PPy).

Micron-sized agglomerates of Fe_3O_4 NPs formed in the conventional process result in great barrier for ion/electron transport in the electrode, which is the key factor preventing active material from full utilization especially at high current density. In contrast, uniformly dispersed Fe_3O_4 NPs in the framework of CPGs provides successive pathways for electron transport and 3D porous tunnels for ion diffusion, thus exhibiting

high rate capability. The rate capability of P-PPy/ Fe_3O_4, C-PPy/ Fe_3O_4 and control samples charged and discharged from 0.1C up to 2C (1C = 926 mA/g) are shown in Figure 10. The hybrid gel electrodes reached stable capacities of 1260 mAh/g, 1002 mAh/g, and 845 mAh/g, when current rates increased from 0.1 C to 1C, 2C, respectively. At each current density, both hybrid gel samples showed much higher capacity than the control sample. Especially at a high rate, hybrid gels could maintain more than 900 mAh/g of capacity while the control sample could only deliver around 500 mAh/g (charge/discharge profiles are shown in Figure 11), indicating greatly enhanced rate performance of hybrid gel samples. This rate performance achieved represents the best performance compared to current literature for various carbon-magnetite composites based electrodes (Table 1). Based on the exceptionally high mass ratio of active materials (85-90%), highest specific capacities based on total electrode mass (active materials plus binder/additive) were achieved for hybrid gel electrodes. C-PPy/Fe_3O_4 also shows recovery of capacity to around 1200 mAh/g when the current density was decreased to 0.1C again while the other two samples can't. Best rate characteristics for C-PPy/Fe_3O_4 hybrid gel frameworks are achieved by optimizing the amount of CuPcTs (Figure 12). The enhancement of rate capability is mainly due to higher conductivity of the whole network of PPy by CuPcTs doping since CuPcTs is a semiconductor. The greatly enhanced rate capability of hybrid gel electrodes comes from their advantageous features that the conductive framework of PPy gels constructs a 3D network for electron transport; the polymer coating connects each particle and the particles with current collector; and the porous structure facilitates the motion of liquid electrolyte and transport ions.

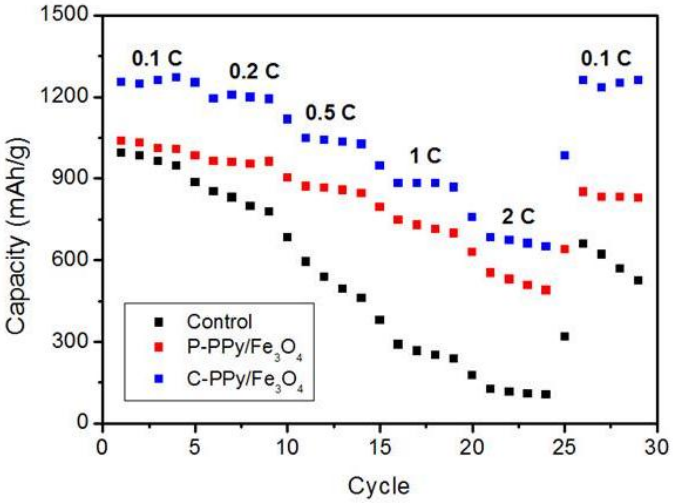

Figure 3.10 Rate characteristics of P-PPy/Fe_3O_4, C-PPy/Fe_3O_4 and control samples.

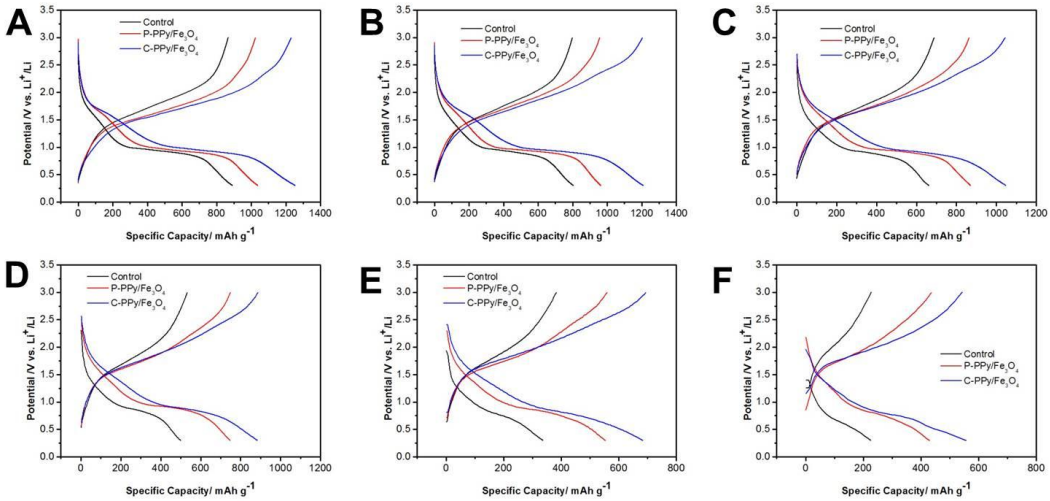

Figure 3.11 Charge/discharge profiles of different samples at different rates from 0.1C to 5C.

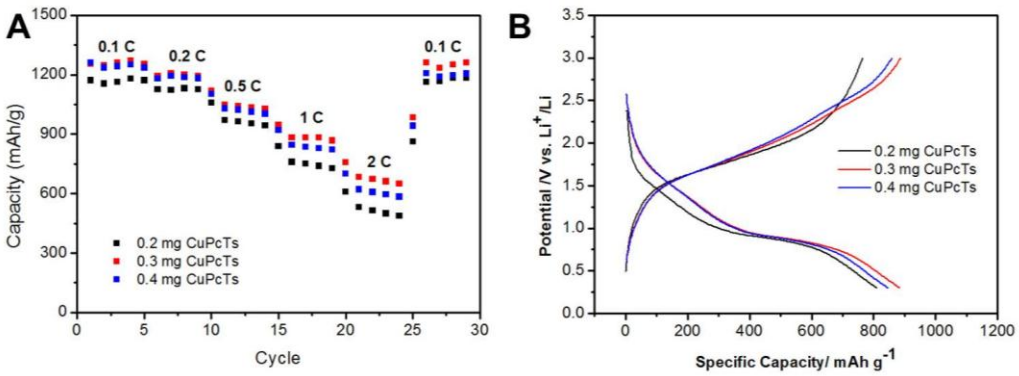

Figure 3.12 Rate performance of C-PPy/Fe_3O_4 hybrid gels with tuned amount of CuPcTs.

Figure 13 shows the cyclic tests of gel framework based electrodes and conventional electrodes at low current density. The conventional electrode delivers an initial discharging specific capacity of 850 mAh/g at a current density of 100 mA/g, which is close to its theoretical specific capacity but only retained ~300 mAh/g after 50 cycles, indicating fast decay. The hybrid electrode of P-PPy/ Fe_3O_4 shows higher specific capacity and much better cyclic stability that a stable capacity of ~1000 mAh/g is achieved, which exceeds/comparable to best-reported results in literature including carbon-encapsulated Fe_3O_4 nanoparticles embedded in graphitic carbon nanosheets, Fe_3O_4 nanoparticles confined in mesocellular carbon foam, and Fe_3O_4 microspheres encapsulated in graphene (a comprehensive comparison of performance of reported magnetite-based anode materials for lithium ion batteries is summarized in Table 1).[40, 47, 48] The decomposition of electrolyte and the formation of polymeric gel-like SEI layers may cause the excess capacity higher than theoretical value at the first cycle.[49] The formation and decomposition of SEI layers are partially reversible and have a continuous contribution to the capacity in following cycles. That the C-PPy/Fe_3O_4 electrode shows a much higher initial capacity up to ~2100 mAh/g which could be attributed to two

reasons. Firstly, the excellent dispersion of Fe_3O_4 nanoparticles in the framework results in a large interface between the active materials and electrolyte for the formation of SEI layers.[50] Furthermore, CuPcTs with catalytic functionality could promote the decomposition of electrolyte and the formation of SEI films, as demonstrated by a relatively lower initial Coulombic efficiency. Nevertheless, the as-grown SEI layers are very stable, resulting in higher Coulombic efficiency from the second cycle. The C-PPy/ Fe_3O_4 hybrid gel electrode maintains a capacity up to 1100 mAh/g within 50 cycles, demonstrating good stability. As discussed in Chapter 2, the conductivity and the structure of the gel frameworks can be tuned by adjusting the amount of the crosslinker. As a result of improved conductivity and fine-tuned 3D network microstructure, the C-PPy/ Fe_3O_4 electrode shows better cyclic stability as well as higher specific capacity. In addition, the contribution of the conducting polymer to capacity is very low, as demonstrated by cyclic voltammograms of the pure P-PPy and C-PPy (Figure 14). The specific capacities of pure P-PPy and C-PPy are calculated to be ~40 and ~50 mAh/g, respectively and the capacity contributions of pure P-PPy and C-PPy in the total electrode is less than 1%.

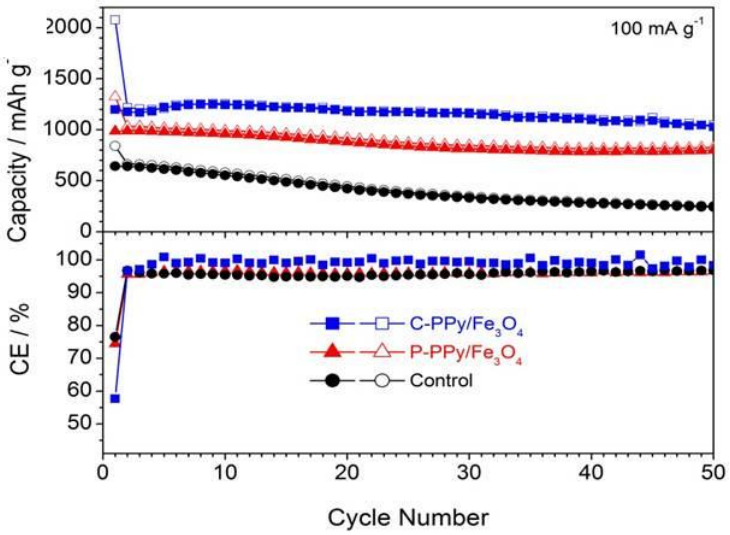

Figure 3.13 Cyclic characteristics and corresponding Coulombic efficiency of P-PPy/Fe_3O_4, C-PPy/Fe_3O_4 and control samples at a current density of 100 mA/g.

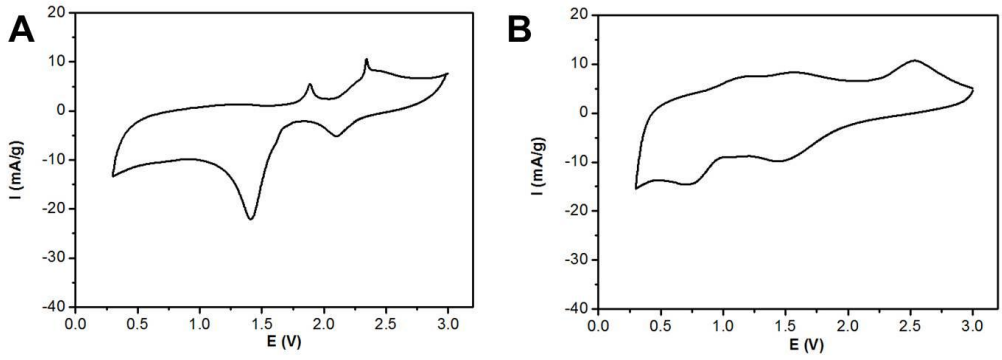

Figure 3.14 Cyclic voltammograms of electrodes with pure P-PPy (A) and C-PPy (B).

Anode structure	Mass ratio of active material in electrode	Specific capacity	Cyclic stability	Rate capability (capacity at highest rate)
Fe_3O_4 NPs/PPy gel framework (this work)	85%	1260 mAh g^{-1} at 0.1C, 1002 mAh g^{-1} at 1C	1100 mAh g^{-1} after 50 cycles	845 mAh g^{-1} at 2C
Fe_3O_4 NPs in porous carbon fibers[51]	36%	1015 mAh g^{-1} at 0.1C	856 mAh g^{-1} after 90 cycles	596 mAh g^{-1} at 2C
Graphene nanosheets and carbon-coated hollow Fe_3O_4 nanoparticles[52]	64%	939 mAh g^{-1} at 0.1C	870.4 mAh g^{-1} after 100 cycles	445 mAh g^{-1} at 5C
Sandwich-like C@ Fe_3O_4@C coaxial nanotubes[47]	49%	900 mAh g^{-1} at 0.1C	1087 mAh g^{-1} after 150 cycles	650 mAh g^{-1} at 1C
Sandwich-Structured Graphene-Fe_3O_4@Carbon Nanocomposites[53]	56%	960 mAh g^{-1} at 0.1C	860 mAh g^{-1} after 100 cycles	480 mAh g^{-1} at 2C
Fe_3O_4 microspheres in hollow graphene shells[47]	49%	1236 mAh g^{-1} at 1C	1260 mAh g^{-1} after 250 cycles	533 mAh g^{-1} at 5C
Carbon encapsulated Fe_3O_4 nanoparticles[40]	55%	1021 mAh g^{-1} at 1C	998 mAh g^{-1} after 100 cycles	905 mAh g^{-1} at 2C
Graphene-wrapped Fe_3O_4-graphene nanoribbons[54]	48%	800 mAh g^{-1} at 0.4C	708 mAh g^{-1} after 100 cycles	500 mAh g^{-1} at 1C
Fe_3O_4 nanoparticles confined in mesocellular carbon foam[48]	36%	1007 mAh g^{-1} at 0.1C	1118 mAh g^{-1} after 150 cycles	700 mAh g^{-1} at 2C
Fe_3O_4@polypyrrole nanocages[55]	62%	970 mAh g^{-1} at 0.2C	950 mAh g^{-1} after 100 cycles	490 mAh g^{-1} at 5C

Table 3.1 Performance of reported magnetite-based anode materials for lithium ion batteries

Electrochemical impedance spectra were conducted to study the mechanism of the enhancement of rate performance of gel framework based electrodes. A Randles circuit (shown in Figure 15) is used to fit the results including Rs as the electrolyte resistance, Q as the constant phase element of the double layer capacity, Rct as the charge transfer resistance and a specific electrochemical element (Warburg element) of diffusion W. The as assembled batteries with hybrid gels showed larger charge transfer resistance but lower Warburg coefficient when compared to control sample which could be explained by the reason that before charge/discharge, the conductive polymer layer and the interface between polymer and active particles were not activated. However, the porous structure could facilitate the transport of ions. EIS tests on the samples after one cycle's charge/discharge between 0.3 to 3 V vs Li (Figure 15) show significantly decreased charge transport resistance of all samples, especially for hybrid gel samples. This is due to the activation of particles and polymer framework. Notably, at low frequency (10 mHz to 10 Hz), the hybrid electrodes show much lower impedance, which is only ~1/5 that of control sample, suggesting a much-improved ion diffusion ability in the hybrid 3D networks. After one cycle's charge/discharge, the electrolyte was infiltrated into the polymer layer and the ionic transport was greatly improved for hybrid gels, as demonstrated by the decreased Warburg coefficient. In addition, the ion conductivity of C-PPy/Fe_3O_4 is higher than that of P-PPy/Fe_3O_4, which may be attributed to higher porosity and better dispersion of C-PPy/Fe_3O_4 electrodes. This demonstrates that the control of microstructure of our gel framework can help tune the ionic transport properties of hybrid gel electrode.

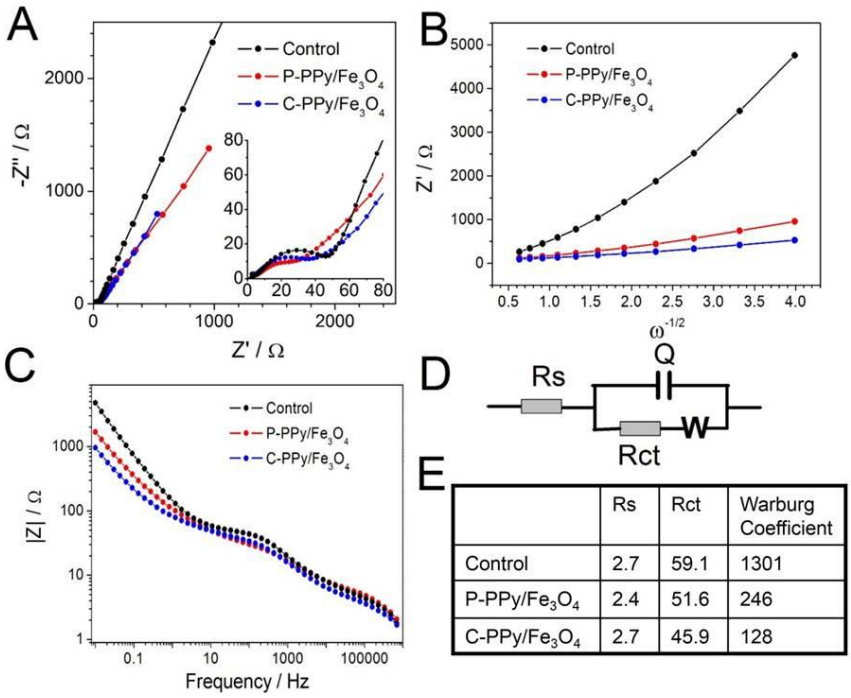

	Rs	Rct	Warburg Coefficient
Control	2.7	59.1	1301
P-PPy/Fe_3O_4	2.4	51.6	246
C-PPy/Fe_3O_4	2.7	45.9	128

Figure 3.15 Impedance analysis of different electrodes. (A) Nyquist curves of different samples, (B) the Warburg plot of different samples, (C) the Bode plot of different samples, (D) Randle's circuit used for fitting, (E) the fitted and calculated results of different samples.

To demonstrate the role of CPGs in the improvement of the ionic transport in hybrid gels, pure PPy without Fe_3O_4 NPs were tested. The pure PPy gel cells exhibited lower Warburg coefficient than P-PPy/Fe_3O_4 and P-PPy/Fe_3O_4 after 1st cycle's charge/discharge, demonstrating that the hierarchically porous structure of conductive polymer gel can facilitate the transport of ions and the polymer matrix is compatible with the liquid electrolyte.

EIS tests were also used to examine the stability of the framework after charge/discharge cycling. An additional semicircle is found at high frequency for hybrid gel samples, which could be attributed to the formation of SEI layers. The charge transport resistance of hybrid gels increased a little while that of control sample increased

significantly (Table 2). The increase is caused by the decomposition of polymer framework during charge/discharge and side reactions of conductive polymers in gel-based electrodes. While in the PVDF-based electrode, it is caused by severe aggregation of Fe_3O_4 NPs because of volume expansion during cycling, resulting in the destruction of electric connections. The Warburg coefficient of gel electrodes also increased little while that of control sample remained large. This was caused by the morphology change which was further examined by SEM tests.

	Rs /Ω	Rsl /Ω	Rct /Ω	Warburg Coefficient
Control	11.1	-	280	9323
P-PPy/Fe3O4	7.1	5.6	61.5	788
C-PPy/Fe3O4	5.5	8.5	64.2	333

Table 3.2 EIS test results of different samples after 50 cycles.

The morphologies of gel framework based electrodes after charge/discharge were examined by SEM (Figure 16). Dendritic structures form in both P-PPy/Fe_3O_4 and C-PPy/Fe_3O_4 samples and the polymer layer became thicker after 50 cycle's charge/discharge, which is caused by the formation of SEI layers and the volume change of conductive polymer during insertion and desertion of lithium ions. Although morphologies change could be detected, the hybrid gel frameworks maintain porous structures and the interconnections between active particles. From the STEM image, it can be seen that Fe_3O_4 NPs were still wrapped in a polymer coating. In comparison, the control sample after cycling showed severe aggregation of Fe_3O_4 NPs which can explain the significant decay of capacity (Figure 17). EDX mapping test was further conducted

on C-PPy/Fe_3O_4 sample after cycling test. Same as the sample before charge/discharge, Cu element can be detected within the whole framework which demonstrated that the gel framework and the polymer shell/particle core structure were well maintained. This could explain the well-maintained capacity and small impedance of battery system after cycling.

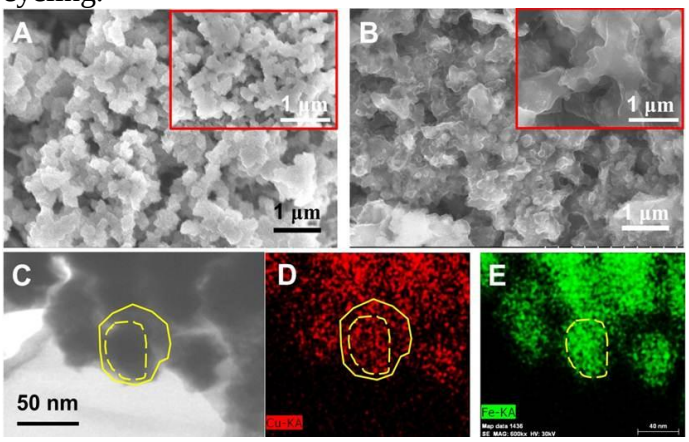

Figure 3.16 (A) SEM image of P-PPy/Fe_3O_4 after cycling test, (B) SEM image of C-PPy/Fe_3O_4 after cycling test, (C) STEM image of C-PPy/Fe_3O_4 after cycling test, (D) and (E) EDX mapping of C-PPy/Fe_3O_4 after cycling test.

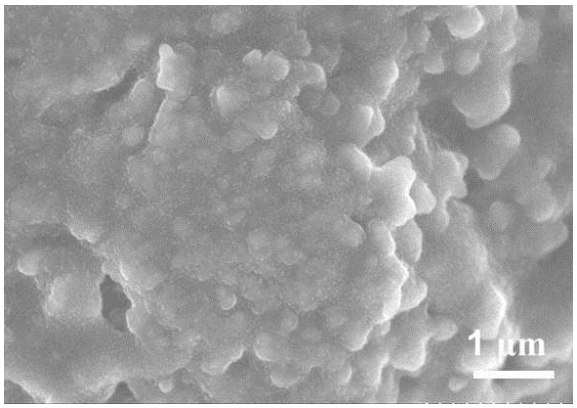

Figure 3.17 SEM image of the control sample.

3.3.2 CPG/$LiFePO_4$ hybrid gel electrode with improved electrochemical performance as cathode materials in lithium ion batteries

To verify the versatility of CPG binder system and investigate the electrochemical properties of CPG binder in the high potential window, nanostructured CPGs are used as a general framework material to enable much higher performance of conventional inorganic cathode materials, lithium iron phosphate (LFP) for Li-ion batteries.[13] CuPcTs crosslinked polypyrrole was used (C-PPy) as a multifunctional framework and commercial lithium iron phosphate (C-LFP) particles were adopted as model cathode materials (Figure 18). A 3D nanostructured electrode in which C-LFP particles were uniformly coated with the conductive polymer and embedded in the gel framework was built up by this in-situ polymerization. The structure of gel framework can be well maintained during electrode fabrication owing to the excellent mechanical strength of PPy backbones.

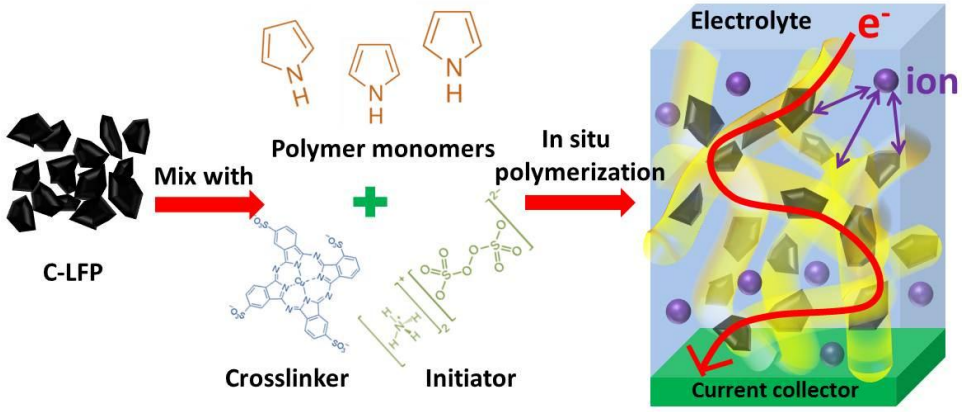

Figure 3.18 Schematic illustration of the synthesis of PPy/LFP hybrid gel electrode.

SEM and STEM were employed to investigate the morphology and structure of resulted electrode. The SEM images in Figure 19A show integrated hybrid gel framework with 3D networked structure in which C-LFP particles are interconnected with each other by conductive polymers. The hierarchical pores within the electrode form in framework

also facilitate ion diffusion. As a comparison, the hybrid gel framework was compared to control electrode fabricated by a conventional method (C-LFP: SuperP: PVDF=85:10:5), which shows low porosity and random distribution of organic domains (Figure 19B). The STEM images in Figure 19C show that C-LFP particles are wrapped by a layer of conductive polymer with a thickness of 5 to 10 nm. TEM imaging further confirmed the polymer coating. Figure 19D clearly shows the highly crystalline structure of C-LFP particle and an amorphous layer on its surface, which can be attributed to the conductive polymer coating. In Energy dispersive X-ray (EDX) analysis (Figure 19E), while Fe element can be only detected from the restricted area with the C-LFP particle, N element coming from the backbone of PPy and S element from CuPcTs molecules can be found from the whole area covered with the gel framework. These results demonstrate that CuPcTs crosslinks conductive polymer chains into a gel framework, which interconnects and coats active particles.

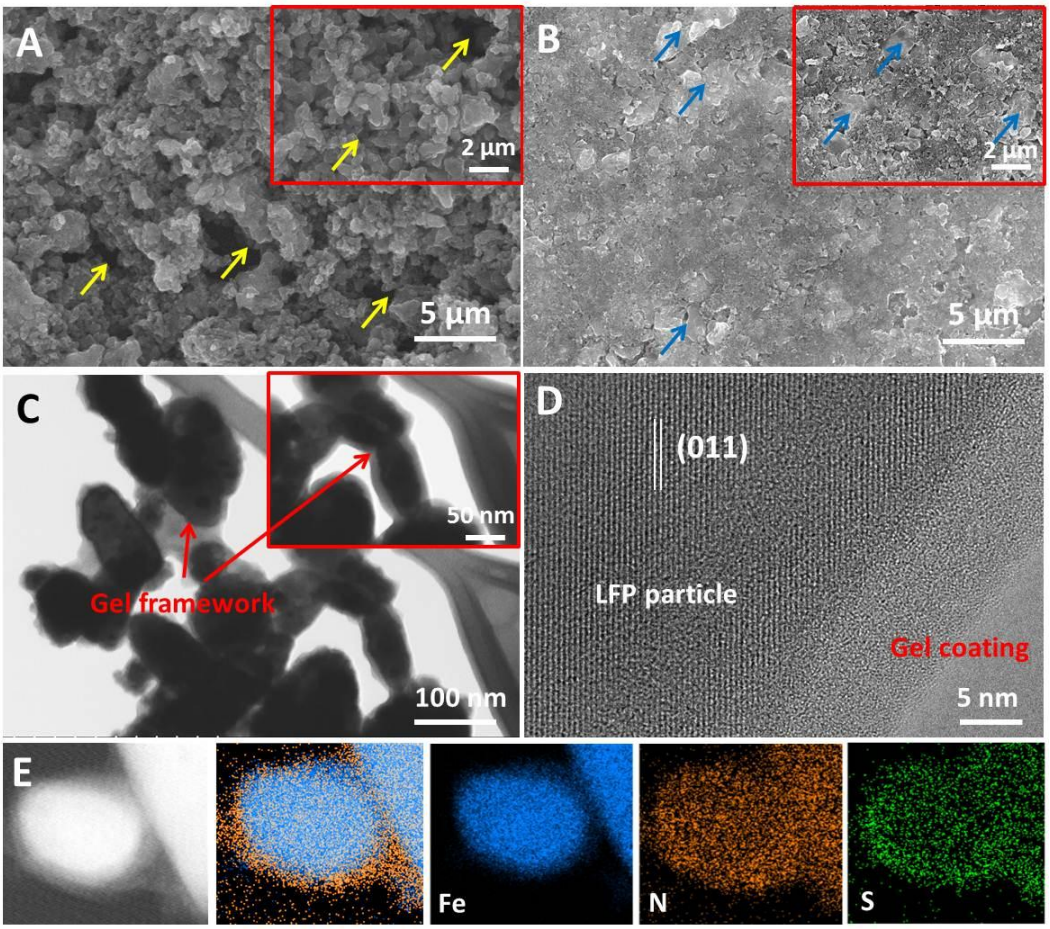

Figure 3.19 (A) SEM images of C-LFP/C-PPy hybrid gel framework with different magnification. The yellow arrows indicate pores with different sizes. (B) SEM images of control electrode with different magnification. The blue arrows indicate PVDF domains. (C) STEM images of C-LFP/C-PPy hybrid gel framework with different magnification. (D) High-resolution TEM image of C-LFP particle coated by C-PPy layer in hybrid gel framework. (E) EDX mapping of C-LFP/C-PPy hybrid gel framework.

X-ray powder diffraction (XRD) and thermogravimetric analysis (TGA) were used to examine the composition of the hybrid gel framework. The XRD pattern of hybrid gel framework (Figure 20A) shows sharp and strong characteristic peaks which can be attributed to LFP crystals, indicating that the crystal structure of C-LFP is well maintained during in situ synthesis, despite a strong oxidant APS is used. [56, 57] In the TGA

curve (Figure 20B), PPy is completely removed before the temperature reaches 450 ℃, thus the weight ratio of C-LFP particles is calculated to be ~85%, which is comparable to those in commercialized batteries. It is worthy to mention that the C-LFP ratio is optimized to 85% since it shows the best rate performance.

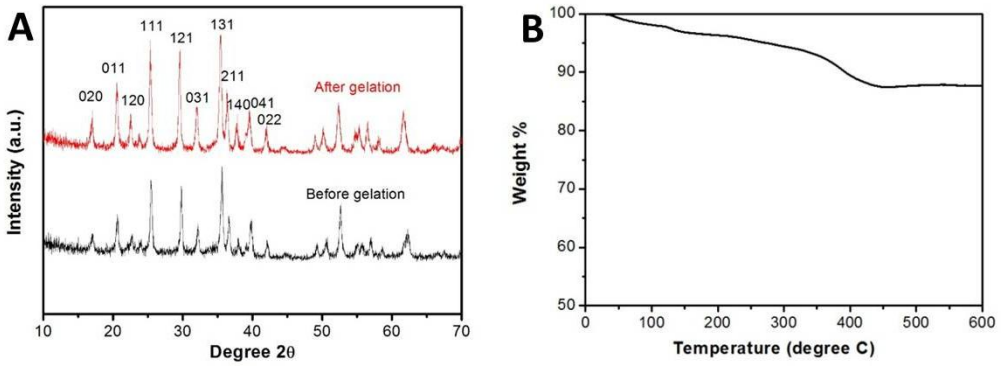

Figure 3.20 (A) XRD pattern of hybrid gel framework. (B) TGA curve of hybrid gel framework.

X-Ray photoelectron spectroscopy (XPS) was further adopted to study the chemical structures of C-LFP/C-PPy framework. The existence of oxygen, nitrogen, and carbon is confirmed in the full XPS spectra (Figure 21A). Figure 21B and 21C show the high-resolution spectra of N 1s and Fe 2p3/2 signals from the hybrid gel framework. The N 1s peaks can be divided into two parts. The two peaks at higher binding energy can be attributed to two kinds of N atoms in CuPcTs molecules under different chemical environments: C-N=C and C-N(-Cu)-C.[58] The other two peaks of N from PPy can be attributed to nitrogen that is least influenced by CuPcTs anions and the nitrogen that electrostatically interacts with CuPcTs.[59] The peak area ratio of electrostatically unscreened to screened nitrogen atoms is 1: 1, indicating a high doping level of C-PPy, which supports the high electronic conductivity of C-PPy gel framework. The Fe 2p peak shown in Figure 21C can be deconvoluted to Fe^{II}, which is corresponding to signals

from LFP and can confirm the existence of C-LFP in the hybrid gel framework.

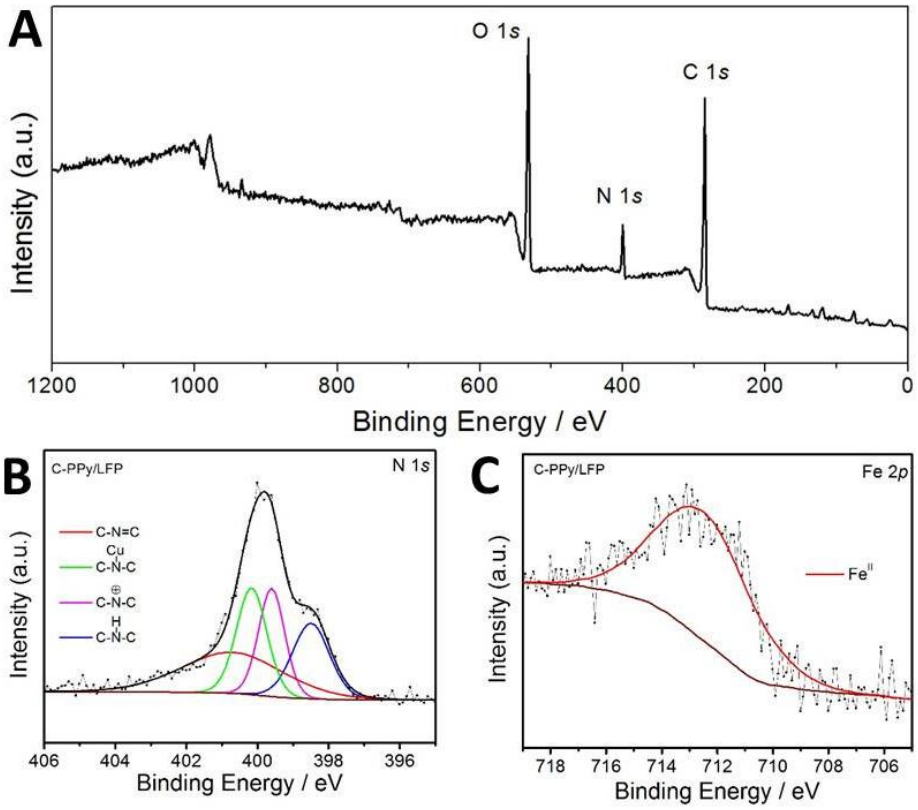

Figure 3.21 (A) XPS full spectrum of C-LFP/C-PPy hybrid gel framework. (B-C) High-resolution spectra of N 1s and Fe 2p3/2 signals from the hybrid gel framework.

The distribution of different components within the hybrid gel framework was examined by TEM. In Figure 22A, micron length (light gray) regions of organic material are presented with a clear distinction between the organic content and the C-LFP particles. This is further highlighted in the false colored images in Figure 22B. Many more regions of isolated C-LFP particles (blue) and organic domains (red) can be found in control sample but not in the C-LFP/C-PPy hybrid gel framework. The C-LFP particles and organic component in C-LFP/C-PPy electrode show a much more uniform distribution

(22C). The false color images of the C-LFP/C-PPy electrode (Figure 22D) show a PPy network that is homogeneously dispersed with the PPy regions less than 200 nm. These images illustrate that the electrode preparation using the PPy gel framework provides a well dispersed, homogeneous C-LFP particle and conductive gel distribution within the electrode and stands in contrast to the electrode prepared by conventional binders. The improved dispersion can be explained by the in situ polymerization and good compatibility between solvents and ingredients. It has been demonstrated that slurries comprising LFP powder, carbon black and polymeric binder in solvent N-methyl-2-pyrrolidone (NMP) without any surfactant usually result in poor dispersion qualities due to the hydrophilic nature of LFP particles.[60]

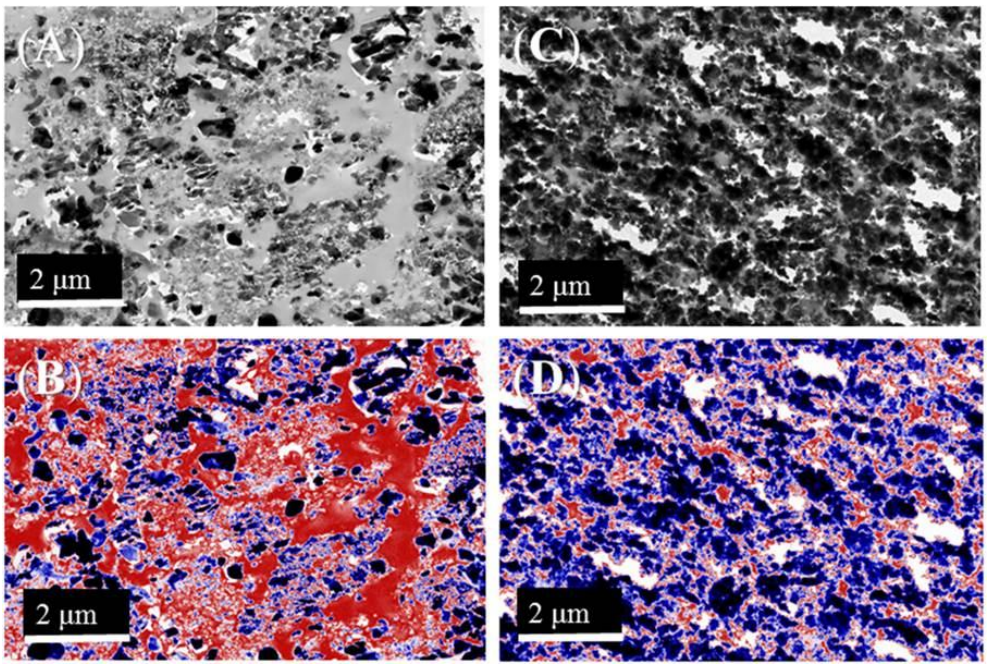

Figure 3.22 TEM images (A-B) as-prepared C-LFP control electrode and (C-D) C-LFP/C-PPy electrode. B and D are false-color images where organic areas are shown in red and inorganic areas are in blue.

The electrochemical properties of C-LFP/C-PPy hybrid gel framework were investigated. Cyclic voltammetry (CV) test at a fixed scan rate of 0.3 mV s^{-1} shows symmetric and sharp anodic and cathodic peaks, demonstrating the high redox kinetics of the hybrid gel framework.[57] It should be noted that the potential window was confined to 2.5 to 4 V to avoid side reactions between conductive polymer gel and electrolyte occurred when the voltage was above 4 V, which consumed electrolyte and led to low Coulombic efficiency. Within this potential window, the C-LFP/C-PPy hybrid gel framework can deliver a specific capacity of ~150 mAh g^{-1} at 1C (1C=170 mAh g^{-1}). According to the CV tests on pure C-PPy, the specific capacity of pure C-PPy in the potential range of 2.5 to 4 V is calculated to be ~15 mAh g^{-1} and the capacity contribution of polymer gel in the total electrode is negligible when considering that the mass ratio of gel framework is only 15% in the total electrode.

The rate characteristics of C-LFP/C-PPy hybrid gel framework were examined by charging/discharging it from 0.2C up to 30C (Figure 23A and 23B). At each current density, C-LFP/C-PPy hybrid gel framework shows much higher capacity than the control sample. The gel framework also shows excellent capacity recovery to ~150 mAh g^{-1} when the current density is back to 0.5C again. These results demonstrate that the rate capability of C-LFP/C-PPy hybrid gel framework is among best values.

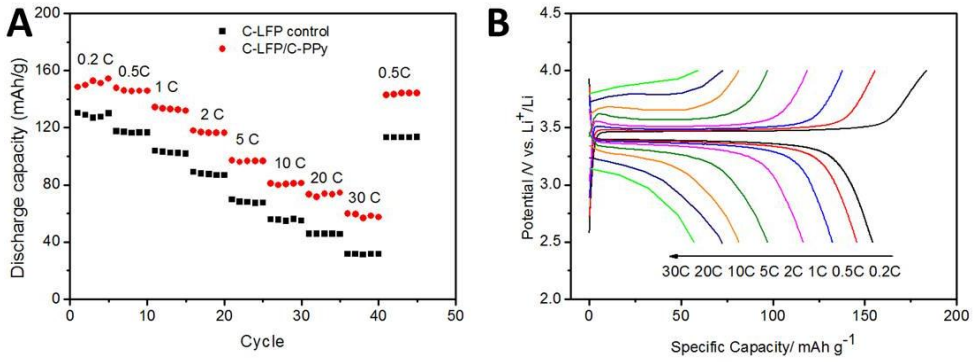

Figure 3.23 (A) Rate properties of different electrodes. (B) Voltage profiles of C-LFP/C-PPy hybrid gel framework at different charge/discharge rates.

To understand enhanced rate capability of C-LFP/C-PPy hybrid gel framework, electrochemical impedance spectra (EIS) studies were conducted on both C-LFP/C-PPy hybrid gel framework electrodes and control samples (Figure 24A). Both control and hybrid gel electrodes exhibit greatly decreased impedance after 1st cycle's charge/discharge, mainly due to the activation effect.[61] The hybrid gel framework and control sample after the first cycle show charge transfer resistances of 35.4 and 44.8 Ω, respectively according to semicircles of EIS curves at high frequency (Table 3). This result implied that the conductive gel framework promotes electrons transport to encounter with Li ions at active sites for charge transfer reactions. C-LFP/C-PPy hybrid gel framework exhibited higher impedance in low frequency (10 mHz to 10 Hz) which can be attributed to ion diffusion resistance in the electrode than control sample because the interfaces between polymer and active particles are not activated. However, after one cycle charge/discharge, the C-LFP/C-PPy hybrid gel framework shows much lower impedance when compared to control sample. The Warburg coefficients for C-LFP/C-

PPy hybrid gel framework and control sample are 91 and 237 Ω $s^{-1/2}$, respectively, indicating much improved ionic conductivity in the 3D gel framework (Figure 24B).

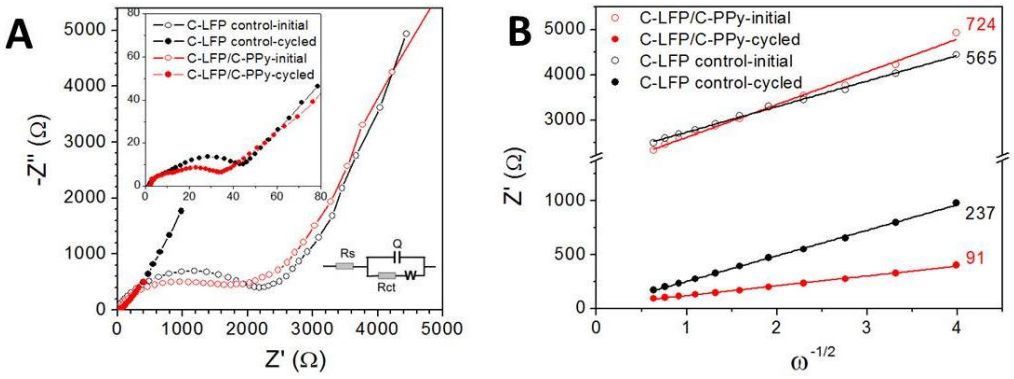

Figure 3.24 Nyquist curves and the Warburg plots of different electrodes before and after the first cycle.

	Rsl	**Rct**	**Warburg Coefficient**
C-LFP control_initial	2.5	1868	565
C-LFP control_after one cycle	2.5	35	237
C-LFP/C-PPy_initial	45.3	1563	724
C-LFP/C-PPy_after one cycle	1.85	35.4	91

Table 3.3 EIS test results of different samples before and after first cycle's charge/discharge.

Randles-Sevcik equation was also used to calculate the lithium ion diffusion coefficients of C-LFP/C-PPy hybrid gel framework during charge/discharge:[57]

$$I_{pc} = 2.69 \times 10^5 n^{3/2} A D^{1/2} C \upsilon^{1/2}$$

where I_{pc} is the peak current (A), n is the number of electrons in the charge-transfer step (for $LiFePO_4$, n = 1), A is the surface area of electrode (cm^2), D is the Li-ion diffusion

coefficient in $LiFePO_4$ at 298 K ($cm^2\ s^{-1}$), C is the molar concentration of Li ions in $LiFePO_4$ (2.28×10^{-2} mol cm^{-3}), and υ is the scan rate ($V\ s^{-1}$). Cyclic voltammetry profiles of C-LFP/C-PPy hybrid gel framework at different scanning rates are shown in Figure 25A and the peak current is in linear response to the square root of scanning rate (Figure 25B). The C-LFP/C-PPy hybrid gel framework shows average cathodic and anodic diffusion coefficients of 1.42×10^{-12} $cm^2\ s^{-1}$ and 8.34×10^{-13} $cm^2\ s^{-1}$, respectively. The average cathodic and anodic diffusion coefficients of the control sample are calculated to be 3.49×10^{-13} $cm^2\ s^{-1}$ and 1.91×10^{-13} $cm^2\ s^{-1}$, respectively (Figure 25C and 25D). The results from EIS and CV studies demonstrate that the improved rate performance of hybrid gel framework results from the promoted diffusion of lithium ions in the whole electrode, which contributes to. The hierarchically porous structure of gel framework can improve the uptake of electrolyte and the uniform polymer coating with high solvent compatibility may lower the ion transfer resistance.

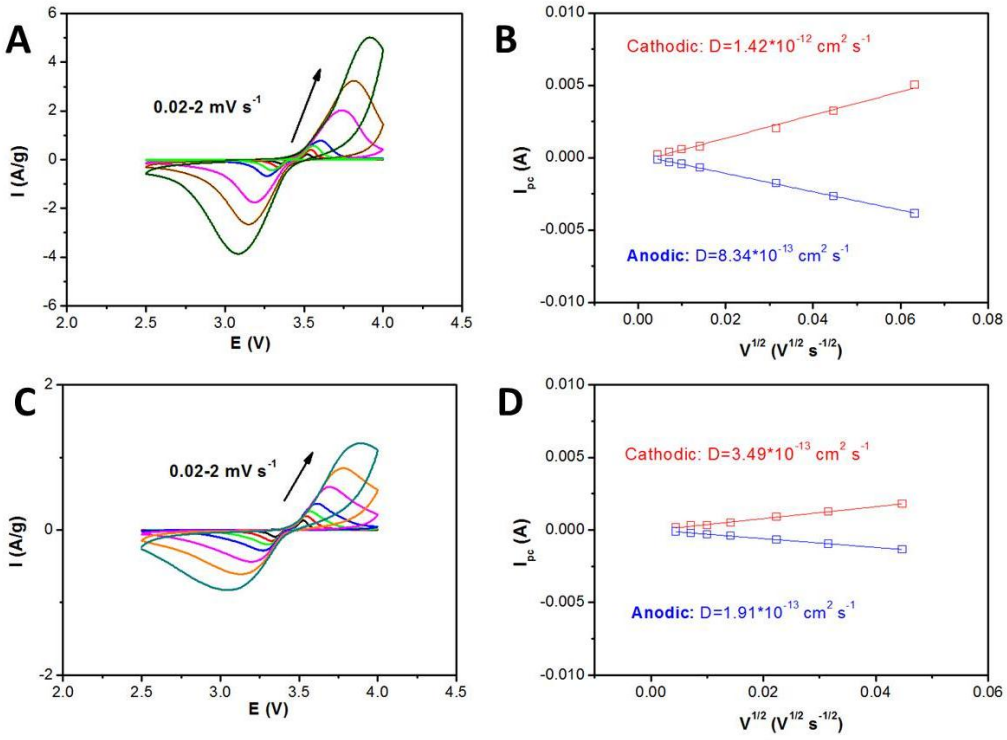

Figure 3.25 (A) Cyclic voltammetry profiles of C-LFP/C-PPy hybrid gel framework at different scanning rates. (B) The average cathodic and anodic diffusion coefficients of C-LFP/C-PPy hybrid gel framework were calculated from the linear relationship between peak current and the square root of scanning rate. (C) Cyclic voltammetry profiles of control sample at different scanning rates. (D) The average cathodic and anodic diffusion coefficients of control sample were calculated from the linear relationship between peak current and the square root of scanning rate.

The cyclic stability of C-LFP/C-PPy hybrid gel framework was also investigated at both low and high current densities. Figure 26A shows the cyclic performance of C-LFP/C-PPy hybrid gel framework and control sample at 1C. The C-LFP/C-PPy hybrid gel framework delivers an initial discharge capacity of 140 mAh g^{-1} and achieved capacity retention of 75% after 500 cycles while the control sample exhibits an initial discharge capacity of 102 mAh g^{-1} and 55.4% capacity retention after 500 cycles' charge/discharge. Figure 26B shows the cyclic performance of C-LFP/C-PPy hybrid gel

framework and control sample at 20C. The gel framework can maintain a discharge capacity of ~80 mAh g^{-1} for over 1000 cycles while the control sample shows the capacity less than 40 mAh g^{-1}. Notably, except for the first cycle, the Coulombic efficiency of C-LFP/C-PPy hybrid gel framework stays near 100% during the whole cyclic tests at 1C and 20C, demonstrating its excellent reversibility.

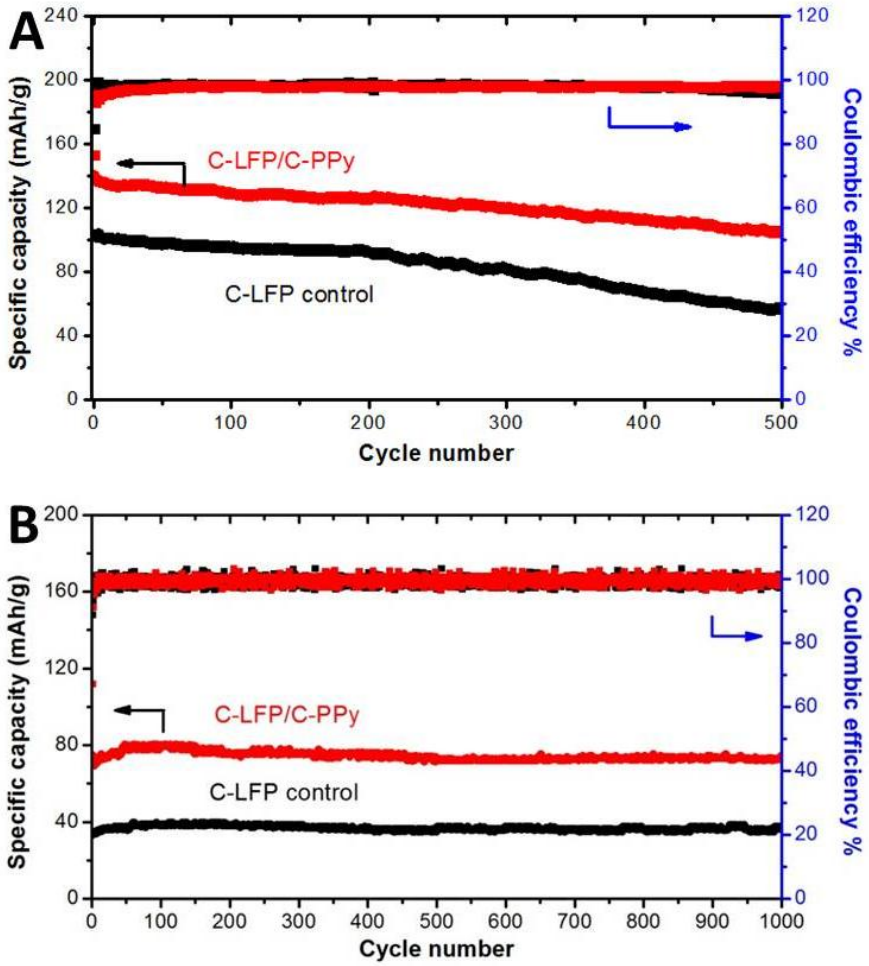

Figure 3.26 Cyclic performance of different electrodes at (A) 1C and (B) 20C, respectively.

The microstructure and morphology of C-LFP/C-PPy hybrid gel framework and control sample after cycling were also studied. As shown in Figure 27A, the C-LFP/C-PPy hybrid gel framework maintains its porous structure and connects active particles with each other after 500 cycles' charge/discharge, indicating the decent mechanical robustness of the gel framework (Figure 27B). Nanostructured PPy gel framework overcomes poor flexibility due to their rigid backbones caused by highly conjugated ring structure and exhibits structure derived elastic modulus to sustain the mechanical change and maintain the 3D nanostructure during electrochemical reactions.[12] EDX mapping on the cycled gel framework is shown in Figure 28C, indicating firm coating of a polymer layer on the LFP particles. The conductive polymer layer demonstrates its excellent chemical/physical stability owing to the strong interactions between polymeric chains and active particles, as well as the mechanical flexibility of gel framework.[62, 63]

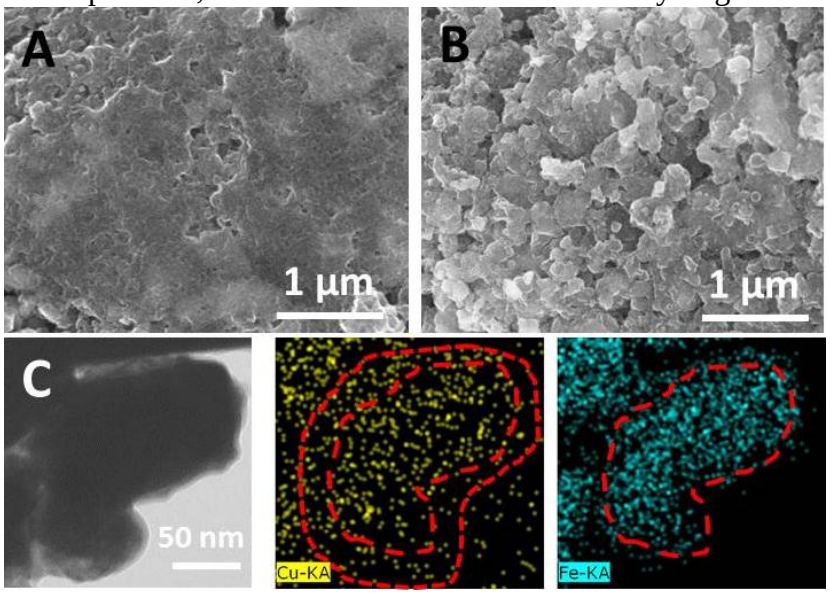

Figure 3.27 (A-B) SEM images of the control electrode and C-LFP/C-PPy hybrid gel after cycling, respectively. (C) EDX mapping of C-LFP/C-PPy hybrid gel electrode after cycling.

3.4 CONCLUSIONS

In summary, a supramolecular self-assembly approach is developed to controllably synthesize nanostructured conductive gels using a disc-shaped liquid crystal molecular CuPcTs as a dopant and cross-linking gelator. The supramolecular self-assembled conductive polymer gels show greatly improved electrical conductivity, thus boosting high-performance when they are used as supercapacitor electrode materials.

A facile and scalable synthesis route is also developed for a conductive PPy gel with tunable 3D microstructures as electroactive materials for high-performance flexible solid-state supercapacitors. Flexible symmetric PPy hydrogel supercapacitors were demonstrated promising capacitive properties and good electrochemical stability during long-term cycling. Even with high PPy loading and at bending/folding states, the electrodes can still offer good rate capabilities and high specific capacitance. The structure-controlled conductive hydrogels with tunable electrochemical properties and mechanical flexibility represent a promising material platform for emerging flexible energy storage devices.

CPGs have been also demonstrated as a high-performance binder system for lithium ion battery electrodes. The 3D nanostructured conductive polymer gel framework can significantly improve performance of active inorganic nanoparticle based electrodes in next-generation high-capacity LIBs for markedly enhanced rate capability and cycling stability. It's attributed to the unique 3D nanostructured conductive gel framework serving as both binder material and 3D conductive network, thus ensuring electron transport to every part of the electrode. The porous structure also facilitates ion transport through the matrix. In addition, the polymer gel can form a uniform coating on each active particle, which can prevent the aggregation of active particles. The robust gel framework can also accommodate the volume change during electrochemical reactions

and maintain the integrity of electrodes. The mass ratio of active material in the hybrid gel based electrode can reach as high as 85%, which can significantly enhance the gravimetric energy density of the battery. As a result, the hybrid electrode with PPy gel framework and both anode and cathode materials showed significantly enhanced electrochemical characteristics, as the high specific capacities and rate characteristics were achieved. In addition, the tunable microstructure and conductive properties of the gel framework also help control transport properties within electrodes. It was demonstrated that the distribution of active particles, the microstructure of the electrode and conductivity of the conductive matrix play important roles in both electron and ion transport, thus determining the resulting electrochemical performance. The conductive gel framework can be applied for other high-capacity inorganic electrode materials and represents a promising framework electrode material for next-generation LIBs.

3.5 REFERENCES

1. G. Yu, X. Xie, L. Pan, Z. Bao and Y. Cui, *Nano Energy*, 2013, **2**, 213-234.
2. A. Yoshino, *Angewandte Chemie International Edition*, 2012, **51**, 5798-5800.
3. J. B. Goodenough and K.-S. Park, *Journal of the American Chemical Society*, 2013, **135**, 1167-1176.
4. J. B. Goodenough, *Energy & Environmental Science*, 2013.
5. Z. Wang, D. O. Carlsson, P. Tammela, K. Hua, P. Zhang, L. Nyholm and M. Strømme, *ACS Nano*, 2015, **9**, 7563-7571.
6. A. Rudge, J. Davey, I. Raistrick, S. Gottesfeld and J. P. Ferraris, *Journal of Power Sources*, 1994, **47**, 89-107.
7. L. Pan, G. Yu, D. Zhai, H. R. Lee, W. Zhao, N. Liu, H. Wang, B. C.-K. Tee, Y. Shi, Y. Cui and Z. Bao, *Proceedings of the National Academy of Sciences*, 2012, **109**, 9287-9292.
8. N. J. Dudney and J. Li, *Science*, 2015, **347**, 131-132.
9. H. Zhao, Z. Wang, P. Lu, M. Jiang, F. Shi, X. Song, Z. Zheng, X. Zhou, Y. Fu, G. Abdelbast, X. Xiao, Z. Liu, V. S. Battaglia, K. Zaghib and G. Liu, *Nano Letters*, 2014.

10. A. S. Arico, P. Bruce, B. Scrosati, J.-M. Tarascon and W. van Schalkwijk, *Nat Mater*, 2005, **4**, 366-377.

11. Y. Wang, Y. Shi, L. Pan, Y. Ding, Y. Zhao, Y. Li, Y. Shi and G. Yu, *Nano Letters*, 2015.

12. Y. Shi, L. Pan, B. Liu, Y. Wang, Y. Cui, Z. Bao and G. Yu, *Journal of Materials Chemistry A*, 2014, **2**, 6086-6091.

13. Y. Shi, X. Zhou, J. Zhang, A. M. Bruck, A. C. Bond, A. C. Marschilok, K. J. Takeuchi, E. S. Takeuchi and G. Yu, *Nano Letters*, 2017, **17**, 1906-1914.

14. G. H. Gelinck, H. E. A. Huitema, E. van Veenendaal, E. Cantatore, L. Schrijnemakers, J. B. P. H. van der Putten, T. C. T. Geuns, M. Beenhakkers, J. B. Giesbers, B.-H. Huisman, E. J. Meijer, E. M. Benito, F. J. Touwslager, A. W. Marsman, B. J. E. van Rens and D. M. de Leeuw, *Nat Mater*, 2004, **3**, 106-110.

15. V. L. Pushparaj, M. M. Shaijumon, A. Kumar, S. Murugesan, L. Ci, R. Vajtai, R. J. Linhardt, O. Nalamasu and P. M. Ajayan, *Proceedings of the National Academy of Sciences*, 2007, **104**, 13574-13577.

16. M. Armand and J. M. Tarascon, *Nature*, 2008, **451**, 652-657.

17. T. Janoschka, M. D. Hager and U. S. Schubert, *Advanced Materials*, 2012, **24**, 6397-6409.

18. P. Simon and Y. Gogotsi, *Nat Mater*, 2008, **7**, 845-854.

19. M. Winter and R. J. Brodd, *Chemical Reviews*, 2004, **104**, 4245-4270.

20. W. Chen, R. B. Rakhi, L. Hu, X. Xie, Y. Cui and H. N. Alshareef, *Nano Letters*, 2011, **11**, 5165-5172.

21. F. Meng and Y. Ding, *Advanced Materials*, 2011, **23**, 4098-4102.

22. M. Wu, X. Xiao, N. Vukmirovic, S. Xun, P. K. Das, X. Song, P. Olalde-Velasco, D. Wang, A. Z. Weber, L.-W. Wang, V. S. Battaglia, W. Yang and G. Liu, *Journal of the American Chemical Society*, 2013, **135**, 12048-12056.

23. P. L. Taberna, S. Mitra, P. Poizot, P. Simon and J. M. Tarascon, *Nature Materials*, 2006, **5**, 567-573.

24. Y. Orikasa, Y. Gogyo, H. Yamashige, M. Katayama, K. Chen, T. Mori, K. Yamamoto, T. Masese, Y. Inada, T. Ohta, Z. Siroma, S. Kato, H. Kinoshita, H. Arai, Z. Ogumi and Y. Uchimoto, *Scientific Reports*, 2016, **6**, 26382.

25. Y. Shi, L. Peng, Y. Ding, Y. Zhao and G. Yu, *Chemical Society Reviews*, 2015, **44**, 6684-6696.

26. X. Yang, Y. Chen, M. Wang, H. Zhang, X. Li and H. Zhang, *Advanced Functional Materials*, 2016, DOI: 10.1002/adfm.201604229.

27. R. C. de Guzman, J. Yang, M. M.-C. Cheng, S. O. Salley and K. Y. Simon Ng, *Journal of Materials Science*, 2013, **48**, 4823-4833.

28. J. K. Lee, K. B. Smith, C. M. Hayner and H. H. Kung, *Chemical Communications*, 2010, **46**, 2025-2027.

29. K. W. Knehr, N. W. Brady, C. A. Cama, D. C. Bock, Z. Lin, C. N. Lininger, A. C. Marschilok, K. J. Takeuchi, E. S. Takeuchi and A. C. West, *Journal of The Electrochemical Society*, 2015, **162**, A2817-A2826.

30. K. W. Knehr, N. W. Brady, C. N. Lininger, C. A. Cama, D. C. Bock, Z. Lin, A. C. Marschilok, K. J. Takeuchi, E. S. Takeuchi and A. C. West, *ECS Transactions*, 2015, **69**, 7-19.

31. A. M. Bruck, C. A. Cama, C. N. Gannett, A. C. Marschilok, E. S. Takeuchi and K. J. Takeuchi, *Inorg Chem Front*, 2016, **3**, 26-40.

32. Y. H. Kwon, M. M. Huie, D. Choi, M. Chang, A. C. Marschilok, K. J. Takeuchi, E. S. Takeuchi and E. Reichmanis, *ACS Applied Materials & Interfaces*, 2016, **8**, 3452-3463.

33. D. C. Bock, C. J. Pelliccione, W. Zhang, J. Wang, K. W. Knehr, J. Wang, F. Wang, A. C. West, A. C. Marschilok, K. J. Takeuchi and E. S. Takeuchi, *ACS Applied Materials & Interfaces*, 2016, **8**, 11418-11430.

34. H. Ji, L. Zhang, M. T. Pettes, H. Li, S. Chen, L. Shi, R. Piner and R. S. Ruoff, *Nano Letters*, 2012, **12**, 2446-2451.

35. H. Zhong, A. He, J. Lu, M. Sun, J. He and L. Zhang, *Journal of Power Sources*, 2016, **336**, 107-114.

36. J.-M. Kim, H.-S. Park, J.-H. Park, T.-H. Kim, H.-K. Song and S.-Y. Lee, *ACS Applied Materials & Interfaces*, 2014, **6**, 12789-12797.

37. G. Liu, S. Xun, N. Vukmirovic, X. Song, P. Olalde-Velasco, H. Zheng, V. S. Battaglia, L. Wang and W. Yang, *Advanced Materials*, 2011, **23**, 4679-4683.

38. Y. H. Kwon, K. Minnici, M. M. Huie, K. J. Takeuchi, E. S. Takeuchi, A. C. Marschilok and E. Reichmanis, *Chemistry of Materials*, 2016.

39. K. Kirshenbaum, D. C. Bock, C.-Y. Lee, Z. Zhong, K. J. Takeuchi, A. C. Marschilok and E. S. Takeuchi, *Science*, 2015, **347**, 149-154.

40. C. He, S. Wu, N. Zhao, C. Shi, E. Liu and J. Li, *ACS Nano*, 2013, **7**, 4459-4469.

41. Y. Chen, H. Xia, L. Lu and J. M. Xue, *J. Mater. Chem.*, 2012, **22**, 5006-5012.

42. Y. Wang, Y. Shi, L. Pan, Y. Ding, Y. Zhao, Y. Li, Y. Shi and G. Yu, *Nano Letters*, 2015, **15**, 7736-7741.

43. W.-M. Zhang, X.-L. Wu, J.-S. Hu, Y.-G. Guo and L.-J. Wan, *Advanced Functional Materials*, 2008, **18**, 3941-3946.

44. M. T. Ramesan, *Journal of Applied Polymer Science*, 2013, **128**, 1540-1546.

45. D. He, L. Li, F. Bai, C. Zha, L. Shen, H. H. Kung and N. Bao, *Chemistry – A European Journal*, 2016, **22**, 4454-4459.

46. X. Y. Qin, H. R. Zhang, J. X. Wu, X. D. Chu, Y. B. He, C. P. Han, C. Miao, S. A. Wang, B. H. Li and F. Y. Kang, *Carbon*, 2015, **87**, 347-356.

47. Y. Jiang, Z.-J. Jiang, L. Yang, S. Cheng and M. Liu, *Journal of Materials Chemistry A*, 2015, **3**, 11847-11856.

48. E. Kang, Y. S. Jung, A. S. Cavanagh, G.-H. Kim, S. M. George, A. C. Dillon, J. K. Kim and J. Lee, *Advanced Functional Materials*, 2011, **21**, 2430-2438.

49. S. Laruelle, S. Grugeon, P. Poizot, M. Dollé, L. Dupont and J.-M. Tarascon, *Journal of The Electrochemical Society*, 2002, **149**, A627-A634.

50. S. H. Lee, S.-H. Yu, J. E. Lee, A. Jin, D. J. Lee, N. Lee, H. Jo, K. Shin, T.-Y. Ahn, Y.-W. Kim, H. Choe, Y.-E. Sung and T. Hyeon, *Nano Letters*, 2013, **13**, 4249-4256.

51. X. Qin, H. Zhang, J. Wu, X. Chu, Y.-B. He, C. Han, C. Miao, S. Wang, B. Li and F. Kang, *Carbon*, 2015, **87**, 347-356.

52. Y. Zuo, G. Wang, J. Peng, G. Li, Y. Ma, F. Yu, B. Dai, X. Guo and C.-P. Wong, *Journal of Materials Chemistry A*, 2016, **4**, 2453-2460.

53. L. Zhao, M. Gao, W. Yue, Y. Jiang, Y. Wang, Y. Ren and F. Hu, *ACS Applied Materials & Interfaces*, 2015, **7**, 9709-9715.

54. L. Li, A. Kovalchuk, H. Fei, Z. Peng, Y. Li, N. D. Kim, C. Xiang, Y. Yang, G. Ruan and J. M. Tour, *Advanced Energy Materials*, 2015, **5**, 1500171.

55. J. Liu, X. Xu, R. Hu, L. Yang and M. Zhu, *Advanced Energy Materials*, 2016, **6**, 1600256.

56. C. Nan, J. Lu, L. Li, L. Li, Q. Peng and Y. Li, *Nano Res.*, 2013, **6**, 469-477.

57. Y. Zhao, L. Peng, B. Liu and G. Yu, *Nano Letters*, 2014, **14**, 2849-2853.

58. R. A. Hatton, N. P. Blanchard, V. Stolojan, A. J. Miller and S. R. P. Silva, *Langmuir*, 2007, **23**, 6424-6430.

59. L. Atanasoska, K. Naoi and W. H. Smyrl, *Chemistry of Materials*, 1992, **4**, 988-994.

60. Zhang, W. J.; He, X. M.; Pu, W. H.; Li, J. J.; Wan, C. R. *Ionics* **2011**, *17*, 473-477.

61. F. Croce, M. L. Focarete, J. Hassoun, I. Meschini and B. Scrosati, *Energy & Environmental Science*, 2011, **4**, 921-927.

62. L. Luo, P. Zhao, H. Yang, B. Liu, J.-G. Zhang, Y. Cui, G. Yu, S. Zhang and C.-M. Wang, *Nano Letters*, 2015, **15**, 7016-7022.

63. Y. Shi, J. Zhang, A. Bruck, Y. Zhang, J. Li, E. Stach, K. Takeuchi, A. Marschilok, E. Takeuchi, G. Yu, *Advanced Materials*, 2017, DOI: 10.1002/adma.201603922.

Chapter 4 Thermally self-regulating electrochemical energy storage devices based on smart electrolyte and conductive polymer gel electrode*

4.1 INTRODUCTION

During past years, the performance of electrochemical energy storage devices such as lithium-ion batteries and supercapacitors have been significantly enhanced in terms of energy density, power density and cycle life and they have been widely used for consumer electronics.[1-3] However, in large-scale and high-power applications such as electrical vehicles and grid storage, their safety still remains an important issue.[4-7] Due to their high power and current density, electrochemical storage devices generate vast heat, especially in ultrafast charging and discharging processes or abusive conditions such as shorting and overcharging could increase the internal cell temperature and pressure, which may lead to risks of fire or explosion.[8] Hence, it is very important to control thermal runaway and develop safe electrochemical energy storage devices with high rate and capacity.

It is difficult to detect thermal runaway by external devices since temperature and pressure increases can occur in such a short time, researchers believe internal safety strategies are more effective in preventing thermal runaway and have been widely studied.[9, 10] People developed alternative electrolytes, such as solid-state electrolytes or polymer gel electrolytes with low conductivity to suppress the origin of heat generation, but they may lead to an invariably low charge and discharge rate at different temperatures.[11, 12] Physical designs such as safety vents, thermal fuses, shutdown separators, and extinguishing agents can release or absorb the heat accumulated in the

* Y. Shi, H. Ha, A. Al-Sudani, C.J. Ellison, G. Yu, Thermoplastic Elastomer Enabled Smart Electrolyte for Thermoresponsive Self-Protection of Electrochemical Storage Devices, *Adv. Mater.*, 2016, 28, 7921.
Y. S. carried out the experimental work and participated in the preparation of manuscript.

devices before thermal runaway, but they are passive strategies to solve the problem.[13-15] Conductive polymers with positive temperature coefficients (PTC) can shut down the current passage in or between neighboring particles at elevated temperature,[16-18] but they exhibit low room-temperature conductivity and considerable leakage current. People also incorporate additives including flame retardant (FR) and overcharge additives in electrochemical devices.[6, 19-21] However, the overall ionic conductivity of the electrolyte decreases due to that large amounts of these additives are required to ensure a high level of cell safety. These above-mentioned strategies lack reversibility or low conductivity, resulting in electrochemical devices without a smart, self-adaptive response to temperature change.

Recently, responsive polymers with sol-gel transition properties were used for electrolytes to address the thermal runaway of electrochemical storage devices.[8, 22] Electrochemical devices with dynamic and reversible thermal self-protection can be fabricated through this smart and active strategy since the device can change charge–discharge rates depending on temperature yet return to original states once the temperature is restored to normal. Poly(N-isopropylacrylamide) (PNIPAM) based copolymers have been explored for this purpose.[8, 22] However, since the synthesis is complicated and the fact the transition temperature is restricted to a narrow range around the lower critical solution temperature (LCST) of PNIPAM, this strategy is not desirable for practical applications.

In this chapter, a thermoresponsive gel system based on a thermoplastic elastomer is used to develop electrolyte with a reversible sol-gel transition (Figure 1).[23] Thermoplastic elastomers are a class of copolymers or a physical mix of polymers which combine both thermoplastic and elastomeric properties.[24] In this study, a Pluronic [poly(ethylene oxide)-block-poly(propylene oxide)-block-poly(ethylene oxide) (PEO-

PPO-PEO)] aqueous solution dissolved with ions such as H^+ or Li^+ is developed as a smart electrolyte which enables a thermoresponsive electrochemical device with a highly desirable self-protection function. Mechanistic studies reveal that at low temperature, the ions can move freely since the Pluronic-based electrolyte is in the solution state. When temperature increases, the motion of ions is inhibited due to the transformation of electrolyte to a gel state, which finally shuts down the electrochemical devices. This smart electrolyte system shows several advanced features: 1) because the sol-gel transition of the Pluronic solution is fast, significant and reversible, the system is sensitive to temperature change and the self-protection behavior is highly effective and reversible. 2) It is easy to tune the temperature threshold for triggering device self-protection since the transition temperature of the Pluronic solution can be tuned over a wide range by various methods, such as tuning concentration, changing average molecular weight (MW) of the polymer, etc.[25, 26] 3) It is possible to control the degree of capacity loss from ~50% to nearly 100% by using Pluronic with different molecular weights. 4) Pluronic is commercially available at low cost, and the smart electrolyte is compatible with different electrode materials and different conductive ions, thus being suitable for a wide range of applications. This suggests that thermoplastic elastomers dissolved in organic solvents are promising for thermoresponsive electrochemical devices such as lithium ion batteries and fuel cells.

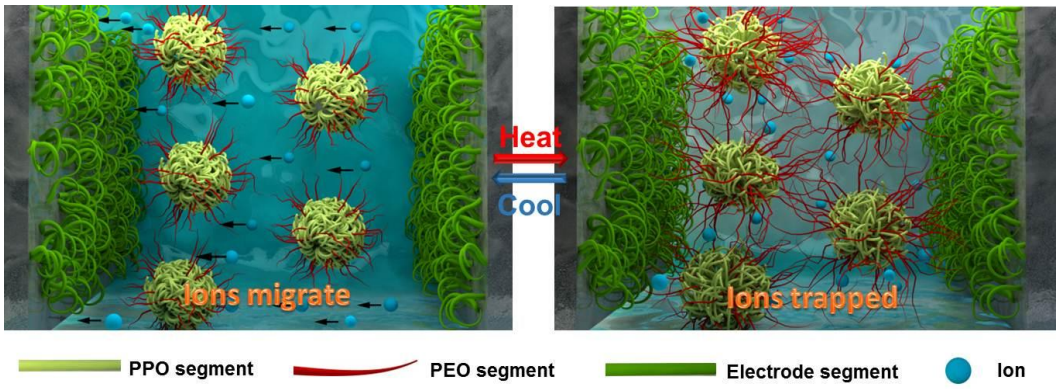

Figure 4.1 Schematic illustration of a thermally responsive gel system used as an electrolyte in electrochemical storage devices. Upon heating, the sol-gel transition of the thermoplastic elastomer solution inhibits the motion of ions, thus actively shutting down the device at high temperature.

4.2 THERMORESPONSIVE ELECTROLYTE BASED ON PLURONIC SOLUTIONS

Chosen amount of Pluronic was added into 50 mL deionized (DI) water to prepare the electrolyte and the mixture was placed at 0 ℃ under vigorous stirring overnight. After the Pluronic solution was formed, a certain amount of H_2SO_4 or $LiNO_3$ was added into the solution to achieve desired ion concentrations.

A temperature dependent rheological test is used to demonstrate the reversible transitions of Pluronic solutions (Figure 2a) and a corresponding general phase diagram is shown in Figure 2b.[27] The 30 wt% Pluronic solution (MW ~5800 Da, henceforth referred to as P5800) first shows a sol to gel transition around 20 ℃ with a significant increase in storage modulus (G'). The block structure of the hydrophilic and hydrophobic polymer segments drives the Pluronic to form micelles at a low temperature such that the solution flows freely. As the temperature increases, the entanglement of stretched PEO segments causes the formation of closely packed spherical micelles and thus the first sol-gel transition. A second sol-gel transition occurs for Pluronic solutions with concentrations higher than the critical concentration (which is related to molecular weight and ratio of

the PEO block to PPO block), as the temperature further increases. The gel first transfers to sol state by dehydrating the hydrophilic shell layer in the packed micelles and then changes to a gel state again because of the physical crosslinking effect between hydrophobic chains.[27, 28] Figure 1c shows the organization of a corresponding Pluronic solution in the sol and gel states.

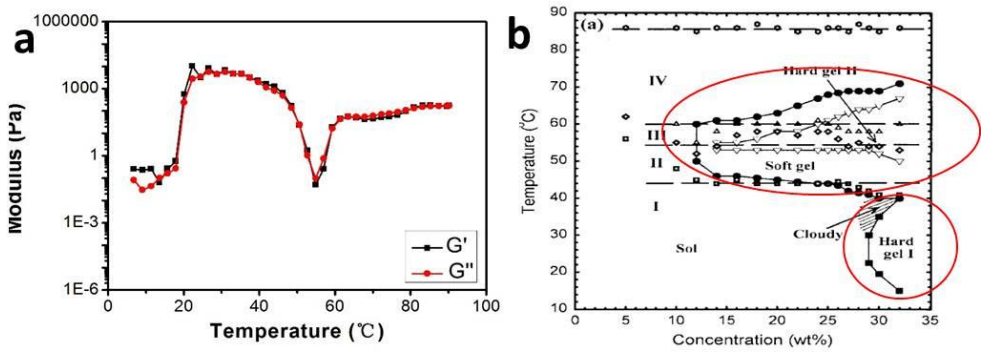

Figure 4.2 (a) The temperature dependent rheological behavior of a 30 wt% Pluronic solution where G' and G" signify the storage and loss modulus, respectively. (b) A general phase diagram of 30 wt% Pluronic solution.

In the smart electrolyte system, it is possible to tune the transition temperature by adjusting the concentration of Pluronic in the solution. The temperature dependent G' values for P5800 at different concentrations is shown in Figure 3. The sol-gel transition temperature of a Pluronic solution can be roughly presented by the temperature at which the G' value increases suddenly.[29, 30] The results indicate that the transition temperature can be tuned from 20 ℃ to above 80 ℃ when the concentration varies from 30 wt% to 5 wt%. The reason is that the decreased concentration of Pluronic solution increases the average inter-distance between micelles and leads to higher thermal energy to drive the polymer chains to stretch enough to entangle with each other.[31]

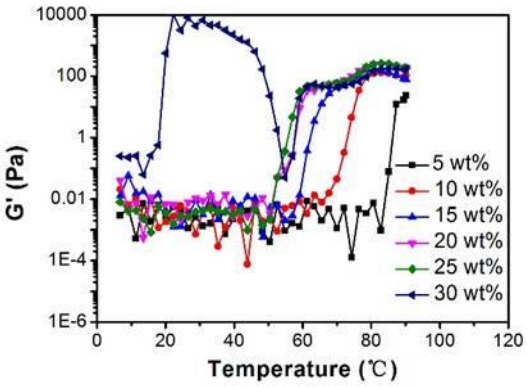

Figure 4.3 The temperature dependent G' value curves for P5800 with different concentrations.

It is also possible to tune the sol-gel transition behavior of Pluronic-based smart electrolyte by changing the MW of polymers. Figure 4 shows the sol-gel transition temperatures of Pluronic solutions with different MWs calculated from temperature-dependent rheological experiments. Clearly, as the molecular weight is increased, the sol-gel transition temperature of the Pluronic solution decreased, showing the temperature can be tuned from above 90 ℃ to room temperature. More importantly, more dramatic changes in G' values after the sol-gel transition can be observed in Pluronic solutions with higher MWs. The solutions with higher MW behave more solid-like in their gel state, indicating greater potential to restrict the motion of ions. It is postulated that as the MW of polymer chains is increased, the polymer chains become more stretched in the solution and have increased possibility of forming entanglements with each other, thus reaching the gelation point at lower temperature.[32]

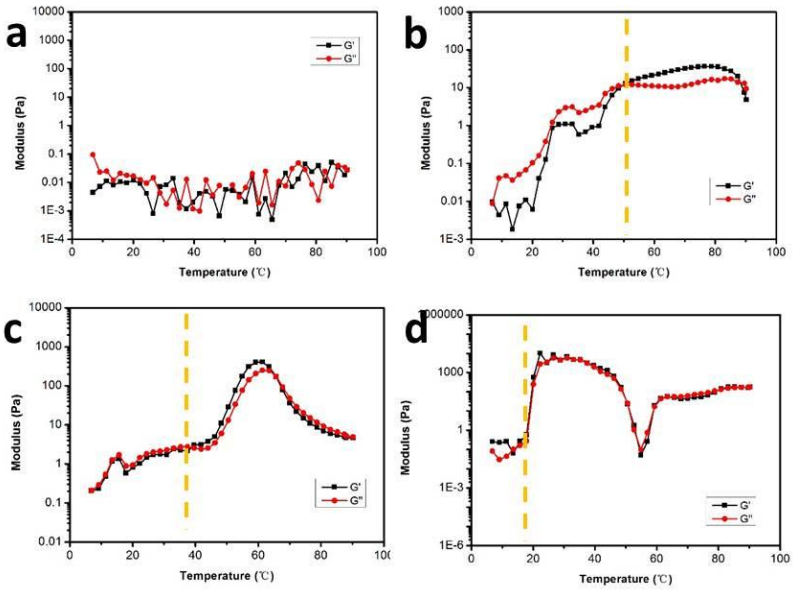

Figure 4.4 Temperature dependent rheological experiments for Pluronic solutions with different average molecular weight: the Pluronic solutions with (a) P2000, (b) P2800, (c) P4400, and (d) P5800.

Impedance tests on coin cell based devices without electrode materials were conducted to understand the inhibition effect of ion transport during the sol-gel transition of the Pluronic-based electrolyte. The impedance of a supercapacitor is mainly determined by two processes: the charge transfer at the electrode–electrolyte interface during a fast change in voltage and the diffusion of conductive ions in the electrolyte during a slow change in voltage. A Nyquist impedance plot reflects the carrier transport properties and the reaction in the electrode interface and can be used to estimate the values of the circuit parameters. The ionic conductivity (δ) can be calculated by Equation 1:[33]

$$\delta = \frac{1}{R_b} \frac{\mathrm{d}}{S} \quad (1)$$

where d is the thickness of electrolyte layer, S is the area of an electrode and R_b is the bulk resistance which can be estimated according to the diameter of the semicircle in the

high-frequency region in the impedance plot. Four Pluronic-based electrolytes using polymers with different MW and different ions in the sol and gel states were tested. The corresponding ionic conductivities were calculated and are listed in Table 1. For all electrolytes, two orders of magnitude decrease of the ionic conductivities can be found from the sol to the gel state, indicating the restriction of ion transport in the gel matrix. The electrolytes using P4400 exhibited lower ionic conductivities in the gel state, which was reasonable since larger polymer chains would be entangled more densely. The electrolytes using Li^+ ions showed lower ionic conductivities when compared to those using H^+ as the transporting ions since ions with larger radius are easier to be trapped by the entangled polymer chains. This is another indication that the self-protection behavior of our electrochemical devices is induced by the inhibition effect of gelation behavior.

Electrolyte	**Ionic conductivity (S/cm)**	
	Sol	Gel
MW 2800-H_2SO_4	3.90×10^{-3}	2.72×10^{-5}
MW 2800-$LiNO_3$	7.80×10^{-4}	5.52×10^{-5}
MW 4400-H_2SO_4	4.65×10^{-3}	1.62×10^{-5}
MW 4400-$LiNO_3$	1.89×10^{-3}	1.58×10^{-5}

Table 4.1 Ionic conductivities in the sol and gel states of four Pluronic-based electrolytes using polymers with different average molecular weights and different ions.

4.3 ELECTROCHEMICAL ENERGY STORAGE DEVICES WITH THERMORESPONSIVE SELF-PROTECTION BEHAVIOR

Thermoresponsive self-protection for electrochemical storage devices can be achieved since the first sol-gel transition of Pluronic solutions can be triggered by temperature. When the temperature is higher than the sol-gel transition point, the gelation

of Pluronic solution can inhibit the motion of ions in the gel matrix, thus shutting down the device. The thermoresponsive self-protection was first demonstrated in a three-electrode system. P5800 dissolved with 0.5 M H_2SO_4 was used as the electrolyte and the conductive polymer polypyrrole gel (PPy) on carbon paper was used as the working electrode. The capacitor functioned properly in an ice water bath, yielding specific capacitance as high as 220 F/g and good rate performance with ~8% capacitance loss when current density was increased by a factor of 10. When the temperature increased to 25 ℃, the system stopped working due to the gelation of the Pluronic solution within a few seconds, indicating that the motion of ions was significantly restricted in the Pluronic gel. The system was found to work well again when the temperature was decreased below 25 ℃. To further approach electrochemical devices for practical applications, symmetric supercapacitors in coin cells were assembled. They work properly when the electrolyte was in the sol state and electrochemical performance was inhibited successfully the device was heated above the sol-gel transition temperature. To maximize the thermoresponsive behavior of the coin cell devices, the amount of electrolyte was optimized and only 200 μL was required. For both the three-electrode system and coin cell device, the thermoresponsive switching behavior was fast, efficient and reversible.

It is possible to tune the thermal-responsive behavior of electrochemical energy storage devices with the change of polymer concentration. 20 wt% P5800 dissolved with aqueous H_2SO_4 was employed as the electrolyte and coin cell supercapacitor devices were assembled. The electrochemical performance was tested at 20 and 70 ℃ and the CV curves are shown in Figure 5a and 5b, respectively. Due to the gelation of electrolyte, the device delivered large capacitance at 20 ℃ and show 50% of the specific capacitance loss at 70 ℃. The charging/discharging test confirmed the change of electrochemical storage performance in Figure 5c. The device exhibited high impedance at high

temperature which was indicated by the larger diameter of the semicircle in the high-frequency range and deviation of the curve from vertical, as shown in the electrochemical impedance spectroscopy (Figure 5d). The transition temperature could be tuned over a wide range and the thermally responsive behavior was retained even at lower concentrations by adjusting the concentration of the Pluronic solution.

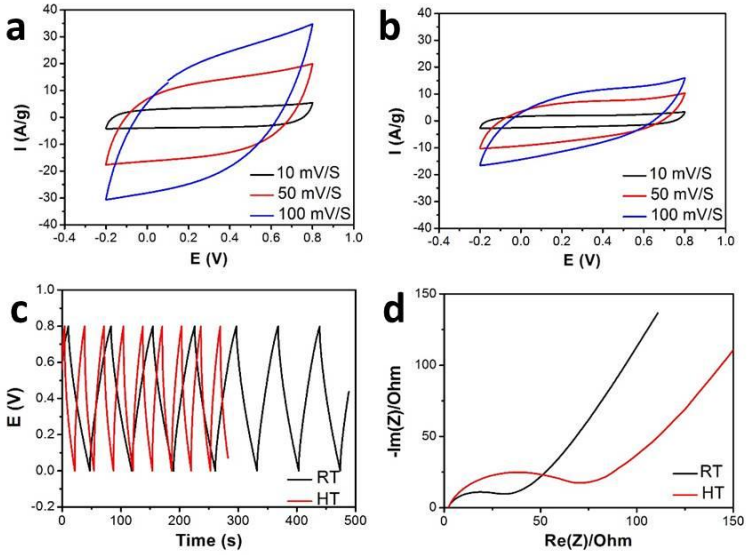

Figure 4.5 (a-d) Electrochemical performance of coin cell based supercapacitor devices using 20 wt% P5800 dissolved with aqueous H_2SO_4 as the electrolyte: The CV curves at 20 (a) and 70 °C (b); (c) The charge/discharge cycle test at room temperature (RT, 20 °C) and high temperature (HT, 70 °C); (d) The impedance test at RT and HT.

Besides the transition temperature, it is also possible to control the extent of capacity loss at high temperature by changing MW. P2800 and P4400 were adopted to prepare thermoresponsive electrolyte (30 wt%). The CV curves at different scanning rates for supercapacitor devices using P2800 dissolved with aqueous H_2SO_4 as the electrolyte at 20 and 70 ℃ are shown Figure 6a and 6b, respectively. Based on the CV tests, the specific capacitances were calculated to be 110 and 10 F/g in the sol and gel states,

indicating significant inhibition of its electrochemical storage performance at high temperature (~91% capacity loss). The supercapacitor device was heated during single charge/discharge tests to validate the effectiveness of the proposed system. And as expected, the device stopped working right after the temperature reached the sol-gel transition point, demonstrating the fast and efficient thermoresponsive self-protection. Similar tests were conducted for supercapacitors using P4400 as the electrolyte at 20 and 60 ℃ (most solid-like state), as shown in Figure 6c and 6d. Nearly 100% capacity loss was achieved, showing even more significant suppression of electrochemical performance. In previous studies of smart electrolytes, the degree of capacity loss after the sol-gel transition was fixed. Only ~35% and ~85% decrease in capacity was obtained in Chen's and Roberts' work, respectively.[8, 22] The strategy of using Pluronic solutions with different concentrations and MWs as electrolytes enabled efficient and controllable thermoresponsive suppression of electrochemical performance within a wide, tunable temperature range.

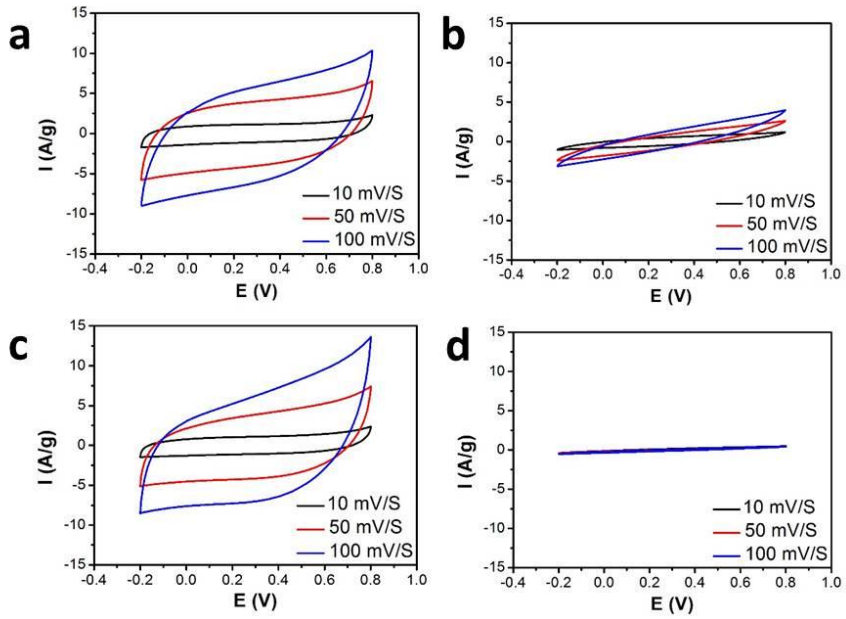

Figure 4.6 (a) and (b) CV curves at different scanning rates for supercapacitor devices using MW ~2800 Da Pluronic solution as the electrolyte at 20 (a) and 70 °C (b). (c) and (d) CV curves at different scanning rates for supercapacitor devices using P4400 as the electrolyte at 20 (c) and 60 °C (d).

In electrochemical devices, the electrode materials contribute to various key properties such as energy densities and different active materials have been developed for different applications. The thermoresponsive electrolyte system should be applicable to different electrode materials without harming their energy density, charging-discharging rates, and mass loading. To demonstrate the universality of our Pluronic-based smart electrolyte, activated carbon (AC) and PPy were used as working electrodes to fabricate coin cells and test their electrochemical storage performances at different temperatures. AC serves as the electrochemical double-layer capacitor material and has been commercially applied for fabricating supercapacitors, while PPy is a typical conducting polymer which can serve as a pseudocapacitor material.[34] High specific capacitance above 100 F/g in coin cells are achieved for both of these two materials based electrolytes

at room temperature (Figure 7a and 7b). As a comparison, the interesting supercapacitor developed by Chen et al. using poly(N-isopropylacrylamide) (PNIPAM) based gel electrolyte can only deliver specific capacitance around 50 F/g. More importantly, all these devices using PPy or AC working electrodes show significant thermal-induced self-protection behaviors owing to the sol-gel transition of Pluronic electrolytes. In addition, different ions such as Li^+ and H^+ ions could move freely in the Pluronic solution and supported high ionic conductivity at room temperature while being trapped within the gel matrix at high temperature. This indicates that the Pluronic-based smart electrolytes are promising for applications that require versatile performance in conditions such as low pH and high salinity.

To experimentally demonstrate the thermal self-protection of the supercapacitor using Pluronic solution based electrolyte, we designed a simple circuit using the thermoresponsive supercapacitor and a light-emitting diode (LED).[8] As shown in Figure 7c, the LED bulb was illuminated with high intensity at room temperature. After the supercapacitor was heated to 70 ℃, the intensity of the LED light decreased significantly, indicating the active thermal self-protection of Pluronic solution based supercapacitors.

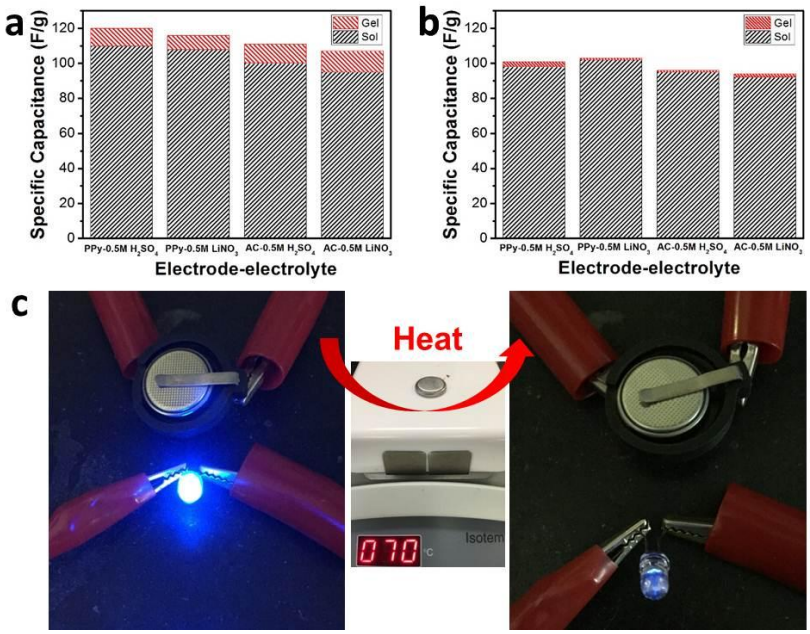

Figure 4.7 Specific capacitance of supercapacitors using Pluronic solution based electrolytes with different electrode materials and conductive ions at sol and gel states: (a) electrolytes based on P2800 and (b) electrolytes based on P4400. (c) Demonstration of thermal self-protection of the supercapacitor using Pluronic solution based electrolyte: the light intensity of the LED bulb decreased significantly upon heating the device to 70 °C.

Temperature dependent CV tests were conducted to demonstrate the effect of the rheological properties of the electrolyte during the sol-gel transition on the electrochemical performance of supercapacitors. We tested the supercapacitors based on an electrolyte containing 30 wt% P2800 from 20 to 70 ℃ at 10 ℃ intervals and compared the electrochemical results with those of temperature dependent rheological experiments. Figure 8a shows the sol-gel transition point of 49 ℃ for 30 wt% P2800 before which the solution shows liquid-like properties with low viscosity. After the transition point, the Pluronic solution becomes more solid-like since the difference between G' and G'' values increases until around 70 °C.[35, 36] The temperature dependent CV tests (Figure 8b) showed a similar trend with the rheological experiments. Before the

transition point, the supercapacitor exhibited almost identical CV curves from 20 to 40 ℃. However, once the temperature was increased to 50 ℃, the specific capacitance showed an obvious loss. The specific capacitance continued to decrease as the temperature increased and finally reached the lowest value at 70 ℃ which is around 10% of the initial capacitance. This indicates that the device can function properly in a wide temperature range before the sol-gel transition then the energy storage capability begins decreasing right after the transition point, thus avoiding burst heat generation. The electrochemical storage performance of the supercapacitor decreased accordingly as shown in both temperature dependent rheological and electrochemical experiments. The steric effect of stretched Pluronic chains at higher temperatures is assumed to inhibit the motion of ions. It should be noted that the diffusion rate of ions in solution and the electronic interaction between Pluronic chains and ions affect the conductivity of electrolyte substantially. The increase in temperature increased the diffusion rate while decreasing the weak electronic interactions between hydroxyl groups on polymer chains and ions resulted in improved electrolyte conductivity. As a result, the sol-gel transition counteracts the temperature effect and efficiently shuts down the device at high temperature.

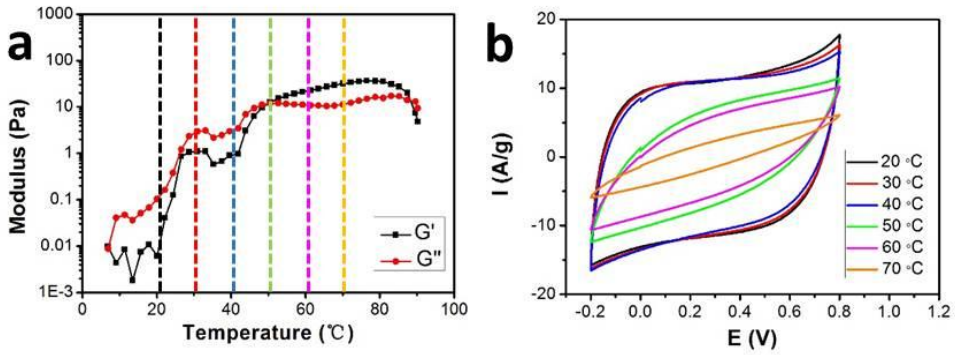

Figure 4.8 (a) Temperature dependent rheological experiments for 30 wt% P2800. (b) Temperature dependent CV tests of supercapacitor based on 30 wt% P2800 electrolyte.

The self-protection behavior of the smart electrolyte system is reversible when compared to traditional strategies for thermally safe electrochemical devices. Supported by the reversibility, it is possible for the device to automatically shut-down at high temperature then later resume its original working state when the device is cooled down. To demonstrate the reversibility of smart electrochemical storage devices based on Pluronic electrolytes, cyclic electrochemical tests were conducted by heating and cooling the devices for multiple times and the specific capacitances were calculated. The cyclic testing results of supercapacitors using P2800 as the electrolyte and PPy and AC as the electrode materials are shown in Figure 9. Both of the devices exhibited high and stable capacitance above 100 F/g during the whole cyclic test in solution states and were able to be shut down successfully when the temperature was increased in each cycle, demonstrating excellent reversibility of the thermoresponsive capacitors.

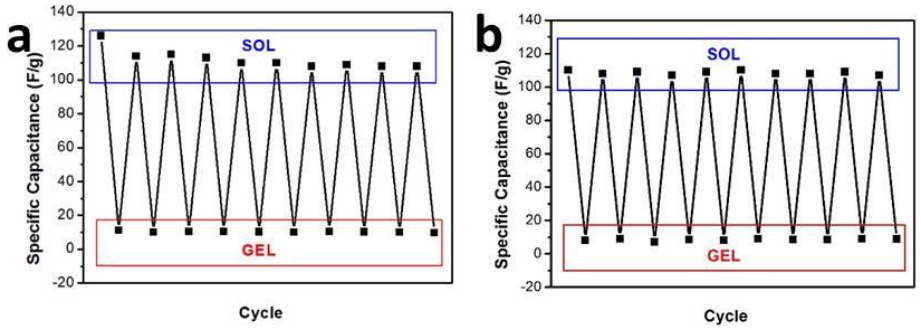

Figure 4.9 Cyclic testing results of supercapacitors using P2800 as the electrolyte and PPy (a) and activated carbon (b) as the electrode materials.

4.4 CONCLUSIONS

In summary, a reversible thermoresponsive electrolyte system is developed to active control and thermal self-protect electrochemical energy storage devices. A commercially available and low-cost thermoplastic elastomer, Pluronic, which shows a fast sol-gel transition process upon heating is employed for the smart electrolyte system. The gelation of Pluronic solution based electrolytes significantly inhibits the migration of ions, leading to a nearly 100% decrease in specific capacitance. Notably, unlike conventional strategies, the device based on this smart electrolyte could deliver high capacitance at normal temperature and the sol-gel transition behavior was highly reversible, which enabled active thermal control of the devices. In addition, it is easy to tune the transition temperature and the degree of capacity loss over a wide range by optimizing the solution concentration and MW of the polymeric material. This system is compatible with various electrode materials and conductive ions, thus being applicable for various applications, such as implantable biodevices and high-temperature energy sources. This Pluronic-based smart electrolyte can be directly employed for designing electrochemical energy storage devices with aqueous electrolytes. Since various thermoplastic elastomers have been synthesized and many of them are soluble in organic

solvents, it is promising to extend the smart electrolyte to other non-aqueous systems such as lithium ion batteries and fuel cells.

4.5 REFERENCES

1. N. Nitta, F. Wu, J. T. Lee and G. Yushin, *Materials Today*, 2015, **18**, 252-264.
2. J. B. Goodenough and K.-S. Park, *Journal of the American Chemical Society*, 2013, **135**, 1167-1176.
3. K. Chen, S. Song, F. Liu and D. Xue, *Chemical Society Reviews*, 2015, **44**, 6230-6257.
4. X. Feng, J. Sun, M. Ouyang, F. Wang, X. He, L. Lu and H. Peng, *Journal of Power* Sources, 2015, **275**, 261-273.
5. J. M. Tarascon and M. Armand, *Nature*, 2001, **414**, 359-367.
6. Q. Wang, P. Ping, X. Zhao, G. Chu, J. Sun and C. Chen, *Journal of Power Sources*, 2012, **208**, 210-224.
7. Z. Chen, P.-C. Hsu, J. Lopez, Y. Li, J. W. F. To, N. Liu, C. Wang, Sean C. Andrews, J. Liu, Y. Cui and Z. Bao, *Nature Energy*, 2016, **1**, 15009.
8. H. Yang, Z. Liu, B. K. Chandran, J. Deng, J. Yu, D. Qi, W. Li, Y. Tang, C. Zhang and X. Chen, *Advanced Materials*, 2015, **27**, 5593.
9. D. P. Finegan, M. Scheel, J. B. Robinson, B. Tjaden, I. Hunt, T. J. Mason, J. Millichamp, M. Di Michiel, G. J. Offer, G. Hinds, D. J. L. Brett and P. R. Shearing, *Nature Communications*, 2015, **6**, 6924.
10. X. M. Feng, X. P. Ai and H. X. Yang, *Electrochemistry Communications*, 2004, **6**, 1021-1024.
11. P.-W. Wu, S. R. Holm, A. T. Duong, B. Dunn and R. B. Kaner, *Chemistry of Materials*, 1997, **9**, 1004-1011.
12. W. H. Meyer, *Advanced Materials*, 1998, **10**, 439-448.
13. H. Wu, D. Zhuo, D. Kong and Y. Cui, *Nat Commun*, 2014, **5**, 5193.
14. Y.-S. Chen, C.-C. Hu and Y.-Y. Li, *Journal of Power Sources*, 2008, **181**, 69-73.
15. T. Yim, M.-S. Park, S.-G. Woo, H.-K. Kwon, J.-K. Yoo, Y. S. Jung, K. J. Kim, J.-S. Yu and Y.-J. Kim, *Nano Letters*, 2015, **15**, 5059-5067.
16. L. Xia, S.-L. Li, X.-P. Ai, H.-X. Yang and Y.-L. Cao, *Energy & Environmental Science*, 2011, **4**, 2845-2848.
17. J.-A. Choi, S. H. Kim and D.-W. Kim, *Journal of Power Sources*, 2010, **195**, 6192-6196.

18. Y. S. Jung, A. S. Cavanagh, L. Gedvilas, N. E. Widjonarko, I. D. Scott, S.-H. Lee, G.-H. Kim, S. M. George and A. C. Dillon, *Advanced Energy Materials*, 2012, **2**, 1022-1027.

19. Y. E. Hyung, D. R. Vissers and K. Amine, *Journal of Power Sources*, 2003, **119–121**, 383-387.

20. L. Zhang, Z. Zhang, H. Wu and K. Amine, *Energy & Environmental Science*, 2011, **4**, 2858-2862.

21. L. Zhang, Z. Zhang, P. C. Redfern, L. A. Curtiss and K. Amine, *Energy & Environmental Science*, 2012, **5**, 8204-8207.

22. J. C. Kelly, M. Pepin, D. L. Huber, B. C. Bunker and M. E. Roberts, *Advanced Materials*, 2012, **24**, 886-889.

23. Y. Shi, H. Ha, A. Al-Sudani, C. J. Ellison and G. Yu, *Advanced Materials*, 2016, **28**, 7921-7928.

24. K. P. Mineart, Y. Lin, S. C. Desai, A. S. Krishnan, R. J. Spontak and M. D. Dickey, *Soft Matter*, 2013, **9**, 7695-7700.

25. V. Lenaerts, C. Triqueneaux, M. Quartern, F. Rieg-Falson and P. Couvreur, *International Journal of Pharmaceutics*, 1987, **39**, 121-127.

26. C. Chaibundit, N. M. P. S. Ricardo, N. M. P. S. Ricardo, C. A. Muryn, M.-B. Madec, S. G. Yeates and C. Booth, *Journal of Colloid and Interface Science*, 2010, **351**, 190-196.

27. M. J. Park, K. Char, H. D. Kim, C.-H. Lee, B.-S. Seong and Y.-S. Han, *Macromolecular Research*, 2002, **10**, 325-331.

28. S. L. Guo, T. J. Hou and X. J. Xu, *The Journal of Physical Chemistry B*, 2002, **106**, 11397-11403.

29. Y. Zhao, Y. Cao, Y. Yang and C. Wu, *Macromolecules*, 2003, **36**, 855-859.

30. K. Nishinari, *Colloid Polym Sci*, 1997, **275**, 1093.

31. Y.-M. Chung, K. L. Simmons, A. Gutowska and B. Jeong, *Biomacromolecules*, 2002, **3**, 511-516.

32. J. P. Mata, P. R. Majhi, C. Guo, H. Z. Liu and P. Bahadur, *Journal of Colloid and Interface Science*, 2005, **292**, 548-556.

33. J. Lopez, Z. Chen, C. Wang, S. C. Andrews, Y. Cui and Z. Bao, *ACS Applied Materials & Interfaces*, 2016, **8**, 2318-2324.

34. G. Yu, X. Xie, L. Pan, Z. Bao and Y. Cui, *Nano Energy*, 2013, **2**, 213-234.

35. C. Ma, Y. Shi, D. A. Pena, L. Peng and G. Yu, *Angewandte Chemie International Edition*, 2015, **54**, 7376-7380.

36. Y. Shi, C. Ma, L. Peng and G. Yu, *Advanced Functional Materials*, 2015, **29**, 1219.

Chapter 5 Multifunctional hybrid gel materials based on conductive polymer gels*

5.1 INTRODUCTION

Multifunctional gel materials are becoming critically important for wide-ranging technological applications, from electronics, biomedical devices, to electrochemical energy devices.[1-3] To enable designed new functionalities, the chemical composition, micro/nano-structures and physical interactions of gel materials need to be delicately controlled. The CPG frameworks possess dense functional groups on the surface and high surface area, thus providing the great possibility for surface modification by either inorganic coatings or polymeric wrapping. With hierarchically porous structure CPGs also serve as a matrix to introduce second polymeric network to construct interpenetrating double network structure. With structure-derived properties and high tunability in structures, the CPGs become a promising platform for the development of multi-functional gel which can be applied for various applications such as responsive electronics, self-healing devices, and smart energy storage devices.

This chapter will firstly discuss on the highly thermoresponsive and conductive hybrid gel synthesized by in situ formation of CPGs within PNIPAM matrix.[4] The resulted hybrid gel exhibits an interpenetrating double network structure which increases the interface and strengthens the interactions between two polymeric networks. This hybrid material successfully inherits the conductive and responsive properties of each component and well maintained the high thermal sensitivity owing to high porosity. More

* Y. Shi, J. Zhang, L. Pan, Y. Shi, G. Yu*, Energy Gels: A Bio-Inspired Material Platform for Advanced Energy Applications, *Nano Today*, 2016, 11, 738.
Y. Shi, C. Ma, L. Peng and G. Yu, Conductive 'Smart' Hybrid Hydrogels with PNIPAM and Nanostructured Conductive Polymers, *Adv. Funct. Mater.*, 2015, 25, 1219.
Y. Shi, M. Wang, C. Ma, Y. Wang, X. Li and G. Yu, A Conductive Self-Healing Hybrid Gel Enabled by Metal–Ligand Supramolecule and Nanostructured Conductive Polymer, *Nano Lett.*, 2015, 15, 6276.
Y. S. carried out the experimental work and participated in the preparation of manuscript.

importantly, the interpenetrating structure excites improved mechanical properties and novel functionalities. The electrical conductivity of hybrid gel can change according to the temperature due to the absorption or desorption of water, thus being applied for a thermoresponsive switcher. The "switching" behavior is highly efficient and reversible owing to the excellent responsive sensitivity and mechanical properties of hybrid gels.

This chapter will also discuss the self-healing hybrid gels based on CPG and supramolecular gel.[5] The interests on self-healing materials with conductive properties are keeping growing in both academia and industry due to their potential applications in a broad range of areas, such as self-healing electronics, medical devices, artificial skins, and soft robotics. In my study, a supramolecular gel is introduced into PPy gel framework, thus forming interpenetrating double networked structure. The hybrid gel shows multi-functionalities in terms of mechanical robustness, high conductivity, and self-healing properties. The hybrid gel shows fast and efficient self-healing behavior on both mechanical and electrical properties without any external stimuli. This self-healing property comes from the dynamic assembly or disassembly, association or dissociation behaviors of supramolecular gel. A self-healing electrical circuit has been fabricated using this hybrid gel and its future applications in self-healing electronics, artificial skins, soft robotics, biomimetic prostheses, and energy storage can be anticipated.

5.2 SYNTHETIC APPROACHES OF CONDUCTIVE POLYMER GEL BASED HYBRID GEL MATERIALS

The development of multi-functional gels with high conductivity and modified chemical and physical properties is of particular importance due to their potential applications in electronics, biomedical devices, and energy conversion and storage.[6, 7] The design and synthesis of interpenetrating double network structured gels has become a powerful tool to create multi-functional gels because the hybrid gel may inherit the

advantages of each component while exciting new features owing to synergic effects between two polymeric networks.[8] CPGs can be an ideal matrix for the introduction of second gel network to build interpenetrating double networked hybrid gel owing to their hierarchically porous structure and a large area of active surfaces (Figure 1). The resulted hybrid gel systems are able to maintain high conductivity; enhance the mechanical properties; as well as bringing new features such as stimuli-responsive property, self-healing property, and enhanced biocompatibility.

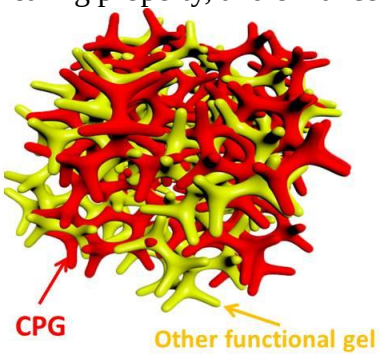

Figure 5.1 The network structured CPG is an ideal matrix for introduction of second polymer network to form interpenetrated double network structure

The interpenetrating double network structured hybrid gels based on CPGs can be synthesized in two ways. The first method is two-step polymerization in which one of the gel networks is firstly constructed and then acts as the supporting matrix for the in-situ polymerization of the second polymeric network. PNIPAM/PANI and PNIPAM/PPy hybrid gels have been successfully synthesized using this method.[4] In a typical synthesis, the PNIPAM gel is firstly synthesized, followed by a de-swelling process. Then the dry PNIPAM gel is swollen by precursor solutions containing conductive polymer monomers and crosslinking molecules. At last, the interpenetrating double network structured hybrid gels are obtained by in situ chemical oxidization of conductive polymers. For another example, a supramolecular gel is introduced into pre-formed CPG network through the

sol-gel transition, resulting in a self-healing hybrid gel. The second method for synthesis of double networked hybrid gel containing CPGs is a one-step method in which two polymers are polymerized and crosslinked within one precursor solution. Hybrid gels consisting of polyelectrolytes PEI and PNIPAM have been prepared using this method.[9]

The two different synthetic methods for CPGs based interpenetrating double network structured hybrid gels share similar features, but also show different advantages and limitations. The chemical and physical properties of hybrid gels synthesized by both methods can be tuned by changing the amount of precursors, synthetic temperature, and solvents used in synthesis. The two-step method is more versatile since the pre-formed gel network can be cleaned and modified before the introduction of the second polymeric network, thus eliminating potential inhibitors for the second polymerization. The one-step method may be limited to a small range of gel precursors since the oxidants used for CPGs can inhibit the polymerization of the second gel network. But this method can provide stronger interactions between two gel networks owing to the enhanced density of entanglement between two polymer chains.

5.3 THERMORESPONSIVE PANIPAM/CONDUCTIVE POLYMER GEL HYBRID MATERIALS

"Smart" hydrogels are receiving increasing attention in recent years since they are sensitive to external stimuli and could react actively to environment changes.[10] However, traditional smart hydrogels are generally electrically non-conductive[8] while conductive gels are promising for a wide range of applications.[6, 7, 11-19] People prepared conductive responsive hydrogels through incorporation of a second ingredient such as conducting fillers,[20] conductive polymers[21] or carbon based gel-like materials[8] into the gel matrix, forming hybrid "smart" hydrogels.

Conducting nanofillers such as carbon nanotubes,[22, 23] carbon black[24] and metal nanoparticles[25] are widely adopted into polymer hydrogels to enhance the conductivity. As nanofillers are randomly distributed in the polymer matrix and tend to form aggregations, a large amount of the fillers are needed and their surfaces need to be functionalized, thus forming a continuous, electrically conductive network.[26] However, this blending method restricts motion of polymer chains due to the strong interaction between fillers and the polymer matrix, thus weakening the mechanical properties of the conductive hybrid gels and reduces the stimuli-responsiveness.[27] When conductive polymers such as PANI and PPy are incorporated into gel systems, they form separately dispersed domains, lowering the electrical performance of the hybrid gel.[21] Recently, graphene aerogels are introduced for conductive smart hydrogels,[8] resulting in a hybrid hydrogel with robust mechanical performance and decent electrical properties. Alternatively, another facile and low-cost method to synthesize smart hydrogels with good conductivity and mechanical properties is the adoption of a conductive polymer.

In this chapter, the synthesis and characterizations of conductive smart gels which are sensitive to temperature change by introducing CPGs into a widely studied thermally responsive hydrogel, poly(N-isopropylcrylamide) (PNIPAM) are presented. Different from the traditional hybrid gel of randomly dispersed conductive polymer and stimuli-responsive hydrogels, a mesh-like hydrogel network of conductive polymer could be in situ formed due to the phytic acid molecule which can react with more than one PANI (or PPy) chain by protonating the nitrogen groups on PANI (or PPy) and thus promote the crosslinked structure.[13]

SEM is used to investigate the morphology and microstructure of PNIPAM/PANI and PNIPAM/PPy hybrid gels. The SEM image of freeze dried PNIPAM/PANI is shown in Figure 2a where the porous structure of the hybrid hydrogel with pores ranging from

several microns to larger than 10 microns. Such hierarchical porous structures facilitate the transport of water molecules owing to both large open channels between the branches and nanoscale porosities within the structures. The hybrid gel of PNIPAM/PPy shows a different morphology with interconnected spheres around 200 nm in Figure 2b. Materials with smooth surface among the spheres can be identified as PNIPAM. The formation of spherical geometry with a structural hierarchy could overcome the rigid nature of PPy chains and endows the hydrogel with effective elasticity.[12] Overall, a highly porous structure with pores ranging from several microns to larger than 10 micron is formed for PNIPAM/PPy hybrid gel, thus facilitating the flowing of water and ensuring the high sensitivity of hybrid gels.

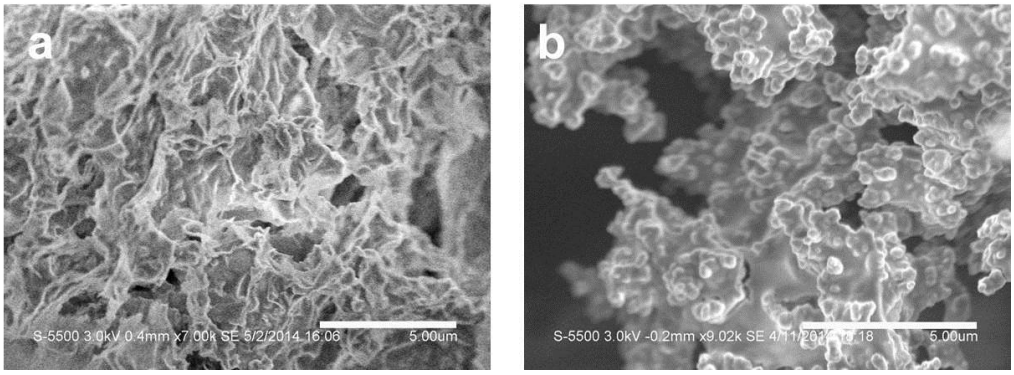

Figure 5.2 SEM images of PNIPAM/PANI (a) and PNIPAM/PPy (b) hybrid gels.

FTIR spectra were used to analyze the chemical structures of as-synthesized PNIPAM/PANI and PNIPAM/PPy hybrid hydrogels. The FTIR spectra of PNIPAM, PANI and PNIPAM/PANI are shown in Figure 3a. In the spectrum (black) of PNIAPM, peaks at 1540 and 1645 cm^{-1} can be attributed to N-H bending and C=O stretching, which are both characteristics of PNIPAM.[28] The red spectrum indicates the emeraldine salt form of PANI with two characteristic absorption peaks at 1570 and 1480 cm^{-1} which are corresponding to the stretching vibration of the quinoid ring and benzenoid ring,

respectively. The FTIR spectrum of synthesized of PNIPAM/PANI hybrid gel exhibits all the characteristic peaks of PNIPAM and PANI, confirming the formation of composites of PNIPAM and PANI. The typical FTIR spectra of PNIPAM, PPy and PNIPAM/PPy are shown in Figure 3b. The spectrum of PPy shows the absorption peaks at 1552 cm^{-1} and 1045 cm^{-1} which are corresponding to the in-ring stretching of C=C bonds in the pyrrole rings and the in-plane deformation of N-H bond, respectively. These two characteristic peaks can also be found in the FTIR spectrum of the as-synthesized hybrid hydrogel, confirming the formation of PPy in the PNIPAM matrix.

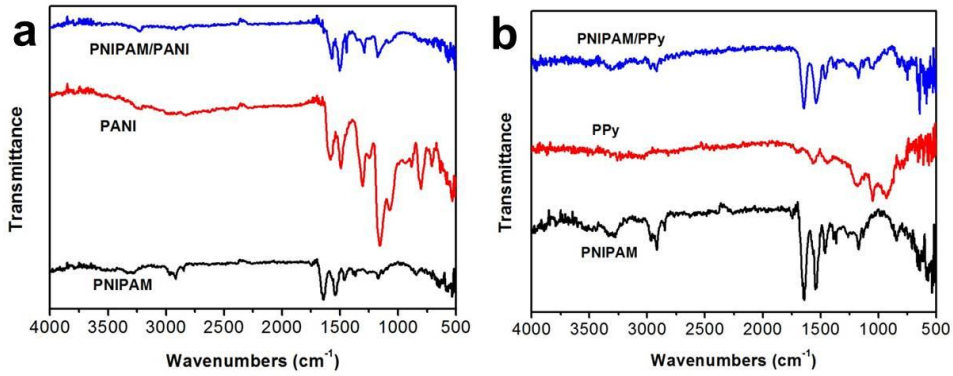

Figure 5.3 (a) FTIR spectra of PNIPAM, PANI, PNIPAM/PANI hydrogels. (b) FTIR spectra of PNIPAM, PPy, PNIPAM/PPy hydrogels.

Responsive hydrogels need desirable mechanical properties, especially when they are applied in practical devices.[29] Hydrogels are viscoelastic materials and they exhibit the properties of storing and dissipation of energy.[10] The amount of energy stored in the gel system and the amount of energy dissipated within the system under the oscillatory stress are indicated by the storage modulus (G') and the loss modulus (G"), respectively. Figure 4 shows the G' and G" values of PNIPAM, PNIPAM/PANI, and PNIPAM/PPy. All gels show a wide linear viscoelastic region in the dynamic frequency sweep experiments. And the value of storage modulus is higher than that of the loss modulus in each case,

confirming their gel state. Hybrid gels show increased mechanical strength due to their significantly higher G' values when compared to pure PNIPAM hydrogel, which is attributed to the reinforcement effect induced by the formation of a continuous and mechanically efficient network of conductive polymer with rigid backbones. The covalent bond of PANI and PPy chains facilitates energy dissipation and the interactions between two networks also contribute to the increase of mechanical strength. The elasticity (G'-G)[30] calculated from the rheological data are 157, 1763 and 3231 Pa for PNIPAM, PNIPAM/PANI and PNIPAM/PPy hydrogels, respectively. The foam-like structure of PANI hydrogel and spherical geometry of PPy hydrogel lead to increased elasticity. Fracture experiments can further demonstrate the enhanced mechanical properties of hybrid hydrogels. When fractured, the pure PNIPAM hydrogel breaks into small pieces while the hybrid hydrogels show a single large crack, indicating that the binary network structure of hybrid hydrogel combining PNIPAM and conductive polymer hydrogels contributes to the relax of local stress and dissipation of micro-crack energy.

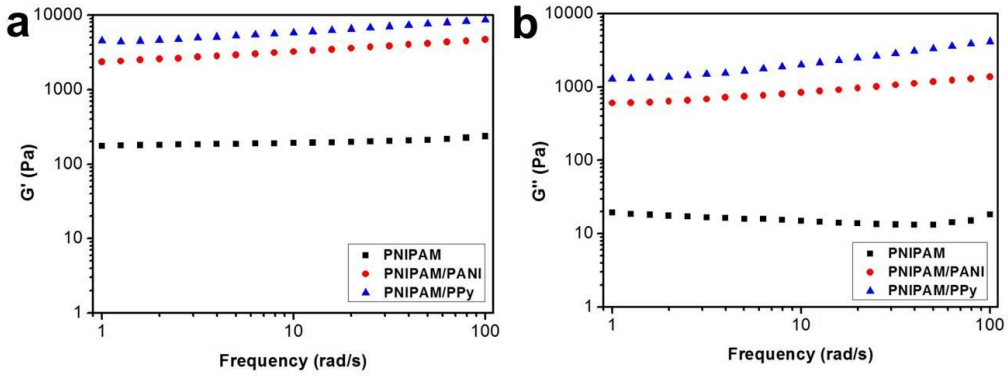

Figure 5.4 (a) and (b) the storage modulus (G') and loss modulus (G") of PNIPAM, PNIAPM/PANI, PNIPAM/PPy hydrogels tested in a frequency sweep mode.

The stability of electrical properties of the hybrid hydrogels under mechanical

strain was also demonstrated. The resistance of both hybrid hydrogels remains almost constant during compressing and relaxing cycle. Even under strain as large as 50%, the decrease of resistance is rather small (< 1%), indicating the excellent electrical stability of hybrid hydrogels under mechanical deformation.

The incorporation of conductive polymers should not negatively affect the thermally responsive functions of PNIPAM hydrogel during practical applications. Figure 5a and 5b show the swelling and deswelling behavior of PNIPAM/PANI and PNIPAM/PPy hybrid hydrogels. PNIPAM/PANI and PNIPAM/PPy show a swelling ratio of 5.2 and 2.3, respectively which are reasonable for the thermo-responsive application. The difference is induced by the different morphologies of two hybrid hydrogels. The PPy particles with smaller size can fill more space when compared to the mesh-like structure of PANI hydrogel, thus resulting in a lower swelling ratio. Besides the swelling ratio, responsive sensitivity is another important factor for thermally responsive hydrogels. As shown in Fig. 5a, 5b, both two hybrid hydrogels show a sharp decrease of mass happens when immersed in water with a temperature of 50 ^{o}C, demonstrating high sensitivity to thermal stimuli. Largest degree of deswelling can be achieved within 1 min for conductive hybrid hydrogels. In the recovering half cycle, both the hybrid hydrogels exhibit a sharp increase in mass during the first several minutes. Then swelling slows down until it takes about 15 h to recover to original swelled status. The hybrid hydrogels show similar swelling and deswelling behavior to PNIPAM hydrogel, confirming the unaffected responsive function of hydrogels after incorporation of conductive polymers. The interpenetrating binary network structure and porous nature which reduce the restriction of PNIPAM chains and facilitates the flow of water molecules within the hydrogel network are mainly responsible for the good thermo-responsive behavior of hybrid hydrogels. The region exhibiting a vertical change of mass in the swelling and

deswelling curves suggests the excellent thermo-responsive sensitivity of the designed hybrid hydrogels and ensures their application in responsive devices.

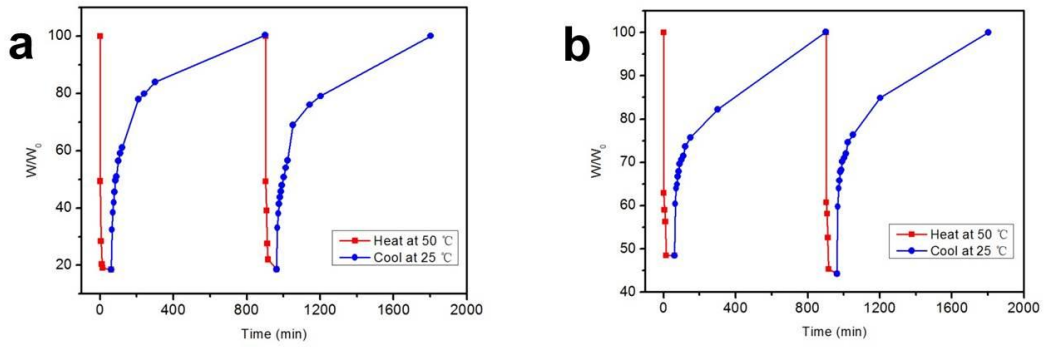

Figure 5.5 The swelling and deswelling behavior of PNIPAM/PANI (a) and PNIPAM/PPy (b) hybrid hydrogels

The hybrid hydrogels based on PNIPAM and conductive polymers also exhibit excellent electrical properties. By using the four-probe method, the bulk electrical conductivities of PNIPAM/PPy and PNIPAM/PANI hydrogels were measured to be 0.8 and 0.2 S m^{-1} at hydrogel states, respectively. The higher conductivity of PNIPAM/PPy hydrogel may be due to the higher loading of PPy in the hybrid gel. Pure conducting polymer hydrogels typically show the electrical conductivity in the range of 0.01~1 S m^{-1} and the highest value reported is 11 S m^{-1} for the PANI hydrogel synthesized by phytic acid as the crosslinker.[31] Compared to recently reported smart hydrogel systems with conductive polymers incorporated, PNIPAM/PPy and PNIPAM/PANI hybrid gels show the electrical conductivities which are approximately two orders of magnitude higher and close to those of pure conductive polymers,[32, 33] demonstrating excellent electrical properties. The in situ formation of networks of conductive polymers which can act as the continuous transporting path for electrons is the reason for excellent electrical properties. In contrast, hybrid hydrogels based on randomly dispersed conductive particles or

monomers consist of point-to-point connected conducting network resulting in a poor electrical conductivity. The hybrid hydrogels are promising for the applications of conductive smart hydrogels owing to their enhanced mechanical performance, high thermo-responsive and electrical properties.

Based on the unique properties of hybrid hydrogels, a thermally responsive switcher is designed. As shown in Figure 6a, a certain amount of hybrid hydrogel is sealed into a cylinder shell with top and bottom electrodes. It becomes a conductor at first because the hydrogel and electrodes are well contacted. When the switcher is heated, the hybrid hydrogel shrinks due to the deswelling. The conductivity of hybrid hydrogel changes due to the loss of water within hydrogel matrix and the decrease of contacting area between conductive hydrogels and the electrodes, leading to increased resistance of the switcher device. When the device is further heated, the hydrogel continuously shrinks and finally loses contact with electrodes, thus switching to open-circuit status. The process is reversible. The hybrid hydrogels swell under LCST and recreate the electrical contact between conductive hydrogels and electrodes, thus forming a transporting path for current. The “switching” behavior could be completed within 10 seconds due to the excellent responsive sensitivity of hybrid hydrogels, ensuring the quick response of switcher device to temperature change.

The stability of conductive hydrogel based switcher device is demonstrated by the cycling performance. Figure 6b shows the 50 cycles of heating and cooling of the switcher during which the switcher maintains around 110 kΩ and 10 kΩ of resistance at heated (deswelled) status at cooled (swelled) status, respectively even after 50 cycles. The good mechanical properties and electrical stability of the hybrid hydrogels support the excellent cycling performance. The change of resistance occurs within 10 seconds and the difference of resistance is significant, demonstrating the highly thermo-responsive

sensitivity of the hybrid gels. And the resistance difference could be tuned by controlling the amount of hybrid gels sealed in between the two electrodes. The switcher can function between totally open-circuit and closed-circuit states by losing and recreating the contact between conductive hybrid hydrogel and electrodes. The demonstrated circuit is shown in Figure 6c. The on/off states of LED are controlled by the closed-circuit/open-circuit states of the electrical circuit. The inset photographs show the swelled and deswelled states of hybrid gels in the device. The hydrogel creates the contact between gel and electrode is created when it is swelled, building the transport path for current. When the temperature is raised and the hydrogel is deswelled, the contact is lost, thus inducing the open-circuit state. The simple demonstration reveals the high thermoresponsive sensitivity, enhanced mechanical properties and good electrical performance of hybrid gels and shows their potential for application in electronic devices.

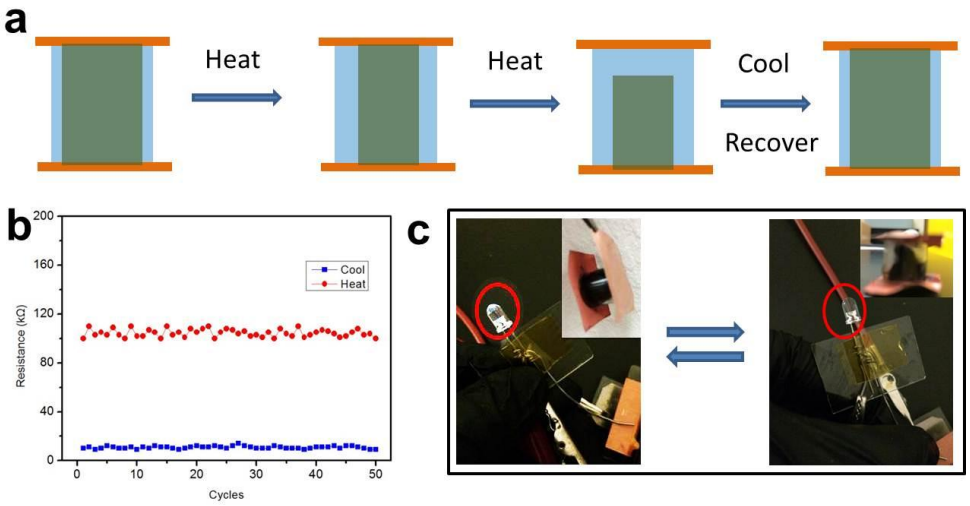

Figure 5.6 (a) Schematic of the working mechanism of the switcher device based on thermal-responsive conductive hydrogels. (b) Cycling performance of the switcher device. (c) The demo circuit in which the on/off states of LED is controlled by the closed-circuit/open-circuit states of the electrical circuit which are determined by the states of the switcher. The inset photographs show the swelled and deswelled states of hybrid hydrogels in the device.

5.4 SELF-HEALING SUPRAMOLECULAR GEL/CONDUCTIVE POLYMER GEL HYBRID MATERIALS

Interests from both academia and industry have been dedicated to self-healing materials with conductive properties due to their potential applications in a broad range of technologies.[25, 34-38] Good conductivity, repeatable mechanical and electrical self-healing properties at room temperature, and decent mechanical strength and flexibility are needed for these materials to meet the requirements for fabrication of flexible devices in practical applications.[39-41]

Various conductive self-healing materials have been developed. White, Moore and co-workers[42-44] used microcapsules containing liquid precursor healing agents for structural healing in which the local healing agent is depleted after capsule rupture. Bao et al.[37] combined a supramolecular organic polymer and nickel microparticles, resulting in a composite with mechanical and electrical self-healing properties at ambient conditions; whereas it needs a large number of inorganic particles. Recently, Park et al.[45] polymerized pyrrole within agarose matrix to form a conductive and self-healing hydrogel. External thermal or optical stimuli, however, are necessary to facilitate the self-healing behavior of the resultant composite. Therefore, the development of self-healing, highly conductive, mechanically strong, and light-weight materials remains a critical challenge.[46]

In the past decades, the supramolecular chemistry has witnessed rapid development of metallo-supramolecular structures based on the highly directional and predictable feature of metal-mediated self-assembly.[47, 48] Hierarchically self-assembly of these materials into higher order nanostructures, i.e., supramolecular gels is driven by directional and conjugated structures and intermolecular forces.[49-51] More importantly, the moderate bond energy of metal-ligand bonds and non-covalent interactions among

supramolecules allow the supramolecular gels to dynamically assemble or disassemble, associate or dissociate at room temperature, thus showing features such as self-healing property and sol-gel phase transitions.[52-54] As discussed in previous chapters, phytic acid was used as the gelator and dopant for the synthesis of conductive polymer hydrogels such as PANI and PPy.[13] The framework of the resulted CPGs is highly conductive. Such 3D hierarchically porous structures offer large open channels to support the introduction of second gel component and provide an ideal interface between conductive hydrogels and other synthetic systems.[4] However, their further applications are inhibited by the fragile nature and lack of self-healing property.

In this chapter, a hybrid gel material is presented by introducing an acetonitrile-based supramolecular gel with cubic architecture, namely, G-Zn-tpy which was synthesized by using 2, 2':6', 2"-terpyridine (tpy) as organic ligand and Zn(II) as gluing element into CPG matrix. In this hybrid gel system, the nanostructured PPy gel constructs a 3D network to promote the transport of electrons and mechanically reinforce the hybrid gel while the supramolecular gel contributes to self-healing property and also conductivity. More importantly, synergic effects such as enhanced mechanical strength and elasticity are excited within the hybrid gel. With these features, films of hybrid gel on various substrates with properties of room-temperature self-healing, high conductivity, and good flexibility are fabricated, showing potential for various applications such as self-healing electronics, artificial skins, soft robotics and biomimetic prostheses. It also demonstrated that a class of functional polymeric materials can be designed and synthesized by the "guest to host" strategy.

The supramolecule was assembled by 12 metal ions and 8 three-armed building blocks which were designed by linking three tpy groups to rigid adamantane core, resulting in a structure of cubic cage (Figure 7a).[55] The intermolecular interactions, such

as hydrophobic forces and π- π stacking drive the formation of a supramolecular gel. The cubic cage structure with rigid and uniform geometry also enhances the hierarchical self-assembly since the supramolecules could be well arranged along three-dimensional directions.[56] In addition, a reversible sol-gel phase transition at 50 ℃ above which G-Zn-tpy becomes a homogeneous solution was observed, as shown in Figure 7b. The disassembly of supramolecules, as well as the dissociation of metal-ligand bonds at high temperature, induces gel to sol transition. These dynamic processes due to relatively weak non-covalent intermolecular interactions and moderate bond energy (15−50 kcal mol^{-1}) of metal-ligand bonds[53, 54] enable good self-healing property of hybrid gel at room temperature. Figure 7c shows the schematic illustration of self-healing behavior of G-Zn-tpy in which the combination of dynamic intermolecular interaction and coordination drives the reassembly of supramolecules at the crack, thus self-healing small cracks within tens of seconds and big cracks in minutes.

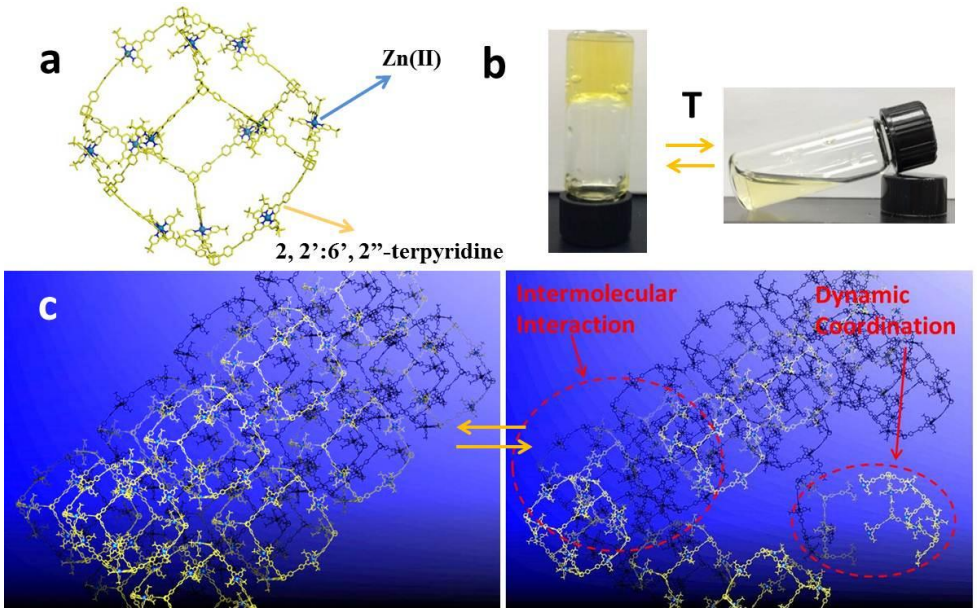

Figure 5.7 The supramolecular gel: (a) The molecular structure of Zn-tpy supramolecule; (b) G-Zn-tpy shows a reversible sol-gel phase transition at 50 °C above which G-Zn-tpy becomes a homogeneous solution; (c) Schematic illustration of proposed mechanisms of supramolecular gels' self-healing behavior. The dynamic intermolecular interaction and coordination at the crack position help heal the gel material.

The hybrid gel is synthesized with the sol-gel transition of G-Zn-tpy. In a typical synthesis, PPy aerogel is obtained by freeze drying and then swollen in the supramolecule solution above 50 ℃ (the weight ratio of PPy to G-Zn-tpy is 6:1; the weight ratio of PPy in the hybrid gel is ~83%). The supramolecular gel in-situ forms within the PPy matrix after it's cooled, resulting in a binary network gel. SEM images in Figure 8a and 8b show the morphologies and microstructures of PPy aerogel and PPy/G-Zn-tpy hybrid gel. Interconnected sphere-like particles with size ranging from 150 nm to 300 nm are formed in PPy aerogel, resulting in a hierarchically porous structure with two levels of pores, including the pores between the nanospheres (the average gap size), and the bigger micron size pores between domains of nanospheres. Thin film-like structures of supramolecule gel forms in PPy matrix. The supramolecular gel wraps the PPy particles

and further connects the PPy domains together, building up a secondary self-crosslinked network to form a binary network gel. Figure 8c shows the FTIR spectra of G-Zn-tpy, PPy, and PPy/G-Zn-tpy hybrid gel. The spectrum of PPy shows the absorption peak at 1552 cm^{-1} and 1045 cm^{-1} which are corresponding to the in-ring stretching of C=C bonds in the pyrrole rings and the in-plane deformation of N-H bond, respectively.[12] Two major characteristic peaks could be found at 995 cm^{-1} and 670 cm^{-1} in the spectrum of G-Zn-tpy which can be attributed to the breathing mode of pyridine and vibration of Zn-N bonds, respectively.[57] Hybrid gel exhibit all the characteristic peaks of PPy and G-Zn-tpy, confirming the formation of composites. The characteristic peaks of G-Zn-tpy slightly shift towards the lower wavenumber side, indicating the interactions between Zn-tpy molecule and PPy backbone which could weaken the bonding strength of supramolecule due to the effect of delocalization of the π electrons.[58]

Gel materials require decent mechanical strength and elasticity to be applied in practical devices.[29] The G' and G" values of G-Zn-tpy gel with acetonitrile as solvent, PPy aerogel, and PPy/G-Zn-tpy hybrid gel with acetonitrile as solvent are shown in Figure 8d and 8e. The wide linear viscoelastic region in the dynamic frequency sweep experiments and the fact that the value of storage modulus is higher than that of the loss modulus in each case reveal their gel states. The G' value of PPy/G-Zn-tpy hybrid gel is significantly enhanced compared to pure supramolecular gel and even higher than that of PPy, indicating the reinforcement effect brought by the continuous and mechanically efficient network of PPy with rigid backbones[8] and the binary network structure of hybrid gel in which the self-crosslinked supramolecule gel wraps and links the PPy particles together. The dissipation of energy is facilitated by covalent bond of PPy chains and metal-ligand bond of supramolecule. The interactions between two networks of gels also contribute to the increase of mechanical strength of hybrid gels. The tangent of the phase

angle – the ratio of the viscous modulus (G") to elastic modulus (G') is a useful quantifier of the presence and extent of elasticity in a gel system.[59] Tanδ values of less than unity indicate elastic-dominant behavior and values greater than unity indicate viscous-dominant behavior. All three samples shown in Figure 8f are elastic-dominant gel systems while the pure Zn-tpy gel is most elastic. The PPy/G-Zn-tpy hybrid gel is much more elastic when compared to the rigid and fragile PPy hydrogel, thus possessing the ability to be applicable and processable in flexible devices.

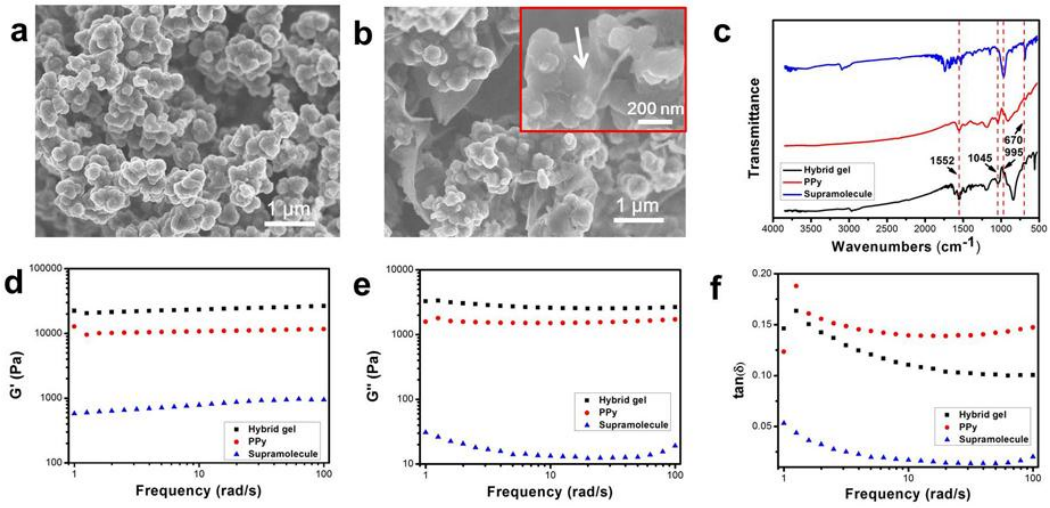

Figure 5.8 Characterization of PPy/G-Zn-tpy hybrid gel: (a) and (b) SEM images of PPy, and PPy/G-Zn-tpy hybrid gel, respectively. (c) FTIR spectra of Zn-tpy supramolecule, PPy, and PPy/G-Zn-tpy hybrid gel; (d) and (e) the storage modulus (G') and loss modulus (G") of Zn-tpy supramolecule, PPy, and PPy/G-Zn-tpy hybrid gel; (f) The tangent of the phase angle (G"/G') values of Zn-tpy supramolecule, PPy, and PPy/G-Zn-tpy hybrid gels.

Thin films of PPy/G-Zn-tpy hybrid gel were successfully fabricated on flexible substrates such as PDMS and Kapton films which are commonly used substrates for flexible electronic devices. Supramolecule gel was introduced to form the hybrid gel film after PPy aerogel was firstly polymerized on flexible substrates. The thickness of films could vary from ~0.1 to 0.5 mm by controlling the amount of PPy precursor and all the

films are uniform and with good quality. The films can maintain uniformity and adhere firmly to substrates when they were significantly bent, demonstrating high flexibility. The controlled sample of PPy aerogel films form cracks and peel off from substrates when they are bent. PPy/G-Zn-tpy hybrid gel can be prepared to free-standing films with various morphologies, revealing good mechanical strength and processability of PPy/G-Zn-tpy hybrid gel. The properties of PPy/G-Zn-tpy hybrid gel films are consistent with the results of rheology tests, indicating its enhanced mechanical strength and elasticity.

The conductivity of PPy/G-Zn-tpy hybrid gel film reaches as high as 12 S m^{-1} in the four-probe test which is comparable to pure conductive polymers and among the highest values of conductive hybrid gels (Figure 9a). It could be attributed to the interconnected networks of conductive polymers which can act as the continuous transporting path for electrons, as well as the conductive nature of G-Zn-tpy. The mechanical stability of electrical properties of PPy/G-Zn-tpy hybrid gel film was demonstrated by bending and stretching tests. Figure 9b shows the result of stretching test using PDMS as the substrate. The hybrid gel film was stretched to 33% and 67% strain and the film resistance increased from 0.68 kΩ to 0.84 and 0.99 kΩ, respectively, which was caused by the formation of small cracks in the film during stretching. The resistance recovered to 0.70 kΩ when the film was released to its original length, which could be explained by the high elasticity and self-healing property of PPy/G-Zn-tpy hybrid gel. The bending tests also demonstrate the good mechanical stability of PPy/G-Zn-tpy hybrid gel film, in which the conductivity of PPy/G-Zn-tpy hybrid gel film remains almost constant under different bending radii, i.e., 1.5, 1.0 and 0.5 cm (Figure 9c). Figure 9d shows the cyclic test in which PPy/G-Zn-tpy hybrid gel film maintains ~10 S m^{-1} up to 100 bending cycles. The enhanced mechanical strength and elasticity of PPy/G-Zn-tpy hybrid gel film help maintain the integrity of 3D continuous network for electron

transport during mechanical deformation and ensure the good contact between gel film and flexible substrates.

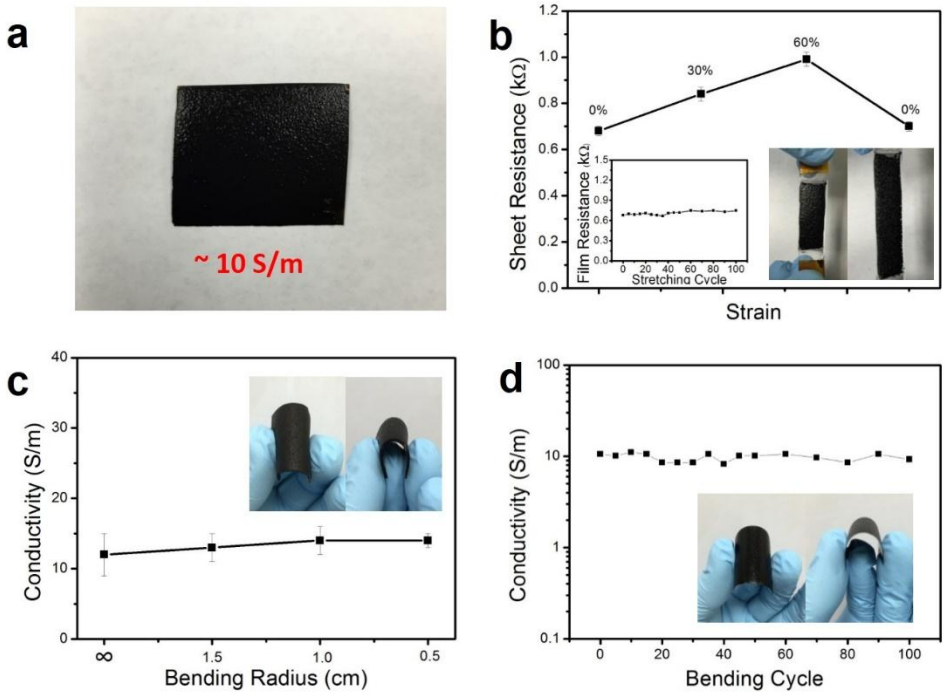

Figure 5.9 Thin film of PPy/G-Zn-tpy hybrid gel: (a) Photograph of PPy/G-Zn-tpy hybrid gel thin film coated on Kapton substrate; (b) Film resistance of PPy/G-Zn-tpy hybrid gel thin film coated on PDMS substrate under different stretching states. Inset (left) shows the film resistance after different stretching cycles and inset (right) shows the optical images of PPy/G-Zn-tpy hybrid gel thin film at initial status and 67% strain. (c) The conductivity of PPy/G-Zn-tpy hybrid gel thin film under different bending states. Inset shows the optical images of bent PPy/G-Zn-tpy hybrid gel thin film coated on PDMS substrate. (d) Conductivities of PPy/G-Zn-tpy hybrid gel thin film after different bending cycles. Inset shows the optical images of bent PPy/G-Zn-tpy hybrid gel thin film coated on Kapton substrate.

The self-healing property is another key feature of G-Zn-tpy. The PPy/G-Zn-tpy hybrid gel inherits this unique feature and is able to self-heal the cracks at room temperature. Compression strength and modulus were measured in compression tests on the samples at different states (original status, right after cutting to pieces, self-healed

status) (Figure 10a). It can be noted that since the cutting direction is parallel to the compression direction, the sample tended to be extruded out during the test, thus further breaking the sample. The original hybrid gel and self-healed gel show similar behavior in compression test while the cut sample shows much lower strength, especially at high strain. The modulus of original gel, self-healed gel, and cut gel was calculated to be 107 Pa, 101 Pa and 29 Pa, respectively. As a reference, modulus of the pure PPy gel was 74 Pa. The gel was much weaker after cutting to pieces since it could not relief the stress well along the horizontal direction. However, the self-healed gel was mechanically integrated and recovered to its initial strength. The self-healing property was also demonstrated by recovered conductivities of hybrid gel (Figure 10b). The conductivity of the sample was measured every 60 S between each cut and every 20 S during its self-healing process. Hybrid gel showed much lower conductivity than original gel after cutting even though the two half samples were physically contacted to each other. After around one minute, the conductivity recovered to initial value due to the reformation of an integrated conductive 3D network.

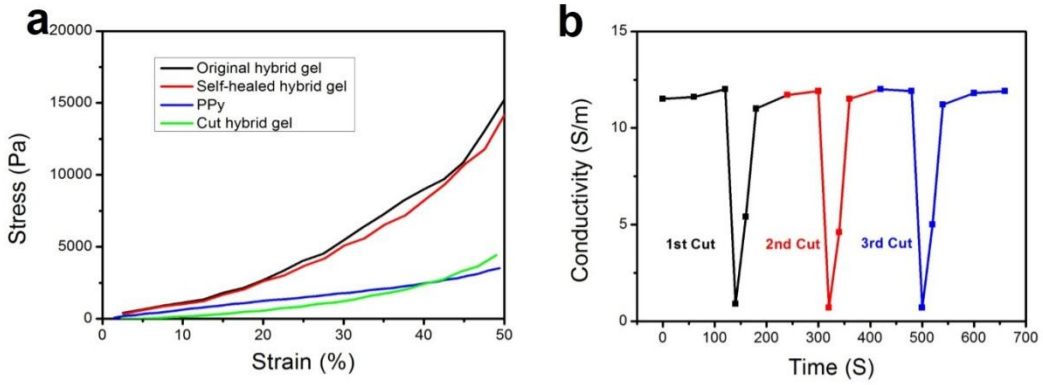

Figure 5.10 (a) Compression test for different samples. (b) The conductivities of the hybrid gel at different stages during cutting and self-healing processes. The cut samples were physically contacted to each other.

The self-healing behavior of PPy/G-Zn-tpy hybrid gel was further demonstrated for both bulk and thin film samples. Initially, one piece of PPy/G-Zn-tpy hybrid gel was shaped to a box with section area of ~1 cm^2 and cut into half as shown in Figure 11a. Then two separated pieces were placed together and after 1 min, the sample self-healed to form an integrated one and can support its own weight when lifted by a pair of tweezers. More importantly, the sample was also electrically healed, showing same resistances before and after cutting. To show the self-healing behavior of PPy/G-Zn-tpy hybrid gel film (Figure 11b), some cracks were created intentionally by bending the PPy aerogel film. After introducing a solution of Zn-tpy supramolecule, the cracks disappeared rapidly. The self-healed thin film of PPy/G-Zn-tpy hybrid gel exhibited excellent flexibility and high conductivity of ~10 S m^{-1}. The supramolecule gel acts as a dynamic "glue" in the hybrid system due to its dynamic assembly or disassembly, association or dissociation behaviors based on relatively weak non-covalent intermolecular interactions and moderate bond energy of metal-ligand bonds. According to the unique binary network structure shown in SEM images, the self-crosslinked supramolecule gel helps to support the PPy network by wrapping and connecting PPy particles together, as well as building a self-supported network. The PPy matrix also plays an important role because its hierarchically porous structure could facilitate the molecule motion and transportation at the cracks and its tough nature favors the mechanical healing behavior.[19]

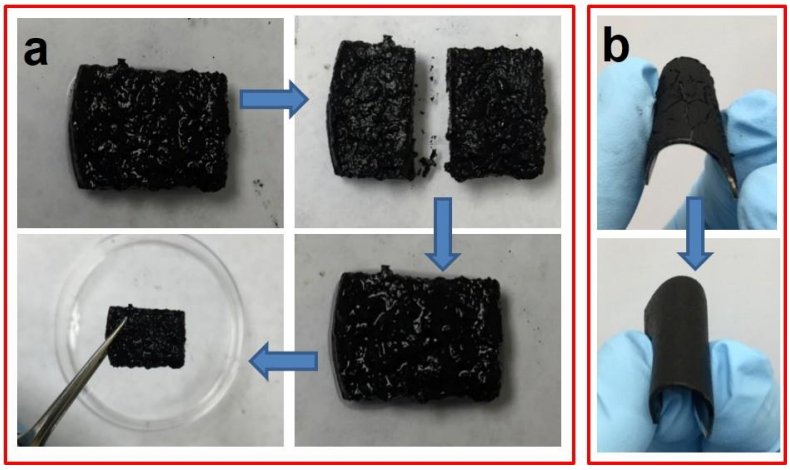

Figure 5.11 Self-healing property of PPy/G-Zn-tpy hybrid gel: The self-healing behavior of PPy/G-Zn-tpy hybrid gel: (a) bulk sample was cut into half and then placed together. After 1 min, the sample self-healed to be an integrated one and can support its own weight when lifted by tweezers; (b) The initially cracked PPy aerogel film was self-healed after introducing G-Zn-tpy.

To further demonstrate the mechanical stability, high conductivity and self-healing feature of PPy/G-Zn-tpy hybrid gel, a complete circuit composed of a LED bulb with driving voltage of 3.0~3.2 V as the electrical load, PPy/G-Zn-tpy hybrid gel film as the conductor and two dry batteries (1.5 V) as the power source was designed. As shown in Figure 12, a circle of PPy/G-Zn-tpy hybrid gel thin film was coated on PDMS substrate, then the LED bulb was involved and the power source was linked into the circuit by two copper wires. Silver paste is used to strengthen the attaching points of LED bulb and copper wires. The bulb was lighted, indicating the high conductivity of PPy/G-Zn-tpy hybrid gel which leads to no apparent voltage drop. Notably, this circuit could work well under bent, even folded states, showing the outstanding flexibility and mechanical strength of the PPy/G-Zn-tpy hybrid gel. At last, the self-healing property of PPy/G-Zn-tpy hybrid gel was also demonstrated on the circuit. In a typical test, the left side of PPy/G-Zn-tpy hybrid gel film was cut and the circuit then became open and the

bulb was extinguished. After about 1 min, the circuit was re-established and the LED bulb could be lighted up again. This self-healing test was successfully conducted for multiple times at the same position and also at other positions. This working circuit shows the great potential of PPy/G-Zn-tpy hybrid gel for practical applications such as self-healing electronics, biosensors, and artificial skins.

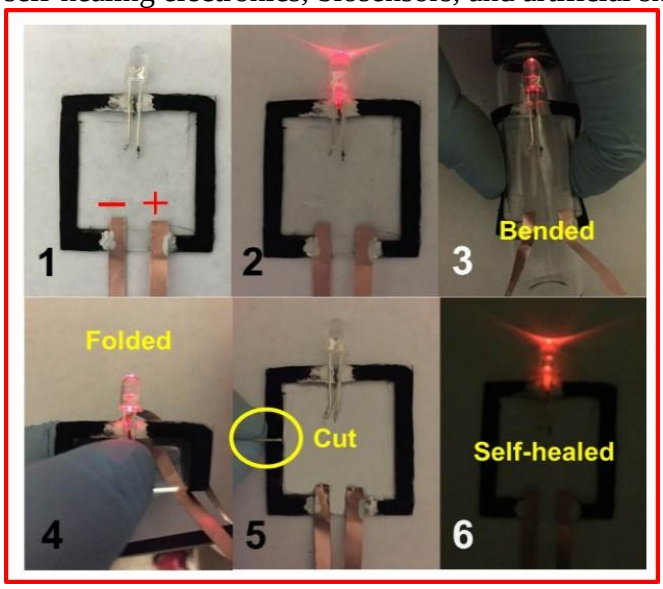

Figure 5.12 Self-healing circuit based on PPy/G-Zn-tpy hybrid gel

5.5 CONCLUSIONS

CPGs is a promising "host" material for the development of responsive gels with the decent conductive property. The network of CPGs can build up continuous pathways for electron transport and provide hierarchical pores to accommodate another responsive gel framework, thus forming interpenetrating double network structured gel. The rich interactions including hydrogen bonding and coulombic effect between conductive polymer chains and responsive gel networks can help maintain the structural integrity during responsive change and tune the responsive behavior of resulted hybrid gel. The

concept to build up multifunctional hybrid gels based on CPGs is successfully demonstrated by two studies.

PNIPAM/conductive polymer based hybrid hydrogels are firstly synthesized by the in situ formation of a continuous network of conductive polymer hydrogels crosslinked by phytic acid in PNIPAM matrix. With the interpenetrating binary network structure, hybrid hydrogels exhibit a unique combination of high electrical conductivity, high thermoresponsive sensitivity, and enhanced mechanical properties. These unique properties are further demonstrated by the switcher device. This hybrid gel demonstrates that the architecture of the filling phase in the hydrogel matrix plays an important role in determining the performance of resulting hybrid material. The hybrid hydrogels are promising for applications in stimuli-responsive electronic devices, the design of self-adaptive electronics, and flexible electronics. And because the performance of hydrogels can be well maintained in an aqueous environment, the conductive hydrogels may be useful for bio-related electronics.

A promising self-healing PPy/G-Zn-tpy hybrid gel was also synthesized by incorporating a G-Zn-tpy supramolecule within the PPy aerogel matrix. The hybrid gel combines the high conductivity of PPy aerogel and self-healing property of G-Zn-tpy, and exhibits enhanced mechanical strength and excellent elasticity due to its unique binary network structure. The self-healing behavior is efficient and could be observed at room temperature without any external stimuli, owing to dynamic assembly or disassembly of supramolecules and association or dissociation of metal-ligand bonds. Supported by these unique features, thin films with good uniformity and flexibility of G-Zn-tpy hybrid gel were successfully fabricated and a self-healable electronic circuit based on hybrid gel films was demonstrated. This conductive, room-temperature self-healing gel material takes unique advantage of supramolecular chemistry and polymer

nanoscience and shows its potential applications in various fields such as self-healing electronics, artificial skins, soft robotics, biomimetic prostheses, and energy storage.

5.6 REFERENCES

1. G. Schottner, *Chemistry of Materials*, 2001, **13**, 3422-3435.
2. Y. Xu, Q. Wu, Y. Sun, H. Bai and G. Shi, *ACS Nano*, 2010, **4**, 7358-7362.
3. J. Lin, Q. Tang, J. Wu and Q. Li, *Journal of Applied Polymer Science*, 2010, **116**, 1376-1383.
4. Y. Shi, C. Ma, L. Peng and G. Yu, *Advanced Functional Materials*, 2015, **25**, 1219.
5. Y. Shi, M. Wang, C. Ma, Y. Wang, X. Li and G. Yu, *Nano Letters*, 2015, **15**, 6276-6281.
6. J. Ma, N. A. Choudhury, Y. Sahai and R. G. Buchheit, *Journal of Power Sources*, 2011, **196**, 8257-8264.
7. L. Zhang and G. Shi, *The Journal of Physical Chemistry C*, 2011, **115**, 17206-17212.
8. L. Qiu, D. Liu, Y. Wang, C. Cheng, K. Zhou, J. Ding, V.-T. Truong and D. Li, *Advanced Materials*, 2014, **26**, 3333.
9. C. Ma, Y. Shi, D. A. Pena, L. Peng and G. Yu, *Angewandte Chemie International Edition*, 2015, **54**, 7376-7380.
10. P. Chakraborty, P. Bairi, B. Roy and A. K. Nandi, *ACS Applied Materials & Interfaces*, 2014.
11. L. Pan, A. Chortos, G. Yu, Y. Wang, S. Isaacson, R. Allen, Y. Shi, R. Dauskardt and Z. Bao, *Nat Commun*, 2014, **5**.
12. Y. Shi, L. Pan, B. Liu, Y. Wang, Y. Cui, Z. Bao and G. Yu, *Journal of Materials Chemistry A*, 2014, **2**, 6086-6091.
13. L. Pan, G. Yu, D. Zhai, H. R. Lee, W. Zhao, N. Liu, H. Wang, B. C.-K. Tee, Y. Shi, Y. Cui and Z. Bao, *Proceedings of the National Academy of Sciences*, 2012, **109**, 9287-9292.
14. Y. Wang, X. Yang, L. Qiu and D. Li, *Energy Environmental Science*, 2013, **6**, 477-481.
15. D. O. Carlsson, G. Nystrom, Q. Zhou, L. A. Berglund, L. Nyholm and M. Stromme, *Journal of Materials Chemistry*, 2012, **22**, 19014-19024.
16. Y. Zhao, B. Liu, L. Pan and G. Yu, *Energy & Environmental Science*, 2013, **6**, 2856-2870.

17. Q. Li, Q. Tang, L. Lin, X. Chen, H. Chen, L. Chu, H. Xu, M. Li, Y. Qin and B. He, *Journal Power Sources*, 2014, **245**, 468.

18. B. Liu, P. Soares, C. Checkles, Y. Zhao and G. Yu, *Nano Letters*, 2013, **13**, 3414-3419.

19. H. Wu, G. Yu, L. Pan, N. Liu, M. T. McDowell, Z. Bao and Y. Cui, *Nat Commun*, 2013, **4**, 1943.

20. C.-H. Zhu, Y. Lu, J. Peng, J.-F. Chen and S.-H. Yu, *Advanced Functional Materials*, 2012, **22**, 4017-4022.

21. R. E. Rivero, M. A. Molina, C. R. Rivarola and C. A. Barbero, *Sensors and Actuators B: Chemical*, 2014, **190**, 270-278.

22. X. Zhang, C. L. Pint, M. H. Lee, B. E. Schubert, A. Jamshidi, K. Takei, H. Ko, A. Gillies, R. Bardhan, J. J. Urban, M. Wu, R. Fearing and A. Javey, *Nano Letters*, 2011, **11**, 3239-3244.

23. Z. Chen, J. W. F. To, C. Wang, Z. Lu, N. Liu, A. Chortos, L. Pan, F. Wei, Y. Cui and Z. Bao, *Advanced Energy Materials*, 2014, **4**, 1400207.

24. W.-J. Chuang, W.-Y. Chiu and H.-J. Tai, *Journal of Materials Chemistry*, 2012, **22**, 20311-20318.

25. C. Wang, H. Wu, Z. Chen, M. T. McDowell, Y. Cui and Z. Bao, *Nat Chem*, 2013, **5**, 1042-1048.

26. H. Kim, A. A. Abdala and C. W. Macosko, *Macromolecules*, 2010, **43**, 6515-6530.

27. K. Haraguchi and H.-J. Li, *Angewandte Chemie International Edition*, 2005, **44**, 6500-6504.

28. T. Munk, S. Baldursdottir, S. Hietala, T. Rades, M. Nuopponen, K. Kalliomäki, H. Tenhu, J. Rantanen and C. J. Strachan, *Polymer*, 2013, **54**, 6947-6953.

29. X. Zhao, *Soft Matter*, 2014, **10**, 672-687.

30. P. Bairi, B. Roy, P. Routh, K. Sen and A. K. Nandi, *Soft Matter*, 2012, **8**, 7436-7445.

31. S.-W. Cao and Y.-J. Zhu, *The Journal of Physical Chemistry C*, 2008, **112**, 6253-6257.

32. H. Huang, W. Li, H. Wang, X. Zeng, Q. Wang and Y. Yang, *ACS Applied Materials & Interfaces*, 2014, **6**, 1595-1600.

33. W. Zhao, L. Glavas, K. Odelius, U. Edlund and A.-C. Albertsson, *Chemistry of Materials*, 2014, **26**, 4265-4273.

34. H. Wang, B. Zhu, W. Jiang, Y. Yang, W. R. Leow, H. Wang and X. Chen, *Advanced Materials*, 2014, **26**, 3638-3643.

35. Y. Zhang, B. Yang, X. Zhang, L. Xu, L. Tao, S. Li and Y. Wei, *Chemical Communications*, 2012, **48**, 9305-9307.

36. N. Holten-Andersen, M. J. Harrington, H. Birkedal, B. P. Lee, P. B. Messersmith, K. Y. C. Lee and J. H. Waite, *Proceedings of the National Academy of Sciences*, 2011, **108**, 2651-2655.

37. B. C. K. Tee, C. Wang, R. Allen and Z. Bao, *Nat Nano*, 2012, **7**, 825-832.

38. R. F. Shepherd, F. Ilievski, W. Choi, S. A. Morin, A. A. Stokes, A. D. Mazzeo, X. Chen, M. Wang and G. M. Whitesides, *Proceedings of the National Academy of Sciences*, 2011, **108**, 20400-20403.

39. D.-H. Kim, N. Lu, R. Ma, Y.-S. Kim, R.-H. Kim, S. Wang, J. Wu, S. M. Won, H. Tao, A. Islam, K. J. Yu, T.-i. Kim, R. Chowdhury, M. Ying, L. Xu, M. Li, H.-J. Chung, H. Keum, M. McCormick, P. Liu, Y.-W. Zhang, F. G. Omenetto, Y. Huang, T. Coleman and J. A. Rogers, *Science*, 2011, **333**, 838-843.

40. S. R. White, N. R. Sottos, P. H. Geubelle, J. S. Moore, M. R. Kessler, S. R. Sriram, E. N. Brown and S. Viswanathan, *Nature*, 2001, **409**, 794-797.

41. K. S. Toohey, N. R. Sottos, J. A. Lewis, J. S. Moore and S. R. White, *Nat Mater*, 2007, **6**, 581-585.

42. B. J. Blaiszik, S. L. B. Kramer, S. C. Olugebefola, J. S. Moore, N. R. Sottos and S. R. White, *Annual Review of Materials Research*, 2010, **40**, 179-211.

43. S. A. Odom, S. Chayanupatkul, B. J. Blaiszik, O. Zhao, A. C. Jackson, P. V. Braun, N. R. Sottos, S. R. White and J. S. Moore, *Advanced Materials*, 2012, **24**, 2578-2581.

44. S. A. Odom, T. P. Tyler, M. M. Caruso, J. A. Ritchey, M. V. Schulmerich, S. J. Robinson, R. Bhargava, N. R. Sottos, S. R. White, M. C. Hersam and J. S. Moore, *Applied Physics Letters*, 2012, **101**, 043106.

45. J. Hur, K. Im, S. W. Kim, J. Kim, D.-Y. Chung, T.-H. Kim, K. H. Jo, J. H. Hahn, Z. Bao, S. Hwang and N. Park, *ACS Nano*, 2014, **8**, 10066-10076.

46. R. J. Wojtecki, M. A. Meador and S. J. Rowan, *Nat Mater*, 2011, **10**, 14-27.

47. R. Chakrabarty, P. S. Mukherjee and P. J. Stang, *Chemical Reviews*, 2011, **111**, 6810-6918.

48. S. Leininger, B. Olenyuk and P. J. Stang, *Chemical Reviews*, 2000, **100**, 853-908.

49. N.-W. Wu, L.-J. Chen, C. Wang, Y.-Y. Ren, X. Li, L. Xu and H.-B. Yang, *Chemical Communications*, 2014, **50**, 4231-4233.

50. Z.-Y. Li, Y. Zhang, C.-W. Zhang, L.-J. Chen, C. Wang, H. Tan, Y. Yu, X. Li and H.-B. Yang, *Journal of the American Chemical Society*, 2014, **136**, 8577-8589.

51. P. Cordier, F. Tournilhac, C. Soulie-Ziakovic and L. Leibler, *Nature*, 2008, **451**, 977-980.

52. K. Harano, S. Hiraoka and M. Shionoya, *Journal of the American Chemical Society*, 2007, **129**, 5300-5301.

53. S. Freye, R. Michel, D. Stalke, M. Pawliczek, H. Frauendorf and G. H. Clever, *Journal of the American Chemical Society*, 2013, **135**, 8476-8479.

54. S. Freye, J. Hey, A. Torras-Galán, D. Stalke, R. Herbst-Irmer, M. John and G. H. Clever, *Angewandte Chemie International Edition*, 2012, **51**, 2191-2194.

55. M. Wang, C. Wang, X.-Q. Hao, X. Li, T. J. Vaughn, Y.-Y. Zhang, Y. Yu, Z.-Y. Li, M.-P. Song, H.-B. Yang and X. Li, *Journal of the American Chemical Society*, 2014, **136**, 10499-10507.

56. Y.-T. Lai, E. Reading, G. L. Hura, K.-L. Tsai, A. Laganowsky, F. J. Asturias, J. A. Tainer, C. V. Robinson and T. O. Yeates, *Nat Chem*, 2014, **6**, 1065-1071.

57. M. Du, Z.-H. Zhang, X.-J. Zhao and Q. Xu, *Inorganic Chemistry*, 2006, **45**, 5785-5792.

58. J. Joseph and E. D. Jemmis, *Journal of the American Chemical Society*, 2007, **129**, 4620-4632.

59. M. J. Taylor, S. Tanna, T. S. Sahota and B. Voermans, *European Journal of Pharmaceutics and Biopharmaceutics*, 2006, **62**, 94-100.

References

Chapter 1

1. A. G. Macdiarmid, J. C. Chiang, A. F. Richter and A. J. Epstein, *Synthetic Metals*, 1987, **18**, 285-290.
2. R. Gangopadhyay and A. De, *Chemistry of Materials*, 2000, **12**, 608-622.
3. G. Wegner, *Angewandte Chemie International Edition in English*, 1981, **20**, 361-381.
4. S. Sadki, P. Schottland, N. Brodie and G. Sabouraud, *Chemical Society Reviews*, 2000, **29**, 283-293.
5. Z. Yin and Q. Zheng, *Advanced Energy Materials*, 2012, **2**, 179-218.
6. G. Giri, E. Verploegen, S. C. B. Mannsfeld, S. Atahan-Evrenk, D. H. Kim, S. Y. Lee, H. A. Becerril, A. Aspuru-Guzik, M. F. Toney and Z. Bao, *Nature*, 2011, **480**, 504-508.
7. A. J. Heeger, *Angewandte Chemie International Edition*, 2001, **40**, 2591-2611.
8. K. Lee, S. Cho, S. Heum Park, A. J. Heeger, C.-W. Lee and S.-H. Lee, *Nature*, 2006, **441**, 65-68.
9. D. Li, J. Huang and R. B. Kaner, *Accounts of Chemical Research*, 2009, **42**, 135-145.
10. C. Li, H. Bai and G. Shi, *Chemical Society Reviews*, 2009, **38**, 2397-2409.
11. Y. Shi, L. Peng, Y. Ding, Y. Zhao and G. Yu, *Chemical Society Reviews*, 2015, **44**, 6684-6696.
12. R. K. Joshi and J. J. Schneider, *Chemical Society Reviews*, 2012, **41**, 5285-5312.
13. H. D. Tran, K. Shin, W. G. Hong, J. M. D'Arcy, R. W. Kojima, B. H. Weiller and R. B. Kaner, *Macromolecular Rapid Communications*, 2007, **28**, 2289-2293.
14. L. Qu, G. Shi, F. e. Chen and J. Zhang, *Macromolecules*, 2003, **36**, 1063-1067.
15. L. Pan, H. Qiu, C. Dou, Y. Li, L. Pu, J. Xu and Y. Shi, *International Journal of Molecular Sciences*, 2010, **11**, 2636.
16. Y.-Z. Long, M.-M. Li, C. Gu, M. Wan, J.-L. Duvail, Z. Liu and Z. Fan, *Progress in Polymer Science*, 2011, **36**, 1415-1442.
17. L. J. Pan, L. Pu, Y. Shi, S. Y. Song, Z. Xu, R. Zhang and Y. D. Zheng, *Advanced Materials*, 2007, **19**, 461-464.
18. X. Zhang and S. K. Manohar, *Journal of the American Chemical Society*, 2004, **126**, 12714-12715.

19. X. Zhang, J. Zhang, Z. Liu and C. Robinson, *Chemical Communications*, 2004, 1852-1853.

20. J. Jang and H. Yoon, *Chemical Communications*, 2003, 720-721.

21. L. Xia, Z. Wei and M. Wan, *Journal of Colloid and Interface Science*, 2010, **341**, 1-11.

22. S. J. Killoran and R. D. O'Neill, *Electrochimica Acta*, 2008, **53**, 7303-7312.

23. D. Xie, Y. Jiang, W. Pan, D. Li, Z. Wu and Y. Li, *Sensors and Actuators B: Chemical*, 2002, **81**, 158-164.

24. C. Liu, H. Ohta, T. Kuwahara and M. Shimomura, *European Polymer Journal*, 2008, **44**, 1114-1122.

25. S. Han, A. L. Briseno, X. Shi, D. A. Mah and F. Zhou, *The Journal of Physical Chemistry B*, 2002, **106**, 6465-6472.

26. G. Lu, C. Li and G. Shi, *Polymer*, 2006, **47**, 1778-1784.

27. J. Zang, C. M. Li, S.-J. Bao, X. Cui, Q. Bao and C. Q. Sun, *Macromolecules*, 2008, **41**, 7053-7057.

28. J. M. Pringle, M. Forsyth, G. G. Wallace and D. R. MacFarlane, *Macromolecules*, 2006, **39**, 7193-7195.

29. X. Lu, W. Zhang, C. Wang, T.-C. Wen and Y. Wei, *Progress in Polymer Science*, 2011, **36**, 671-712.

30. Y. Liao, C. Zhang, Y. Zhang, V. Strong, J. Tang, X.-G. Li, K. Kalantar-zadeh, E. M. V. Hoek, K. L. Wang and R. B. Kaner, *Nano Letters*, 2011, **11**, 954-959.

31. J. Zhang, J. Jiang, H. Li and X. S. Zhao, *Energy & Environmental Science*, 2011, **4**, 4009-4015.

32. Z. Gui, J. Duay, J. Hu and S. B. Lee, *Physical Chemistry Chemical Physics*, 2014, **16**, 12332-12340.

33. X. Xia, D. Chao, X. Qi, Q. Xiong, Y. Zhang, J. Tu, H. Zhang and H. J. Fan, *Nano Letters*, 2013.

34. Y. Hou, Y. Cheng, T. Hobson and J. Liu, *Nano Letters*, 2010, **10**, 2727-2733.

35. H. Zhang, X. Yu and P. V. Braun, *Nat Nano*, 2011, **6**, 277-281.

36. G. Yu, X. Xie, L. Pan, Z. Bao and Y. Cui, *Nano Energy*, 2013, **2**, 213-234.

37. J. Huang and R. B. Kaner, *Journal of the American Chemical Society*, 2003, **126**, 851-855.

38. D. P. Dubal, S. H. Lee, J. G. Kim, W. B. Kim and C. D. Lokhande, *Journal of Materials Chemistry*, 2012, **22**, 3044-3052.

39. J. Xu, K. Wang, S.-Z. Zu, B.-H. Han and Z. Wei, *ACS Nano*, 2010, **4**, 5019-5026.

40. Q. Wu, Y. Xu, Z. Yao, A. Liu and G. Shi, *ACS Nano*, 2010, **4**, 1963-1970.

41. G. Wang, L. Zhang and J. Zhang, *Chemical Society Reviews*, 2012, **41**, 797-828.

42. R. Liu and S. B. Lee, *Journal of the American Chemical Society*, 2008, **130**, 2942-2943.

43. C. Zhou, Y. Zhang, Y. Li and J. Liu, *Nano Letters*, 2013, **13**, 2078-2085.

44. P. Novák, K. Müller, K. S. V. Santhanam and O. Haas, *Chemical Reviews*, 1997, **97**, 207-282.

45. F. Cheng, W. Tang, C. Li, J. Chen, H. Liu, P. Shen and S. Dou, *Chemistry – A European Journal*, 2006, **12**, 3082-3088.

46. M. Zhou, J. Qian, X. Ai and H. Yang, *Advanced Materials*, 2011, **23**, 4913-4917.

47. K. S. Park, S. B. Schougaard and J. B. Goodenough, *Advanced Materials*, 2007, **19**, 848-851.

48. M. N. Hyder, R. Kavian, Z. Sultana, K. Saetia, P.-Y. Chen, S. W. Lee, Y. Shao-Horn and P. T. Hammond, *Chemistry of Materials*, 2014, **26**, 5310-5318.

49. D. Lepage, C. Michot, G. Liang, M. Gauthier and S. B. Schougaard, *Angewandte Chemie International Edition*, 2011, **50**, 6884-6887.

50. M. Wu, X. Xiao, N. Vukmirovic, S. Xun, P. K. Das, X. Song, P. Olalde-Velasco, D. Wang, A. Z. Weber, L.-W. Wang, V. S. Battaglia, W. Yang and G. Liu, *Journal of the American Chemical Society*, 2013, **135**, 12048-12056.

51. G. Liu, S. Xun, N. Vukmirovic, X. Song, P. Olalde-Velasco, H. Zheng, V. S. Battaglia, L. Wang and W. Yang, *Advanced Materials*, 2011, **23**, 4679-4683.

52. K. Deligkaris, T. S. Tadele, W. Olthuis and A. van den Berg, *Sensors and Actuators B: Chemical*, 2010, **147**, 765-774.

53. R. Chakrabarty, P. S. Mukherjee and P. J. Stang, *Chemical Reviews*, 2011, **111**, 6810-6918.

54. N. A. Peppas, J. Z. Hilt, A. Khademhosseini and R. Langer, *Advanced Materials*, 2006, **18**, 1345-1360.

55. Q. Zhang, E. Uchaker, S. L. Candelaria and G. Cao, *Chemical Society Reviews*, 2013, **42**, 3127-3171.

56. L. Pan, G. Yu, D. Zhai, H. R. Lee, W. Zhao, N. Liu, H. Wang, B. C.-K. Tee, Y. Shi, Y. Cui and Z. Bao, *Proceedings of the National Academy of Sciences*, 2012, **109**, 9287-9292.

57. C. R. Martin, *Accounts of Chemical Research*, 1995, **28**, 61-68.

58. L. Li, Y. Shi, L. Pan, Y. Shi and G. Yu, *Journal of Materials Chemistry B*, 2015, **3**, 2920-2930.

59. Y. Zhao, B. Liu, L. Pan and G. Yu, *Energy & Environmental Science*, 2013.

60. S. Brahim, D. Narinesingh and A. Guiseppi-Elie, *Biomacromolecules*, 2003, **4**, 497-503.

Chapter 2

1. A. S. Arico, P. Bruce, B. Scrosati, J.-M. Tarascon and W. van Schalkwijk, *Nat Mater*, 2005, **4**, 366-377.

2. R. K. Joshi and J. J. Schneider, *Chemical Society Reviews*, 2012, **41**, 5285-5312.

3. D. R. Rolison, J. W. Long, J. C. Lytle, A. E. Fischer, C. P. Rhodes, T. M. McEvoy, M. E. Bourg and A. M. Lubers, *Chemical Society Reviews*, 2009, **38**, 226-252.

4. N. Sahiner, *Progress in Polymer Science*, 2013, **38**, 1329-1356.

5. L. Pan, G. Yu, D. Zhai, H. R. Lee, W. Zhao, N. Liu, H. Wang, B. C.-K. Tee, Y. Shi, Y. Cui and Z. Bao, *Proceedings of the National Academy of Sciences*, 2012, **109**, 9287-9292.

6. J. Janata and M. Josowicz, *Nat Mater*, 2003, **2**, 19-24.

7. Y. Zhao, B. Liu, L. Pan and G. Yu, *Energy & Environmental Science*, 2013.

8. L. Xia, Z. Wei and M. Wan, *Journal of Colloid and Interface Science*, 2010, **341**, 1-11.

9. H. D. Tran, D. Li and R. B. Kaner, *Advanced Materials*, 2009, **21**, 1487-1499.

10. Y. Wang, Y. Shi, L. Pan, Y. Ding, Y. Zhao, Y. Li, Y. Shi and G. Yu, *Nano Letters*, 2015.

11. Y. Shi, L. Pan, B. Liu, Y. Wang, Y. Cui, Z. Bao and G. Yu, *Journal of Materials Chemistry A*, 2014, **2**, 6086-6091.

12. Y. Shi and G. Yu, *Chemistry of Materials*, 2016, **28**, 2466-2477.

13. J. Huang and R. B. Kaner, *Angewandte Chemie International Edition*, 2004, **43**, 5817-5821.

14. W. Zhang, Z. Pan, F. K. Yang and B. Zhao, *Advanced Functional Materials*, 2015, **10**, 1588-1597.

15. T. Aida, E. W. Meijer and S. I. Stupp, *Science*, 2012, **335**, 813-817.

16. S. I. Stupp, V. LeBonheur, K. Walker, L. S. Li, K. E. Huggins, M. Keser and A. Amstutz, *Science*, 1997, **276**, 384-389.

17. S. I. Stupp and L. C. Palmer, *Chemistry of Materials*, 2014, **26**, 507-518.

18. H. D. Tran, Y. Wang, J. M. D'Arcy and R. B. Kaner, *ACS Nano*, 2008, **2**, 1841-1848.

19. R. Buitrago-Sierra, M. J. Garcia-Fernandez, M. M. Pastor-Blas and A. Sepulveda-Escribano, *Green Chemistry*, 2013, **15**, 1981-1990.

20. S. P. Lim, A. Pandikumar, Y. S. Lim, N. M. Huang and H. N. Lim, *Scientific Reports*, 2014, **4**, 5305.

21. J.-G. Wang, B. Wei and F. Kang, *RSC Advances*, 2014, **4**, 199-202.

22. M.-K. Song, Y.-T. Kim, B.-S. Kim, J. Kim, K. Char and H.-W. Rhee, *Synthetic Metals*, 2004, **141**, 315-319.

23. M. Massi, C. Albonetti, M. Facchini, M. Cavallini and F. Biscarini, *Advanced Materials*, 2006, **18**, 2739-2742.

24. V. L. Pushparaj, M. M. Shaijumon, A. Kumar, S. Murugesan, L. Ci, R. Vajtai, R. J. Linhardt, O. Nalamasu and P. M. Ajayan, *Proceedings of the National Academy of Sciences*, 2007, **104**, 13574-13577.

25. M. Armand and J. M. Tarascon, *Nature*, 2008, **451**, 652-657.

26. T. Janoschka, M. D. Hager and U. S. Schubert, *Advanced Materials*, 2012, **24**, 6397-6409.

27. L. Pan, A. Chortos, G. Yu, Y. Wang, S. Isaacson, R. Allen, Y. Shi, R. Dauskardt and Z. Bao, *Nat Commun*, 2014, **5**, 3002.

28. J. M. Pringle, O. Ngamna, C. Lynam, G. G. Wallace, M. Forsyth and D. R. MacFarlane, *Macromolecules*, 2007, **40**, 2702-2711.

29. S. Konwer and S. K. Dolui, *Materials Chemistry and Physics*, 2010, **124**, 738-743.

Chapter 3

1. G. Yu, X. Xie, L. Pan, Z. Bao and Y. Cui, *Nano Energy*, 2013, **2**, 213-234.

2. A. Yoshino, *Angewandte Chemie International Edition*, 2012, **51**, 5798-5800.

3. J. B. Goodenough and K.-S. Park, *Journal of the American Chemical Society*, 2013, **135**, 1167-1176.

4. J. B. Goodenough, *Energy & Environmental Science*, 2013.

5. Z. Wang, D. O. Carlsson, P. Tammela, K. Hua, P. Zhang, L. Nyholm and M. Strømme, *ACS Nano*, 2015, **9**, 7563-7571.

6. A. Rudge, J. Davey, I. Raistrick, S. Gottesfeld and J. P. Ferraris, *Journal of Power Sources*, 1994, **47**, 89-107.

7. L. Pan, G. Yu, D. Zhai, H. R. Lee, W. Zhao, N. Liu, H. Wang, B. C.-K. Tee, Y. Shi, Y. Cui and Z. Bao, *Proceedings of the National Academy of Sciences*, 2012, **109**, 9287-9292.

8. N. J. Dudney and J. Li, *Science*, 2015, **347**, 131-132.

9. H. Zhao, Z. Wang, P. Lu, M. Jiang, F. Shi, X. Song, Z. Zheng, X. Zhou, Y. Fu, G. Abdelbast, X. Xiao, Z. Liu, V. S. Battaglia, K. Zaghib and G. Liu, *Nano Letters*, 2014.

10. A. S. Arico, P. Bruce, B. Scrosati, J.-M. Tarascon and W. van Schalkwijk, *Nat Mater*, 2005, **4**, 366-377.

11. Y. Wang, Y. Shi, L. Pan, Y. Ding, Y. Zhao, Y. Li, Y. Shi and G. Yu, *Nano Letters*, 2015.

12. Y. Shi, L. Pan, B. Liu, Y. Wang, Y. Cui, Z. Bao and G. Yu, *Journal of Materials Chemistry A*, 2014, **2**, 6086-6091.

13. Y. Shi, X. Zhou, J. Zhang, A. M. Bruck, A. C. Bond, A. C. Marschilok, K. J. Takeuchi, E. S. Takeuchi and G. Yu, *Nano Letters*, 2017, **17**, 1906-1914.

14. G. H. Gelinck, H. E. A. Huitema, E. van Veenendaal, E. Cantatore, L. Schrijnemakers, J. B. P. H. van der Putten, T. C. T. Geuns, M. Beenhakkers, J. B. Giesbers, B.-H. Huisman, E. J. Meijer, E. M. Benito, F. J. Touwslager, A. W. Marsman, B. J. E. van Rens and D. M. de Leeuw, *Nat Mater*, 2004, **3**, 106-110.

15. V. L. Pushparaj, M. M. Shaijumon, A. Kumar, S. Murugesan, L. Ci, R. Vajtai, R. J. Linhardt, O. Nalamasu and P. M. Ajayan, *Proceedings of the National Academy of Sciences*, 2007, **104**, 13574-13577.

16. M. Armand and J. M. Tarascon, *Nature*, 2008, **451**, 652-657.

17. T. Janoschka, M. D. Hager and U. S. Schubert, *Advanced Materials*, 2012, **24**, 6397-6409.

18. P. Simon and Y. Gogotsi, *Nat Mater*, 2008, **7**, 845-854.

19. M. Winter and R. J. Brodd, *Chemical Reviews*, 2004, **104**, 4245-4270.

20. W. Chen, R. B. Rakhi, L. Hu, X. Xie, Y. Cui and H. N. Alshareef, *Nano Letters*, 2011, **11**, 5165-5172.

21. F. Meng and Y. Ding, *Advanced Materials*, 2011, **23**, 4098-4102.

22. M. Wu, X. Xiao, N. Vukmirovic, S. Xun, P. K. Das, X. Song, P. Olalde-Velasco, D. Wang, A. Z. Weber, L.-W. Wang, V. S. Battaglia, W. Yang and G. Liu, *Journal of the American Chemical Society*, 2013, **135**, 12048-12056.

23. P. L. Taberna, S. Mitra, P. Poizot, P. Simon and J. M. Tarascon, *Nature Materials*, 2006, **5**, 567-573.

24. Y. Orikasa, Y. Gogyo, H. Yamashige, M. Katayama, K. Chen, T. Mori, K. Yamamoto, T. Masese, Y. Inada, T. Ohta, Z. Siroma, S. Kato, H. Kinoshita, H. Arai, Z. Ogumi and Y. Uchimoto, *Scientific Reports*, 2016, **6**, 26382.

25. Y. Shi, L. Peng, Y. Ding, Y. Zhao and G. Yu, *Chemical Society Reviews*, 2015, **44**, 6684-6696.

26. X. Yang, Y. Chen, M. Wang, H. Zhang, X. Li and H. Zhang, *Advanced Functional Materials*, 2016, DOI: 10.1002/adfm.201604229.

27. R. C. de Guzman, J. Yang, M. M.-C. Cheng, S. O. Salley and K. Y. Simon Ng, *Journal of Materials Science*, 2013, **48**, 4823-4833.

28. J. K. Lee, K. B. Smith, C. M. Hayner and H. H. Kung, *Chemical Communications*, 2010, **46**, 2025-2027.

29. K. W. Knehr, N. W. Brady, C. A. Cama, D. C. Bock, Z. Lin, C. N. Lininger, A. C. Marschilok, K. J. Takeuchi, E. S. Takeuchi and A. C. West, *Journal of The Electrochemical Society*, 2015, **162**, A2817-A2826.

30. K. W. Knehr, N. W. Brady, C. N. Lininger, C. A. Cama, D. C. Bock, Z. Lin, A. C. Marschilok, K. J. Takeuchi, E. S. Takeuchi and A. C. West, *ECS Transactions*, 2015, **69**, 7-19.

31. A. M. Bruck, C. A. Cama, C. N. Gannett, A. C. Marschilok, E. S. Takeuchi and K. J. Takeuchi, *Inorg Chem Front*, 2016, **3**, 26-40.

32. Y. H. Kwon, M. M. Huie, D. Choi, M. Chang, A. C. Marschilok, K. J. Takeuchi, E. S. Takeuchi and E. Reichmanis, *ACS Applied Materials & Interfaces*, 2016, **8**, 3452-3463.

33. D. C. Bock, C. J. Pelliccione, W. Zhang, J. Wang, K. W. Knehr, J. Wang, F. Wang, A. C. West, A. C. Marschilok, K. J. Takeuchi and E. S. Takeuchi, *ACS Applied Materials & Interfaces*, 2016, **8**, 11418-11430.

34. H. Ji, L. Zhang, M. T. Pettes, H. Li, S. Chen, L. Shi, R. Piner and R. S. Ruoff, *Nano Letters*, 2012, **12**, 2446-2451.

35. H. Zhong, A. He, J. Lu, M. Sun, J. He and L. Zhang, *Journal of Power Sources*, 2016, **336**, 107-114.

36. J.-M. Kim, H.-S. Park, J.-H. Park, T.-H. Kim, H.-K. Song and S.-Y. Lee, *ACS Applied Materials & Interfaces*, 2014, **6**, 12789-12797.

37. G. Liu, S. Xun, N. Vukmirovic, X. Song, P. Olalde-Velasco, H. Zheng, V. S. Battaglia, L. Wang and W. Yang, *Advanced Materials*, 2011, **23**, 4679-4683.

38. Y. H. Kwon, K. Minnici, M. M. Huie, K. J. Takeuchi, E. S. Takeuchi, A. C. Marschilok and E. Reichmanis, *Chemistry of Materials*, 2016.

39. K. Kirshenbaum, D. C. Bock, C.-Y. Lee, Z. Zhong, K. J. Takeuchi, A. C. Marschilok and E. S. Takeuchi, *Science*, 2015, **347**, 149-154.

40. C. He, S. Wu, N. Zhao, C. Shi, E. Liu and J. Li, *ACS Nano*, 2013, **7**, 4459-4469.

41. Y. Chen, H. Xia, L. Lu and J. M. Xue, *J. Mater. Chem.*, 2012, **22**, 5006-5012.

42. Y. Wang, Y. Shi, L. Pan, Y. Ding, Y. Zhao, Y. Li, Y. Shi and G. Yu, *Nano Letters*, 2015, **15**, 7736-7741.

43. W.-M. Zhang, X.-L. Wu, J.-S. Hu, Y.-G. Guo and L.-J. Wan, *Advanced Functional Materials*, 2008, **18**, 3941-3946.

44. M. T. Ramesan, *Journal of Applied Polymer Science*, 2013, **128**, 1540-1546.

45. D. He, L. Li, F. Bai, C. Zha, L. Shen, H. H. Kung and N. Bao, *Chemistry – A European Journal*, 2016, **22**, 4454-4459.

46. X. Y. Qin, H. R. Zhang, J. X. Wu, X. D. Chu, Y. B. He, C. P. Han, C. Miao, S. A. Wang, B. H. Li and F. Y. Kang, *Carbon*, 2015, **87**, 347-356.

47. Y. Jiang, Z.-J. Jiang, L. Yang, S. Cheng and M. Liu, *Journal of Materials Chemistry A*, 2015, **3**, 11847-11856.

48. E. Kang, Y. S. Jung, A. S. Cavanagh, G.-H. Kim, S. M. George, A. C. Dillon, J. K. Kim and J. Lee, *Advanced Functional Materials*, 2011, **21**, 2430-2438.

49. S. Laruelle, S. Grugeon, P. Poizot, M. Dollé, L. Dupont and J.-M. Tarascon, *Journal of The Electrochemical Society*, 2002, **149**, A627-A634.

50. S. H. Lee, S.-H. Yu, J. E. Lee, A. Jin, D. J. Lee, N. Lee, H. Jo, K. Shin, T.-Y. Ahn, Y.-W. Kim, H. Choe, Y.-E. Sung and T. Hyeon, *Nano Letters*, 2013, **13**, 4249-4256.

51. X. Qin, H. Zhang, J. Wu, X. Chu, Y.-B. He, C. Han, C. Miao, S. Wang, B. Li and F. Kang, *Carbon*, 2015, **87**, 347-356.

52. Y. Zuo, G. Wang, J. Peng, G. Li, Y. Ma, F. Yu, B. Dai, X. Guo and C.-P. Wong, *Journal of Materials Chemistry A*, 2016, **4**, 2453-2460.

53. L. Zhao, M. Gao, W. Yue, Y. Jiang, Y. Wang, Y. Ren and F. Hu, *ACS Applied Materials & Interfaces*, 2015, **7**, 9709-9715.

54. L. Li, A. Kovalchuk, H. Fei, Z. Peng, Y. Li, N. D. Kim, C. Xiang, Y. Yang, G. Ruan and J. M. Tour, *Advanced Energy Materials*, 2015, **5**, 1500171.

55. J. Liu, X. Xu, R. Hu, L. Yang and M. Zhu, *Advanced Energy Materials*, 2016, **6**, 1600256.

56. C. Nan, J. Lu, L. Li, L. Li, Q. Peng and Y. Li, *Nano Res.*, 2013, **6**, 469-477.

57. Y. Zhao, L. Peng, B. Liu and G. Yu, *Nano Letters*, 2014, **14**, 2849-2853.

58. R. A. Hatton, N. P. Blanchard, V. Stolojan, A. J. Miller and S. R. P. Silva, *Langmuir*, 2007, **23**, 6424-6430.

59. L. Atanasoska, K. Naoi and W. H. Smyrl, *Chemistry of Materials*, 1992, **4**, 988-994.

60. Zhang, W. J.; He, X. M.; Pu, W. H.; Li, J. J.; Wan, C. R. *Ionics* **2011**, *17*, 473-477.

61. F. Croce, M. L. Focarete, J. Hassoun, I. Meschini and B. Scrosati, *Energy & Environmental Science*, 2011, **4**, 921-927.

62. L. Luo, P. Zhao, H. Yang, B. Liu, J.-G. Zhang, Y. Cui, G. Yu, S. Zhang and C.-M. Wang, *Nano Letters*, 2015, **15**, 7016-7022.

63. Y. Shi, J. Zhang, A. Bruck, Y. Zhang, J. Li, E. Stach, K. Takeuchi, A. Marschilok, E. Takeuchi, G. Yu, *Advanced Materials*, 2017, DOI: 10.1002/adma.201603922.

Chapter 4

1. N. Nitta, F. Wu, J. T. Lee and G. Yushin, *Materials Today*, 2015, **18**, 252-264.

2. J. B. Goodenough and K.-S. Park, *Journal of the American Chemical Society*, 2013, **135**, 1167-1176.

3. K. Chen, S. Song, F. Liu and D. Xue, *Chemical Society Reviews*, 2015, **44**, 6230-6257.

4. X. Feng, J. Sun, M. Ouyang, F. Wang, X. He, L. Lu and H. Peng, *Journal of Power* Sources, 2015, **275**, 261-273.

5. J. M. Tarascon and M. Armand, *Nature*, 2001, **414**, 359-367.

6. Q. Wang, P. Ping, X. Zhao, G. Chu, J. Sun and C. Chen, *Journal of Power Sources*, 2012, **208**, 210-224.

7. Z. Chen, P.-C. Hsu, J. Lopez, Y. Li, J. W. F. To, N. Liu, C. Wang, Sean C. Andrews, J. Liu, Y. Cui and Z. Bao, *Nature Energy*, 2016, **1**, 15009.

8. H. Yang, Z. Liu, B. K. Chandran, J. Deng, J. Yu, D. Qi, W. Li, Y. Tang, C. Zhang and X. Chen, *Advanced Materials*, 2015, **27**, 5593.

9. D. P. Finegan, M. Scheel, J. B. Robinson, B. Tjaden, I. Hunt, T. J. Mason, J. Millichamp, M. Di Michiel, G. J. Offer, G. Hinds, D. J. L. Brett and P. R. Shearing, *Nature Communications*, 2015, **6**, 6924.

10. X. M. Feng, X. P. Ai and H. X. Yang, *Electrochemistry Communications*, 2004, **6**, 1021-1024.

11. P.-W. Wu, S. R. Holm, A. T. Duong, B. Dunn and R. B. Kaner, *Chemistry of Materials*, 1997, **9**, 1004-1011.

12. W. H. Meyer, *Advanced Materials*, 1998, **10**, 439-448.

13. H. Wu, D. Zhuo, D. Kong and Y. Cui, *Nat Commun*, 2014, **5**, 5193.

14. Y.-S. Chen, C.-C. Hu and Y.-Y. Li, *Journal of Power Sources*, 2008, **181**, 69-73.

15. T. Yim, M.-S. Park, S.-G. Woo, H.-K. Kwon, J.-K. Yoo, Y. S. Jung, K. J. Kim, J.-S. Yu and Y.-J. Kim, *Nano Letters*, 2015, **15**, 5059-5067.

16. L. Xia, S.-L. Li, X.-P. Ai, H.-X. Yang and Y.-L. Cao, *Energy & Environmental Science*, 2011, **4**, 2845-2848.

17. J.-A. Choi, S. H. Kim and D.-W. Kim, *Journal of Power Sources*, 2010, **195**, 6192-6196.

18. Y. S. Jung, A. S. Cavanagh, L. Gedvilas, N. E. Widjonarko, I. D. Scott, S.-H. Lee, G.-H. Kim, S. M. George and A. C. Dillon, *Advanced Energy Materials*, 2012, **2**, 1022-1027.

19. Y. E. Hyung, D. R. Vissers and K. Amine, *Journal of Power Sources*, 2003, **119–121**, 383-387.

20. L. Zhang, Z. Zhang, H. Wu and K. Amine, *Energy & Environmental Science*, 2011, **4**, 2858-2862.

21. L. Zhang, Z. Zhang, P. C. Redfern, L. A. Curtiss and K. Amine, *Energy & Environmental Science*, 2012, **5**, 8204-8207.

22. J. C. Kelly, M. Pepin, D. L. Huber, B. C. Bunker and M. E. Roberts, *Advanced Materials*, 2012, **24**, 886-889.

23. Y. Shi, H. Ha, A. Al-Sudani, C. J. Ellison and G. Yu, *Advanced Materials*, 2016, **28**, 7921-7928.

24. K. P. Mineart, Y. Lin, S. C. Desai, A. S. Krishnan, R. J. Spontak and M. D. Dickey, *Soft Matter*, 2013, **9**, 7695-7700.

25. V. Lenaerts, C. Triqueneaux, M. Quartern, F. Rieg-Falson and P. Couvreur, *International Journal of Pharmaceutics*, 1987, **39**, 121-127.

26. C. Chaibundit, N. M. P. S. Ricardo, N. M. P. S. Ricardo, C. A. Muryn, M.-B. Madec, S. G. Yeates and C. Booth, *Journal of Colloid and Interface Science*, 2010, **351**, 190-196.

27. M. J. Park, K. Char, H. D. Kim, C.-H. Lee, B.-S. Seong and Y.-S. Han, *Macromolecular Research*, 2002, **10**, 325-331.

28. S. L. Guo, T. J. Hou and X. J. Xu, *The Journal of Physical Chemistry B*, 2002, **106**, 11397-11403.

29. Y. Zhao, Y. Cao, Y. Yang and C. Wu, *Macromolecules*, 2003, **36**, 855-859.

30. K. Nishinari, *Colloid Polym Sci*, 1997, **275**, 1093.

31. Y.-M. Chung, K. L. Simmons, A. Gutowska and B. Jeong, *Biomacromolecules*, 2002, **3**, 511-516.

32. J. P. Mata, P. R. Majhi, C. Guo, H. Z. Liu and P. Bahadur, *Journal of Colloid and Interface Science*, 2005, **292**, 548-556.

33. J. Lopez, Z. Chen, C. Wang, S. C. Andrews, Y. Cui and Z. Bao, *ACS Applied Materials & Interfaces*, 2016, **8**, 2318-2324.

34. G. Yu, X. Xie, L. Pan, Z. Bao and Y. Cui, *Nano Energy*, 2013, **2**, 213-234.

35. C. Ma, Y. Shi, D. A. Pena, L. Peng and G. Yu, *Angewandte Chemie International Edition*, 2015, **54**, 7376-7380.

36. Y. Shi, C. Ma, L. Peng and G. Yu, *Advanced Functional Materials*, 2015, **29**, 1219.

Chapter 5

1. G. Schottner, *Chemistry of Materials*, 2001, **13**, 3422-3435.

2. Y. Xu, Q. Wu, Y. Sun, H. Bai and G. Shi, *ACS Nano*, 2010, **4**, 7358-7362.

3. J. Lin, Q. Tang, J. Wu and Q. Li, *Journal of Applied Polymer Science*, 2010, **116**, 1376-1383.

4. Y. Shi, C. Ma, L. Peng and G. Yu, *Advanced Functional Materials*, 2015, **25**, 1219.

5. Y. Shi, M. Wang, C. Ma, Y. Wang, X. Li and G. Yu, *Nano Letters*, 2015, **15**, 6276-6281.

6. J. Ma, N. A. Choudhury, Y. Sahai and R. G. Buchheit, *Journal of Power Sources*, 2011, **196**, 8257-8264.

7. L. Zhang and G. Shi, *The Journal of Physical Chemistry C*, 2011, **115**, 17206-17212.

8. L. Qiu, D. Liu, Y. Wang, C. Cheng, K. Zhou, J. Ding, V.-T. Truong and D. Li, *Advanced Materials*, 2014, **26**, 3333.

9. C. Ma, Y. Shi, D. A. Pena, L. Peng and G. Yu, *Angewandte Chemie International Edition*, 2015, **54**, 7376-7380.

10. P. Chakraborty, P. Bairi, B. Roy and A. K. Nandi, *ACS Applied Materials & Interfaces*, 2014.

11. L. Pan, A. Chortos, G. Yu, Y. Wang, S. Isaacson, R. Allen, Y. Shi, R. Dauskardt and Z. Bao, *Nat Commun*, 2014, **5**.

12. Y. Shi, L. Pan, B. Liu, Y. Wang, Y. Cui, Z. Bao and G. Yu, *Journal of Materials Chemistry A*, 2014, **2**, 6086-6091.

13. L. Pan, G. Yu, D. Zhai, H. R. Lee, W. Zhao, N. Liu, H. Wang, B. C.-K. Tee, Y. Shi, Y. Cui and Z. Bao, *Proceedings of the National Academy of Sciences*, 2012, **109**, 9287-9292.

14. Y. Wang, X. Yang, L. Qiu and D. Li, *Energy Environmental Science*, 2013, **6**, 477-481.

15. D. O. Carlsson, G. Nystrom, Q. Zhou, L. A. Berglund, L. Nyholm and M. Stromme, *Journal of Materials Chemistry*, 2012, **22**, 19014-19024.

16. Y. Zhao, B. Liu, L. Pan and G. Yu, *Energy & Environmental Science*, 2013, **6**, 2856-2870.

17. Q. Li, Q. Tang, L. Lin, X. Chen, H. Chen, L. Chu, H. Xu, M. Li, Y. Qin and B. He, *Journal Power Sources*, 2014, **245**, 468.

18. B. Liu, P. Soares, C. Checkles, Y. Zhao and G. Yu, *Nano Letters*, 2013, **13**, 3414-3419.

19. H. Wu, G. Yu, L. Pan, N. Liu, M. T. McDowell, Z. Bao and Y. Cui, *Nat Commun*, 2013, **4**, 1943.

20. C.-H. Zhu, Y. Lu, J. Peng, J.-F. Chen and S.-H. Yu, *Advanced Functional Materials*, 2012, **22**, 4017-4022.

21. R. E. Rivero, M. A. Molina, C. R. Rivarola and C. A. Barbero, *Sensors and Actuators B: Chemical*, 2014, **190**, 270-278.

22. X. Zhang, C. L. Pint, M. H. Lee, B. E. Schubert, A. Jamshidi, K. Takei, H. Ko, A. Gillies, R. Bardhan, J. J. Urban, M. Wu, R. Fearing and A. Javey, *Nano Letters*, 2011, **11**, 3239-3244.

23. Z. Chen, J. W. F. To, C. Wang, Z. Lu, N. Liu, A. Chortos, L. Pan, F. Wei, Y. Cui and Z. Bao, *Advanced Energy Materials*, 2014, **4**, 1400207.

24. W.-J. Chuang, W.-Y. Chiu and H.-J. Tai, *Journal of Materials Chemistry*, 2012, **22**, 20311-20318.

25. C. Wang, H. Wu, Z. Chen, M. T. McDowell, Y. Cui and Z. Bao, *Nat Chem*, 2013, **5**, 1042-1048.

26. H. Kim, A. A. Abdala and C. W. Macosko, *Macromolecules*, 2010, **43**, 6515-6530.

27. K. Haraguchi and H.-J. Li, *Angewandte Chemie International Edition*, 2005, **44**, 6500-6504.

28. T. Munk, S. Baldursdottir, S. Hietala, T. Rades, M. Nuopponen, K. Kalliomäki, H. Tenhu, J. Rantanen and C. J. Strachan, *Polymer*, 2013, **54**, 6947-6953.

29. X. Zhao, *Soft Matter*, 2014, **10**, 672-687.

30. P. Bairi, B. Roy, P. Routh, K. Sen and A. K. Nandi, *Soft Matter*, 2012, **8**, 7436-7445.

31. S.-W. Cao and Y.-J. Zhu, *The Journal of Physical Chemistry C*, 2008, **112**, 6253-6257.

32. H. Huang, W. Li, H. Wang, X. Zeng, Q. Wang and Y. Yang, *ACS Applied Materials & Interfaces*, 2014, **6**, 1595-1600.

33. W. Zhao, L. Glavas, K. Odelius, U. Edlund and A.-C. Albertsson, *Chemistry of Materials*, 2014, **26**, 4265-4273.

34. H. Wang, B. Zhu, W. Jiang, Y. Yang, W. R. Leow, H. Wang and X. Chen, *Advanced Materials*, 2014, **26**, 3638-3643.

35. Y. Zhang, B. Yang, X. Zhang, L. Xu, L. Tao, S. Li and Y. Wei, *Chemical Communications*, 2012, **48**, 9305-9307.

36. N. Holten-Andersen, M. J. Harrington, H. Birkedal, B. P. Lee, P. B. Messersmith, K. Y. C. Lee and J. H. Waite, *Proceedings of the National Academy of Sciences*, 2011, **108**, 2651-2655.

37. B. C. K. Tee, C. Wang, R. Allen and Z. Bao, *Nat Nano*, 2012, **7**, 825-832.

38. R. F. Shepherd, F. Ilievski, W. Choi, S. A. Morin, A. A. Stokes, A. D. Mazzeo, X. Chen, M. Wang and G. M. Whitesides, *Proceedings of the National Academy of Sciences*, 2011, **108**, 20400-20403.

39. D.-H. Kim, N. Lu, R. Ma, Y.-S. Kim, R.-H. Kim, S. Wang, J. Wu, S. M. Won, H. Tao, A. Islam, K. J. Yu, T.-i. Kim, R. Chowdhury, M. Ying, L. Xu, M. Li, H.-J. Chung, H. Keum, M. McCormick, P. Liu, Y.-W. Zhang, F. G. Omenetto, Y. Huang, T. Coleman and J. A. Rogers, *Science*, 2011, **333**, 838-843.

40. S. R. White, N. R. Sottos, P. H. Geubelle, J. S. Moore, M. R. Kessler, S. R. Sriram, E. N. Brown and S. Viswanathan, *Nature*, 2001, **409**, 794-797.

41. K. S. Toohey, N. R. Sottos, J. A. Lewis, J. S. Moore and S. R. White, *Nat Mater*, 2007, **6**, 581-585.

42. B. J. Blaiszik, S. L. B. Kramer, S. C. Olugebefola, J. S. Moore, N. R. Sottos and S. R. White, *Annual Review of Materials Research*, 2010, **40**, 179-211.

43. S. A. Odom, S. Chayanupatkul, B. J. Blaiszik, O. Zhao, A. C. Jackson, P. V. Braun, N. R. Sottos, S. R. White and J. S. Moore, *Advanced Materials*, 2012, **24**, 2578-2581.

44. S. A. Odom, T. P. Tyler, M. M. Caruso, J. A. Ritchey, M. V. Schulmerich, S. J. Robinson, R. Bhargava, N. R. Sottos, S. R. White, M. C. Hersam and J. S. Moore, *Applied Physics Letters*, 2012, **101**, 043106.

45. J. Hur, K. Im, S. W. Kim, J. Kim, D.-Y. Chung, T.-H. Kim, K. H. Jo, J. H. Hahn, Z. Bao, S. Hwang and N. Park, *ACS Nano*, 2014, **8**, 10066-10076.

46. R. J. Wojtecki, M. A. Meador and S. J. Rowan, *Nat Mater*, 2011, **10**, 14-27.

47. R. Chakrabarty, P. S. Mukherjee and P. J. Stang, *Chemical Reviews*, 2011, **111**, 6810-6918.

48. S. Leininger, B. Olenyuk and P. J. Stang, *Chemical Reviews*, 2000, **100**, 853-908.

49. N.-W. Wu, L.-J. Chen, C. Wang, Y.-Y. Ren, X. Li, L. Xu and H.-B. Yang, *Chemical Communications*, 2014, **50**, 4231-4233.

50. Z.-Y. Li, Y. Zhang, C.-W. Zhang, L.-J. Chen, C. Wang, H. Tan, Y. Yu, X. Li and H.-B. Yang, *Journal of the American Chemical Society*, 2014, **136**, 8577-8589.

51. P. Cordier, F. Tournilhac, C. Soulie-Ziakovic and L. Leibler, *Nature*, 2008, **451**, 977-980.

52. K. Harano, S. Hiraoka and M. Shionoya, *Journal of the American Chemical Society*, 2007, **129**, 5300-5301.

53. S. Freye, R. Michel, D. Stalke, M. Pawliczek, H. Frauendorf and G. H. Clever, *Journal of the American Chemical Society*, 2013, **135**, 8476-8479.

54. S. Freye, J. Hey, A. Torras-Galán, D. Stalke, R. Herbst-Irmer, M. John and G. H. Clever, *Angewandte Chemie International Edition*, 2012, **51**, 2191-2194.

55. M. Wang, C. Wang, X.-Q. Hao, X. Li, T. J. Vaughn, Y.-Y. Zhang, Y. Yu, Z.-Y. Li, M.-P. Song, H.-B. Yang and X. Li, *Journal of the American Chemical Society*, 2014, **136**, 10499-10507.

56. Y.-T. Lai, E. Reading, G. L. Hura, K.-L. Tsai, A. Laganowsky, F. J. Asturias, J. A. Tainer, C. V. Robinson and T. O. Yeates, *Nat Chem*, 2014, **6**, 1065-1071.

57. M. Du, Z.-H. Zhang, X.-J. Zhao and Q. Xu, *Inorganic Chemistry*, 2006, **45**, 5785-5792.

58. J. Joseph and E. D. Jemmis, *Journal of the American Chemical Society*, 2007, **129**, 4620-4632.

59. M. J. Taylor, S. Tanna, T. S. Sahota and B. Voermans, *European Journal of Pharmaceutics and Biopharmaceutics*, 2006, **62**, 94-100.